The Thesis Committee for David Charles Sing
Certifies that this is the approved version of the following thesis:

Direct Measurement of Vanadium Cross-over in an Operating Redox Flow Battery

APPROVED BY
SUPERVISING COMMITTEE:

Supervisor: _____
Arumugam Manthiram

Co-Supervisor: _____
Jeremy P. Meyers

Direct Measurement of Vanadium Cross-over in an Operating Redox Flow Battery

by

David Charles Sing, B.S.; M.S.; Ph.D.

Thesis

Presented to the Faculty of the Graduate School of

The University of Texas at Austin

in Partial Fulfillment

of the Requirements

for the Degree of

Master of Science in Engineering

The University of Texas at Austin

May 2013

Acknowledgements

I would like to thank first and foremost the love and support of my wife Meryl, who likely did not expect to be supporting her graduate student husband at this stage of our lives.

Next, I thank my advisor Dr. Jeremy Meyers for offering a research assistant position to a middle-aged engineer who many would have thought was just suffering through a mid-life career crisis. Thanks also to the other members of the Meyers research group, especially my friend and colleague Philip Michael, who helped me tremendously getting our lab set up and getting our first battery experiments going. It was fun working with Philip while we both plunged ahead into a brand new field for both of us.

Finally I would like to thank the faculty and staff of the Materials Science and Engineering program. I was fortunate to be able to learn from world class professors such as Dr. John Goodenough, Dr. Allan Bard, Dr. Arumugam Manthiram, and the rest of the faculty members of the MS&E program. Thank you also to the talented staff of the Mechanical Engineering Department machine shop, lead by Mr. Scott Allen, especially for putting up with last minute modifications and additions to my job submissions. Finally, I would like to acknowledge the financial supporters of my research, including United Technologies Research Center and the US Department of Energy. This work was supported by the US DOE ARPA-E program under grant # DE-AR00000149.

Abstract

Direct Measurement of Vanadium Cross-over in an Operating Redox Flow Battery

David Charles Sing, M.S.E.

The University of Texas at Austin, 2013

Supervisor: Arumugam Manthiram

Co-Supervisor: Jeremy P. Meyers

A redox flow battery (RFB) is an electrochemical energy storage device in which the storage medium is in the form of liquid electrolyte, which is stored in external reservoirs separate from the cell stack. The storage capacity of such systems is limited by the size of the external tanks, making the RFB an ideal technology for grid level energy storage. The vanadium redox flow battery (VRB) is a particularly attractive variant of the RFB, due to its use of a single transition-metal element in both the positive and negative electrolytes. However, the performance of the VRB is affected by the cross-over of electrolytes through the ion-exchange membrane which separates the positive and negative electrolytes. Cross-over causes degradation of energy storage efficiency and long term capacity loss. Previous studies of ion cross-over have focused primarily on the measurement of ion diffusion across ion exchange membranes in the absence of electrical current. In this work a novel VRB cell is described in which ion cross-over can be measured directly in the presence and absence of electrical current. Measurements are

made of cross-over using this cell with three different types of ion exchange membrane in both charge and discharge modes. The results reported in this work show that the rate of ion cross-over can be greatly enhanced or suppressed depending upon the magnitude of the current flow and its direction relative to the ion concentration gradient.

Table of Contents

List of Tables

List of Figures

Chapter 1: Introduction to Vanadium Redox Flow Batteries

In this chapter, the motivation for the research is briefly discussed, followed by an introduction to redox flow batteries (RFB) and the all-vanadium redox flow battery in particular. The experimental apparatus is described and a brief review of relevant previous experimental results from the literature is discussed. In subsequent chapters of this thesis the use of absorption spectroscopy for determination of the composition of vanadium ion mixtures will be discussed, as well as the methods for calculating cross-over rates from the spectroscopic data. A large chapter is devoted to a discussion of scaling studies of cross-over variation with electric current density, followed by a shorter chapter discussing an experimental study of the effects of convective flows on cross-over. Finally a summary of the results and recommendations for future work is presented in the final chapter.

1.1 Flow batteries for Grid-Level Energy Storage

Grid-level energy storage is essential for widespread integration of renewable energy sources such as wind and solar into the national energy grid. Energy storage capability allows rapid fluctuations in output due to factors such as cloud cover to be buffered, and over longer time periods the storage of energy generated during peak production times for use later during periods of peak demand. Figure 1.1 illustrates how storage can firm up the capacity of a solar power generation facility.

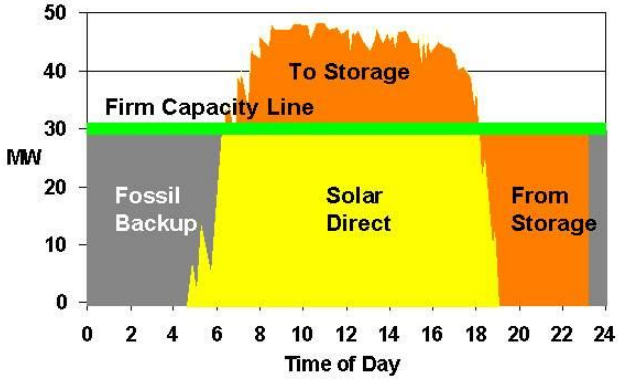

Figure 1.1 Energy storage used to buffer and load shift output from a solar generation facility. Figure adapted from reference [20].

Among the many proposed systems for grid level energy storage is the redox flow battery (RFB). The RFB is an electrochemical energy storage device in which the storage medium is in the form of liquid electrolytes containing ionic species which are either oxidized or reduced to store and release electrical energy. A schematic diagram of a redox flow battery is shown in Figure 1.2. External tanks store the two electrolyte species, the positive electrolyte (catholyte), which is reduced during electrical discharge, and the negative electrolyte (anolyte), which is oxidized during discharge. Many flow battery systems use aqueous electrolytes with a strong acid as supporting electrolyte to provide a ready source of hydrogen ions needed as charge carriers in the electrolyte and ionomer. External pumps circulate the electrolytes through the cell stack, the flow rate is such that in most cases the only a small percentage of the electrolyte is reacted in a single pass. Within the cell stack porous conducting electrodes are separated by an ion exchange membrane which allows hydrogen ions to pass but keeps the electrolyte species from mixing. The porous electrodes provide a large surface area for the heterogeneous electrochemical reactions to occur. Current collectors in contact with the porous

electrodes conduct electrons generated by the electrochemical reactions to and from the external circuit.

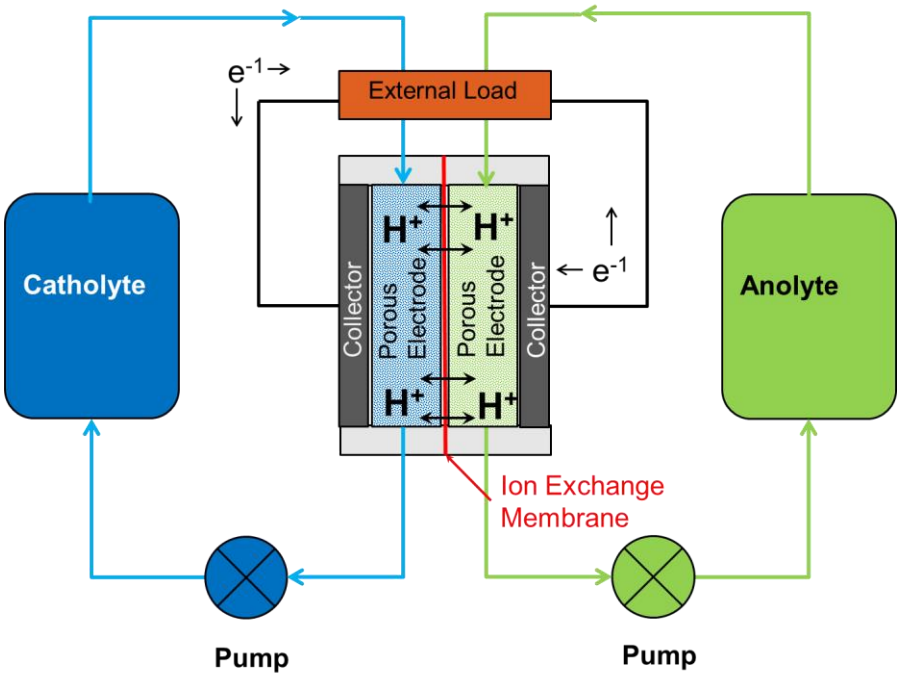

Figure 1.2 Flow Battery Schematic Diagram.

The most important feature of the flow battery is that the energy capacity of the battery depends on the size of the external electrolyte reservoirs, and thus is completely decoupled from the power rating of the system, which is proportional to the cross sectional area of the flow battery cell stack. The decoupling of storage capacity from power capacity makes flow batteries good candidates for large-scale energy storage applications.

The size of the electrolyte reservoirs required for a given energy storage application is easily estimated. The strength of typical anolytes and catholytes used in

most RFB systems is 1 to 2 M, and the energy stored per electron is on the order of 1 eV. Therefore, assuming an electrolyte strength of 1.5 M, each liter of electrolyte can store the following amount of energy:

$$\begin{aligned} &1.5\ \text{(mole/L)} \times 6.02\times10^{23}\ \text{(electrons/mole)} \times 1\ \text{(eV/electron)} \times 1.6\times10^{-19}\ \text{(J/eV)} \\ &\quad = 144480\ \text{(J/L)} \\ &\quad = 40.13\ \text{(W-hr/L)} \end{aligned} \tag{1.1}$$

Storage of the output of a 30 MW solar power plant for 4 hours would require 120 MW-hr of storage capacity, and with a specific capacity of 40.13 W-hr/liter, the volume of electrolyte of each type (anolyte and catholyte) would be 2.99×10^{6} liters. A tank to store that amount of liquid is approximately 65 feet in diameter and 32.5 feet tall, which is comparable to the size of tanks found in a typical petroleum tank farm. Compared to the scale of a typical photovoltaic power plant, tanks of this size are very reasonably sized. Figure 1.3 shows a satellite view of the City of Austin 30 MW photovoltaic power plant in Webberville, TX, with two red dots representing 65 foot diameter electrolyte storage tanks. Compared to the scale of the photovoltaic plant the tanks required for energy storage are quite small. In actual practice a modular set of tanks and RFB stacks would be used, but this example shows that large scale storage facilities can be accommodated by current renewable energy resources.

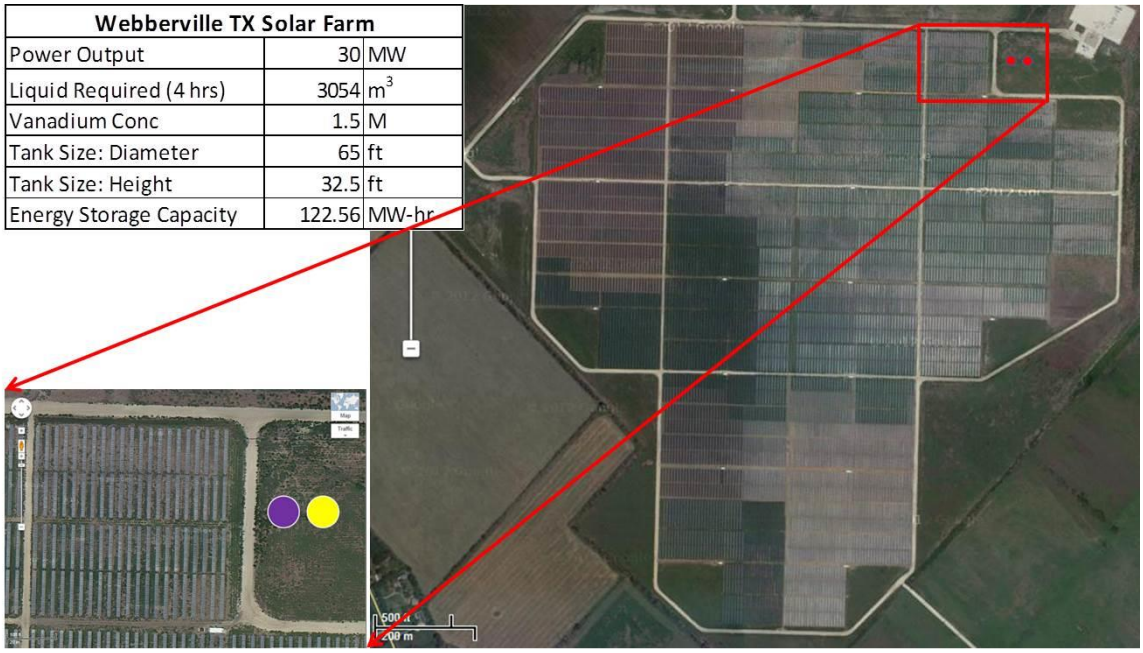

Figure 1.3 Satellite view of a 30 MW photovoltaic power plant. The red dots represent the size of the electrolyte tanks required to provide 4 hours of storage at rated output. Photo from Google Maps.

1.2 VANADIUM REDOX FLOW BATTERIES

The Vanadium Redox Flow Battery (VRB) is a redox flow battery which utilizes vanadium ions in both the catholyte and the anolyte [1]. In the VRB, the catholyte contains a mixture of vanadium ions in the +4 and +5 ionization state, with the charged state corresponding to the +5 ionization state. The chemical formula for the +4 ion is VO^{+2}, and the +5 ion exists in the form VO_2^+. For brevity, the +4 ion will be referred to as V^{+4} in this thesis and the +5 ion as V^{+5} instead of their actual chemical formulations. The anolyte contains a mixture of vanadium ions in the +2 and +3 ionization states, with the charged state corresponding to the +2 state. The electrochemical reactions of the VRB are given by:

$$\begin{aligned} VO^{+2} + H_2O &\underset{DChg}{\overset{Chg}{\rightleftharpoons}} VO_2^+ + 2H^+ + e^{-1}, \; E_o^+ = 1.00 \text{ V} \\ V^{+3} + e^{-1} &\underset{DChg}{\overset{Chg}{\rightleftharpoons}} V^{+2}, \; E_o^- = -0.26 \text{ V} \end{aligned} \tag{1.1}$$

During the charging reaction, water molecules are split at the positive electrode. Oxygen is incorporated into V^{+4} ions forming V^{+5} ions and electrons and hydrogen ions are released. Half of the hydrogen ions flow through the cell to the negative electrode while the electrons pass through the external circuit to the negative current collector. At the negative electrode the electrons combine with V^{+3}, forming V^{+2}. During discharge, V^{+2} is oxidized to V^{+3}, and the electrons liberated pass through the external circuit to the positive electrode. At the positive electrode each V^{+5} ion reacts with two hydrogen ions and an electron to form a V^{+4} ion and a water molecule.

The open circuit voltage can be expressed in terms of the electrolyte concentrations using the Nernst equation [2]:

$$E_0 = E_0^+ - E_0^- + \frac{RT}{F}\ln\left(\frac{c_{V^{+5}} c_{V^{+2}} c^2_{H^+}}{c_{V^{+4}} c_{V^{+3}}}\right) \tag{1.2}$$

where R is the universal gas constant, F is Faraday's constant and T is absolute temperature. At standard (1 M) concentrations, the open circuit voltage (OCV) of a VRB is $E_0 = E_0^+ - E_0^- = 1.26$ V. As the VRB is charged, the concentrations of V^{+4} and V^{+3} decrease while the concentrations of V^{+5} and V^{+2} increase, and the OCV increases logarithmically as the ratio of $c_{V^{+5}} / c_{V^{+4}}$ and $c_{V^{+2}} / c_{V^{+3}}$. If the anolyte and catholyte reservoir volumes are matched, and the initial concentrations of the uncharged electrolytes are the same, then, in the absence of side reactions or crossover, ratios of $c_{V^{+5}} / c_{V^{+4}}$ and $c_{V^{+2}} / c_{V^{+3}}$ will always change in unison and a single state of charge (SOC) metric can be defined as:

$$SOC = \frac{c_{V^{+5}}}{c_{V^{+4}} + c_{V^{+5}}} = \frac{c_{V^{+2}}}{c_{V^{+3}} + c_{V^{+2}}} \tag{1.3}$$

If the contribution due to the hydrogen ion concentration is neglected, then the OCV of a VRB can be expressed in terms of the SOC as:

$$E = E_0 + \frac{2RT}{F}\ln(\frac{SOC}{1-SOC}) \tag{1.4}$$

In practice, the variation of OCV with SOC is more complicated than the simple version given by equation (1.4), especially when transport of electrolyte across the ion exchange membrane and side reactions cause an imbalance in the ratios $c_{V^{+5}}/c_{V^{+4}}$ and $c_{V^{+2}}/c_{V^{+3}}$. Effects of cross membrane transport on cell capacity will be discussed in greater detail in a later section.

1.3 EXPERIMENTAL APPARATUS

Experimental VRB Cell

Several experimental VRB cells were designed and built for the experiments reported in this thesis. Figure 1.4 shows a photograph of one of the experimental cells. In Figure 1.4 (a) a VRB cell is shown with chemical input and output lines and electrical connections attached. The yellow colored lines are the catholyte input and output, the yellow color is characteristic of the V^{+5} ion. The indigo colored lines are the anolyte input and output, the indigo color is characteristic of the V^{+2} ion. The yellow and indigo colors provide a visual indication that the electrolytes are in the charged state. The relationship between the colors of vanadium ion mixtures and chemical composition will be shown to be important for determining the state of charge of the VRB system. Figure 1.4 (b) shows an exploded view of the experimental cell. The porous electrodes are 5 mm thick graphite felt (SGL Sigracell™ GFD5), and the current collectors are machined from graphite and fitted with Viton O-rings and gaskets. When installed the porous electrodes are both compressed approximately 20% to minimize contact resistance between the porous

electrodes and the current collectors. The porous electrode and current collectors fit into PVC frame pieces with manifolds for electrolyte flow and are fitted with acid resistant PVDF tube fittings. An ion exchange membrane is sandwiched between the PVC frame pieces and is sealed with 1.5 mm Viton gaskets. A 75 micron thick Teflon gasket with a 4 cm by 4 cm opening defines the cross sectional area for current flow through the cell.

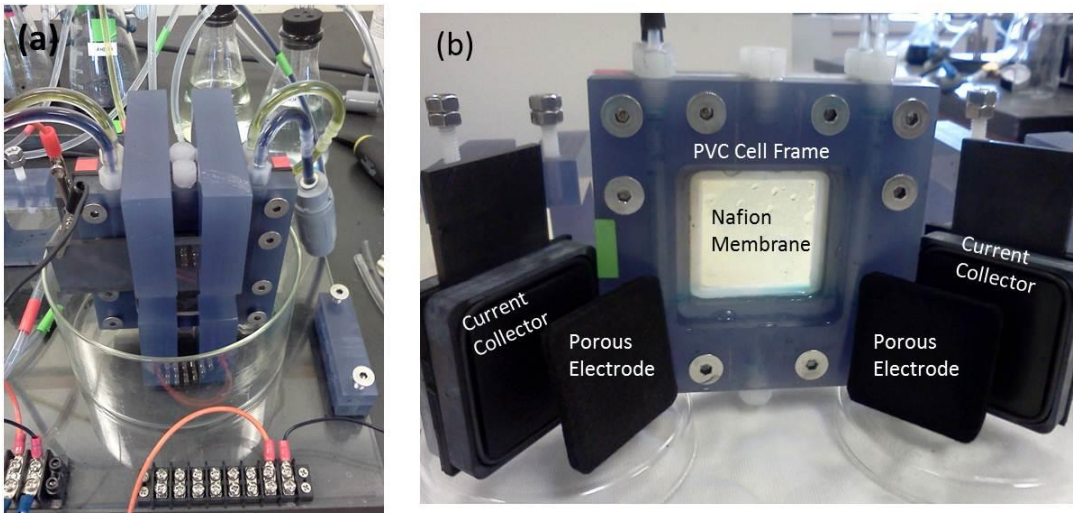

Figure 1.4 Experimental VRB Cell (a) attached to experimental apparatus (b) Exploded view.

Figure 1.5 shows the balance of the equipment used in the experiments. A Gilson Minipuls^{TM} 3 peristaltic pump is used to pump the electrolytes through the VRB Cell. Pyrex flasks with rubber stoppers and glass tubing are used to form the electrolyte reservoirs. Both electrolyte reservoirs can be purged with Argon gas to prevent oxidation from atmospheric oxygen, in practice only the anolyte reservoir requires purging to prevent the V^{+2} ionic species from being oxidized. Acid resistant plastic and Viton tubing are used throughout. Figure 1.5 also shows two additional reservoirs (labeled “Cross-over

Electrolyte Reservoirs") which are used for experiments with a special triple membrane VRB cell, the design and operation of which will discussed in a later section.

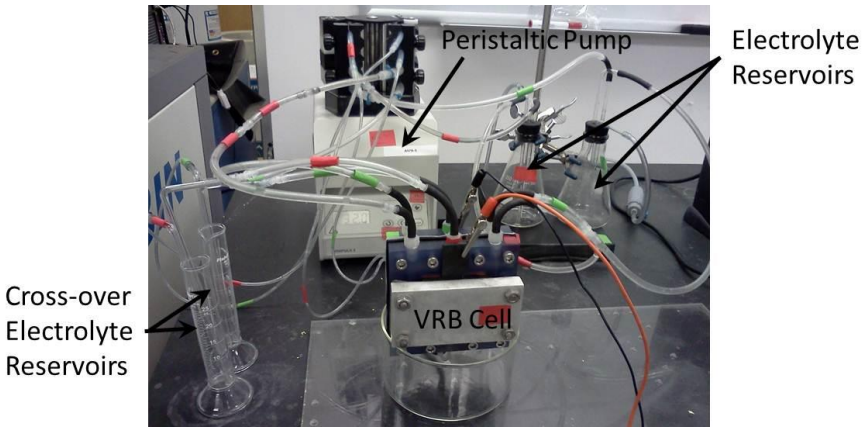

Figure 1.5 VRB Cell and supporting hardware.

Electrolyte Preparation

The starting material for electrolyte preparation is crystalline vanadium (IV) oxide sulfate hydrate, chemical formula $VOSO_4 \cdot xH_2O$ (Sigma-Aldrich stock number 233706-500G). The amount of water which binds with the vanadium complex depends on environmental factors (atmospheric humidity, length of time of exposure). Typical values of x are between 3 and 4. The Vanadyl sulfate is dissolved in di-ionized water with concentrated H_2SO_4 added to achieve a total sulfate concentration of 4 M to 5 M and a vanadium concentration between 0.5 M and 1.5 M. The resulting solution of V^{+4} ions in sulfuric acid forms the uncharged catholyte solution.

The charged catholyte and anolyte are prepared by electrolysis of V^{+4} solution using a procedure based on the method described in [3]. An Arbin BT-2000 battery test system or a Princeton Applied Research Model 2273 potentiostat are used to process the electrolyte solutions. In a typical preparation, the anolyte reservoir is filled with a

quantity of V^{+4} solution while the catholyte reservoir is filled with twice that amount of V^{+4} solution. The anolyte and catholyte solutions are pumped through a VRB cell, and a constant charging current with a current density of 65 mA/cm^2 is injected into the positive electrode of the VRB cell. The applied electrical current drives the following chemical reactions in the VRB:

Positive Electrode:

$$VO^{+2} + H_2O \rightarrow VO_2^{+} + 2H^{+} + e^{-1}$$

Negative Electrode: (1.5)

$$VO^{+2} + 2H^{+} + e^{-1} \rightarrow V^{+3} + H_2O$$

$$V^{+3} + e^{-1} \rightarrow V^{+2}$$

Since the volume of catholyte is twice that of the anolyte, a single oxidation reaction occurs at the positive electrode while two successive reduction reactions occur at the negative electrode. At the positive electrode V^{+4} is oxidized to the V^{+5} ionization state. At the negative electrode, V^{+4} is reduced to V^{+3}, which is further reduced to V^{+2} after all the V^{+4} in the anolyte is exhausted. The endpoint of the reaction is indicated by a sharp rise in the applied voltage and a dramatic color change in the solutions, with the anolyte assuming the indigo color characteristic of V^{+2} and the catholye becoming yellow which is characteristic of V^{+5}.

Ion Exchange Membrane

One of the most important components of a VRB is the ion exchange membrane. The ion exchange membrane has two competing roles: maintaining separation of the electrolyte species while providing a high conductivity path for hydrogen ions to complete the electrical circuit within the VRB. For a given material, a thick membrane will offer increased resistance to mixing of the electrolyte species, but at the cost of higher internal cell resistance. In general, materials which offer superior separation of

electrolytes have higher resistivity. Three different ion exchange membranes were used in this thesis: Dupont Nafion™ 117, Nafion 212, and Fumatech™ FX-7050.

The transport of the anolyte and catholyte across the ion exchange membrane is called electrolyte cross-over. Electrolyte cross-over leads to loss of energy efficiency and cell capacity. In a VRB, V^{+4} and V^{+5} ions from the catholyte which pass through the ion exchange membrane will react with the V^{+2} and V^{+3} ions in the anolyte according to the following reactions:

$$\begin{aligned} &V^{+4} \text{ into } V^{+2}/V^{+3}: \\ &VO^{+2} + V^{+2} + 2H^{+} \rightarrow 2V^{+3} + H_2O \\ &V^{+5} \text{ into } V^{+2}/V^{+3}: \\ &VO_2^{+} + V^{+2} + 2H^{+} \rightarrow V^{+3} + VO^{+2} + H_2O \\ &VO_2^{+} + V^{+3} \rightarrow 2VO^{+2} \end{aligned} \tag{1.6}$$

V^{+4} ions that cross-over into the anolyte can only react with V^{+2} ions, forming two V^{+3} ions for every V^{+4} ion. V^{+5} ions can react with either V^{+2} or V^{+3} ions. If there is sufficient amount of V^{+2} present, a V^{+5} ion will react with V^{+2} to form a V^{+3} and V^{+4} ion. The V^{+4} ion formed will react with additional V^{+2} to form two more V^{+3} ions, which makes a total of three V^{+3} ions for every V^{+5} ion which enters the anolyte. A similar set of reactions occurs when V^{+2} and V^{+3} cross over into the catholyte:

$$\begin{aligned} &V^{+3} \text{ into } V^{+4}/V^{+5}: \\ &V^{+3} + VO_2^{+} \rightarrow 2VO^{+2} \\ &V^{+2} \text{ into } V^{+4}/V^{+5}: \\ &V^{+2} + VO^{+2} + 2H^{+} \rightarrow 2V^{+3} + H_2O \\ &V^{+2} + VO_2^{+} + 2H^{+} \rightarrow V^{+3} + VO^{+2} + H_2O \end{aligned} \tag{1.7}$$

V^{+3} ions which cross-over to the catholyte can only react with V^{+5} ions, forming two V^{+4} ions for every V^{+3} ion. V^{+2} ions can react with either V^{+4} or V^{+5} ions. If there is a sufficient amount of V^{+5} present, a V^{+2} ion will react V^{+5} to form a V^{+3} and V^{+4} ion. The

V^{+3} ion will react with additional V^{+5} to form two more V^{+4} ions, which makes a total of three V^{+4} ions formed for every V^{+2} ion which enters the catholyte. Table 1.1 summarizes the reactants and products of cross-over ion reactions. It is apparent that cross-over ions have the effect of discharging the cell, with V^{+2} and V^{+5} ions having twice the discharge effect of V^{+3} and V^{+4} ions.

Table 1.1 Summary of chemical reactions due to cross-over in a VRB

Cross-Over Ion	Receiving Electrolyte	Available Ions	Ions Lost	Ions Formed
V^{+2}	Catholyte	V^{+4}/V^{+5}	$2V^{+5}$	$3V^{+4}$
V^{+3}	Catholyte	V^{+4}/V^{+5}	V^{+5}	$2V^{+4}$
V^{+4}	Anolyte	V^{+2}/V^{+3}	V^{+2}	$2V^{+3}$
V^{+5}	Anolyte	V^{+2}/V^{+3}	$2V^{+2}$	$3V^{+3}$

In addition to causing self-discharge, cross-over can also lead to a permanent loss of capacity in a flow battery system [4,5]. Capacity loss results when the net flux of ion cross-over is non-zero over a charge and discharge cycle, leading to excess vanadium on one side of the cell and a deficit on the other side. When this occurs, the cell is said to be unbalanced, and the half cell with less vanadium will cycle over larger range of SOC with each charge/discharge cycle, while the cell with more vanadium will cycle over a smaller range of SOC. Unbalancing is a direct result of differences in the transport coefficients of the various ionic species through the ion exchange membrane. Knehr *et.al.* showed that small imbalances in transport, which over a single charge/discharge cycle result in only a fraction of a percent loss in capacity, can over many (45) cycles result in a large (17%) capacity loss [5]. Since VRB's are designed to run many thousands of cycles, capacity loss due to electrolyte imbalance is a serious problem from an operational standpoint.

1.4 BRIEF REVIEW OF PREVIOUS ION CROSS-OVER MEASUREMENTS

Dialysis Cell Experiments

Several groups have reported measurements of vanadium cross-over using dialysis cells [6,7,8]. In these experiments vanadium ion solutions are circulated through a cell in which an ion exchange membrane has been mounted. On the opposite side of the membrane a solution of sulfuric acid is circulated with an equivalent sulfate concentration as the vanadium solution to minimize osmotic pressure effects. Figure 1.6 shows a schematic diagram of a typical dialysis cell experiment.

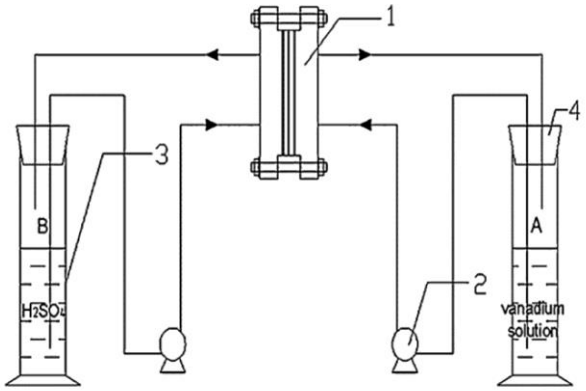

1 - dialysis cell; 2 - pump; 3 - measuring cylinder; 4 - rubber plug.

Figure 1.6 Schematic of Dialysis Cell Experiment. Copied from Reference [7].

Due to the concentration gradient vanadium ions diffuse through the ion exchange membrane into the sulfuric acid solution. The concentration of vanadium in the acid can be measured using UV/VIS spectroscopy [6,7] or by potentiometric titration [8]. Mass transport coefficients and diffusion coefficients for V^{+2}, V^{+3}, V^{+4}, and V^{+5} can be found using this method. Table 1.2 lists the diffusion coefficients for vanadium through Nafion 115 membrane material as reported in Reference [8]. Also listed in Table 1.2 are effective

mass transfer coefficients m_i calculated by dividing the diffusion coefficients by the membrane thickness.

Table 1.2 Vanadium diffusion coefficients and mass transfer coefficients for transport through Nafion N115. Data from Reference [8].

Membrane	Nafion N115	
Thickness	0.0125	cm
Species	D_i (cm^2/sec)	m_i (cm/sec)
V^{+2}	8.77E-08	7.01E-06
V^{+3}	3.22E-08	2.58E-06
V^{+4}	6.83E-08	5.46E-06
V^{+5}	5.90E-08	4.72E-06

However, in an operating VRB, an electrical current primarily carried by the H^+ ions is also present, and with it an electro-osmotic flow of water. vanadium ions can be transported by electro-migration and convective flows in addition to concentration gradient driven diffusion. These effects cannot be measured in dialysis cell experiments.

Redox Flow Battery Experiments

Luo and co-workers [9] measured vanadium ion transport in redox flow battery cells using a mixed vanadium/Fe system. In these experiments vanadium redox couples (V^{+2}/V^{+3} or V^{+4}/V^{+5}) were paired with the Fe^{+2}/Fe^{+3} redox couple to form working flow battery cells. Vanadium which crossed over to the Fe side of the cells can be measured using ICP mass spectroscopy (ICP/MS). In these experiments, the total concentration of vanadium cross-over can be measured but that of the individual ionic components cannot be determined. The authors used the cell configurations shown in Figure 1.7 (a) and (b) to measure cross-over with the mixed V/Fe cells running charge and discharge cycles. The

transport of V^{+4}/V^{+5} was studied using the cell in Figure 1.7 (a) and the transport of V^{+2}/V^{+3} was studied using the cell in Figure 1.7 (b).

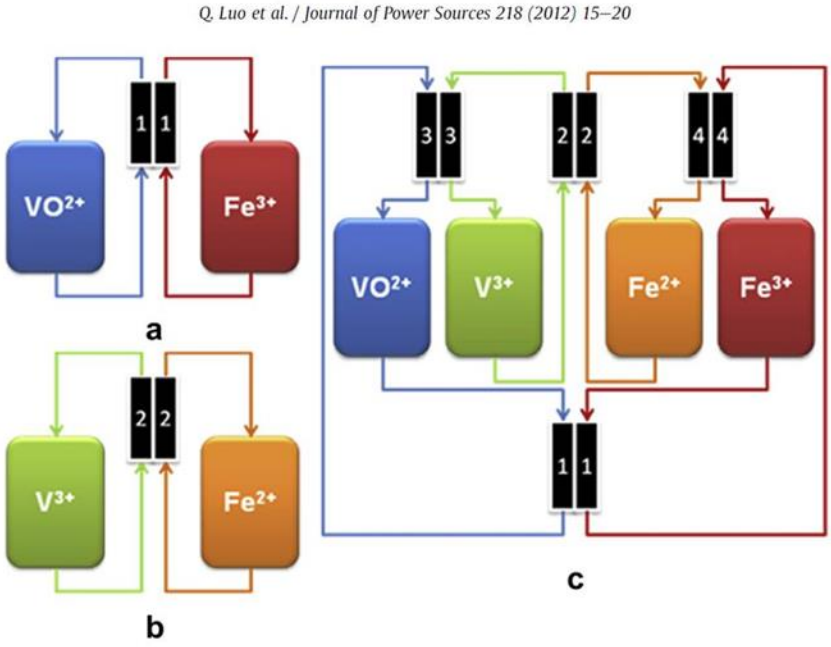

Figure 1.7 Schematic of Fe/V Flow Battery cells to measure V transport across ion exchange membranes with electrical current flowing. Copied from Ref. [9].

Because the chemical compositions of the flow cells change with time as the cells are charged and discharged, the amount of vanadium that passes through the membrane depends on both electrical effects and concentration changes. To isolate concentration changes from electric current effects a complex of four cells as shown in Figure 1.7 (c) was used. Cells (1) and (2) in Figure 1.7 (c) had no current flowing through them, while cells (3) and (4) were run through charge/discharge cycles to reproduce the composition charges in the single cell apparatus shown in Figures 1.7 (a) and (b). In this way the effects of chemical composition changes on vanadium transport could be isolated form the electric current effects. The authors found that transport was enhanced when the electrical current was in the same direction as the ion gradient driven flux and suppressed

with the electric current was in the opposite direction. The transport results were modeled using an equation of the form:

$$N_i = (m_i + k_i J) \times c_i \tag{1.8}$$

In Equation (1.8) N_i is the flux (in moles/cm^2) of species i with concentration c_i passing through the membrane, m_i is the mass transfer coefficient, J is the current density, and k_i is the electro-migration coefficient. Implicit in Equation (1.8) is the assumption that J is a signed quantity, with the positive sign corresponding to current in the same direction as the gradient driven flux. Also, Equation (1.8) also assumes that the concentration of vanadium on the other side of the membrane is negligible compared to c_i. Table 1.3 lists the values of m_i and k_i from Reference [9].

Table 1.3 Vanadium mass transfer and electro-migration coefficients for Nafion N115. Data from Reference [9].

Membrane	Nafion N115	
Thickness	1.25E-02	cm
Species	m_i (cm/sec)	k_i (cm^3/sec/mA)
V^{+2}	7.55E-06	1.05E-07
V^{+3}	1.16E-05	1.48E-07
V^{+4}	3.56E-06	1.10E-07
V^{+5}	1.92E-06	3.50E-08

Note that although the same membrane (Nafion N115) was used in the experiments that generated the data listed in Tables 1.2 and 1.3, the values for the mass diffusion coefficients m_i different significantly. The cause for the variation from experiment to experiment, even for the same ion and membrane, has not been addressed in a systematic way by any other researchers, aside from an acknowledgement that other unknown factors must be coming into play. The most meaningful results are found in comparison studies, in which different membranes are compared under identical conditions [6, 7], or

a single membrane which is tested with only one parameter varied (i.e. current density for the experiment reported in Reference [9]).

To date, the results reported by Luo and co-workers are the only ones published in which the transport of vanadium has been measured across ion exchange membranes in the presence of electrical current. The maximum current density used in these experiments, 50 mA/cm^2, is much less than the current densities that have been reported in experiments with state-of-the-art VRB cells, in which current densities in excess of 500 mA/cm^2 have been demonstrated [10,19]. Also, the use of a number of different flow batteries in a complicated series/parallel arrangement makes the execution of experiments to separate concentration changes from current effects unwieldy at best. A novel new cell design which simplifies the measurement of transport in an operating VRB configuration was developed for this thesis and is described in the next section.

1.5 TRIPLE MEMBRANE CELL

A special VRB cell was designed with the purpose of studying ion cross-over in an operating VRB cell. Two additional electrolyte chambers are incorporated into a standard VRB cell to form the triple-membrane cell. Figure 1.8 shows a schematic diagram of this cell. The triple membrane cell, which, for brevity, will be referred to as the "XO" (for cross-over) cell, is a conventional VRB with positive and negative electrolyte flow chambers, indicated in Figure 1.8 as the "V+" and "V-" chambers. Two additional chambers, labeled "+XO" and "–XO", are filled with sulfuric acid which is circulated through two reservoirs using two additional flow circuits. Three ion exchange membranes separate the four different chambers of the cell. The strength of the sulfuric acid pumped through the XO chambers is adjusted to match the sulfate concentration of the anolyte and catholyte.

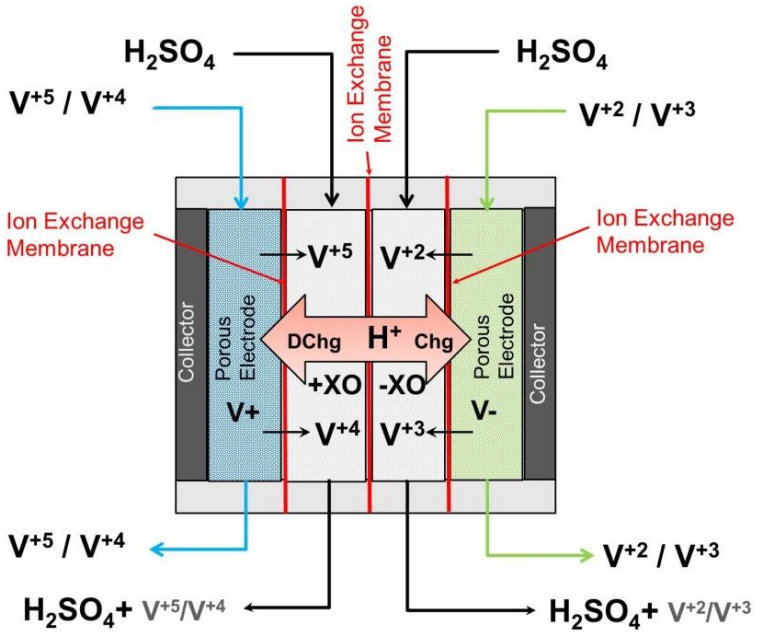

Figure 1.8 Triple Membrane Cell Schematic Diagram.

The XO chambers act like a salt bridge connecting the V+ and V- chambers, allowing a flux of H^+ ions to pass through the +XO and –XO chambers during charge and discharge. Anolyte and catholyte ions which cross-over through the outer ion exchange membranes are collected in the –XO and +XO chambers respectively. Transport into the XO chambers is dominated by the flux of ions from the adjacent V+ and V- chambers, since the concentration gradient across the outer membranes is several orders of magnitude greater than the gradient across the center membrane. All of the cross-over transport data in this thesis was collected with the XO cell.

The XO cell proved to be very successful for measuring the transport of vanadium with and without electrical current. Experiments with current densities up to 900 mA/cm^2 were successfully run with the cell. The exact details and operating conditions will be discussed in Chapter 3.

Chapter 2: Optical Measurement of Vanadium Ion Concentrations and Transport Coefficients

In this chapter methods are described to determine the composition of mixtures of vanadium ions using absorption spectroscopy. The calculation of vanadium transport coefficients is demonstrated with spectroscopy data from a simple experiment.

2.1 Beer's Law for Mixtures of Absorbing Species

In many cases, the intensity of light transmitted through a liquid media varies exponentially with the path length *l*:

$$I = I_0 e^{-\sigma N l} \tag{2.1}$$

where σ is the cross section for light absorption and *N* is the number density of the absorbing molecules. The absorbance is defined as the negative logarithm (base 10) of the fraction of transmitted light:

$$A = -\log\left(\frac{I}{I_0}\right) \tag{2.2}$$

Substituting (2.1) into (2.2) yields Beer's Law, which relates the absorbance to the properties and number density of the absorbing molecules:

$$A = 0.434\sigma N l \tag{2.3}$$

If Beer's law is valid for a particular substance, then equations (2.1) through (2.3) are valid, and the absorbance is proportional to the concentration of the absorbing molecules. Equation (2.3) is often recast in terms of molar concentration *c* and molar absorptivity *a* as:

$$A = acl \tag{2.4}$$

If a mixture of two absorbing species α and β is prepared, then the absorptivity of the mixture will often behave linearly with the concentrations of the component species c_α and c_β according to:

$$A = a_\alpha c_\alpha l + a_\beta c_b l \tag{2.5}$$

where a_α and a_β are the molar absorptivity of species α and β.

Equation (2.5) implies that if the absorptivity is measured at two different wavelengths, λ_1 and λ_2, then the concentrations of the two species can be found by solving the following system of equations:

$$\begin{aligned} A(\lambda_1) &= a_\alpha(\lambda_1)c_\alpha l + a_\beta(\lambda_1)c_\beta l \\ A(\lambda_2) &= a_\alpha(\lambda_2)c_\alpha l + a_\beta(\lambda_2)c_\beta l \end{aligned} \tag{2.6}$$

In practice, the absorption spectra of reference samples of known concentrations of α and β are used to eliminate the molar absorptivity and path length by using the relationship:

$$A_j(\lambda_i) = a_j(\lambda_i)c_j^{ref} l \tag{2.7}$$

where $A_j(\lambda_i)$ is the absorptivity at wavelength λ_i of the reference sample consisting of species j with concentration c_j^{ref}. Using (2.7) the system of equations (2.6) can be rewritten in terms of the absorptivity of the reference samples as:

$$\begin{aligned} A(\lambda_1) &= A_\alpha(\lambda_1)\frac{c_\alpha}{c_\alpha^{ref}} + A_\beta(\lambda_1)\frac{c_\beta}{c_\beta^{ref}} \\ A(\lambda_2) &= A_\alpha(\lambda_2)\frac{c_\alpha}{c_\alpha^{ref}} + A_\beta(\lambda_2)\frac{c_\beta}{c_\beta^{ref}} \end{aligned} \tag{2.8}$$

The solution of (2.8) yields the coefficients $c_\alpha / c_\alpha^{ref}$ and c_β / c_β^{ref}, the concentrations of species α and β relative to the reference sample concentrations.

2.2 SPECTROSCOPIC ANALYSIS OF VANADIUM ION MIXTURES

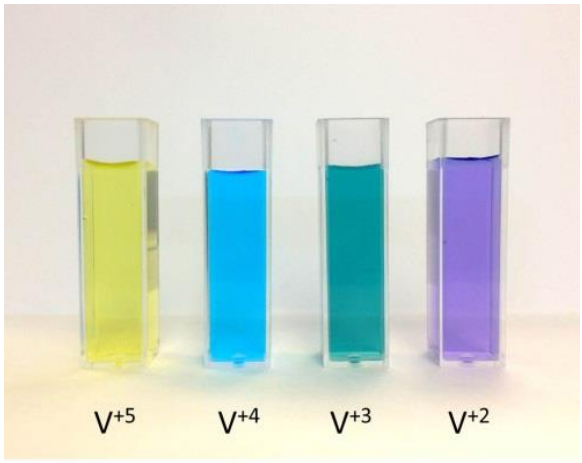

Figure 2.1 Vanadium 0.1 M solutions, ionization states +2 through +5. Photograph by the author.

Aqueous solutions of the four different vanadium ion species used in VRB's have distinctly different colors. Figure 2.1 shows a photograph of 0.1 M samples contained in 1 cm cuvettes. Pure solutions of the two components of the positive electrolyte, V^{+4} and V^{+5}, have blue and yellow colors respectively, while the two components of the negative electrolyte, V^{+2} and V^{+3}, have indigo and green colors. The absorption spectra of the samples pictured in Figure 2.1 are shown in Figure 2.2.

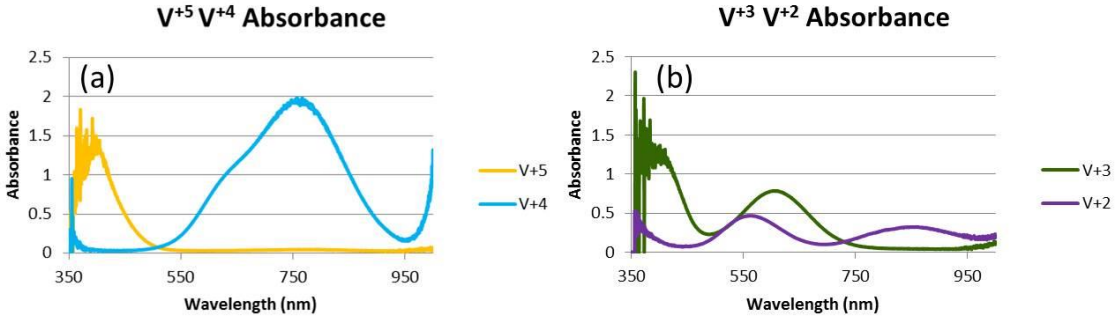

Figure 2.2 Absorption spectra of 0.1 M samples of vanadium cations (a) V^{+4} and V^{+5} (b) V^{+2} and V^{+3}.

Because of these distinctly different colors, several research groups have investigated the use of UV/VIS absorption spectroscopy to determine the state of charge (SOC) of the electrolytes used in VRB's [11,12].

A requirement for spectrophotometry of a mixture of vanadium ions to be useful for determining the composition mixture is that the spectrum must obey Equation (2.5), which states that the mixture spectrum is a linear combination of the spectra of the component species. Tang *et. al*. measured the absorption spectra of mixtures of V^{+2} and V^{+3} typical of the negative electrolyte of a VRB [12]. Figure 2.3 taken from Reference [12] shows the absorption spectra of the negative electrolyte for different SOC, where SOC = 0% is pure V^{+3} and SOC = 100% is pure V^{+2}. The sum of the concentrations of V^{+2} and V^{+3} was kept constant at 1 M, and the path length of the sample used was 0.5 mm. The spectra in Figure 2.3 are well represented by linear combinations of the V^{+2} and V^{+3} spectra with the coefficients consistent with the SOC of the electrolyte mixture. The authors conclude that absorption spectroscopy is useful for determining the SOC of the VRB negative electrolyte.

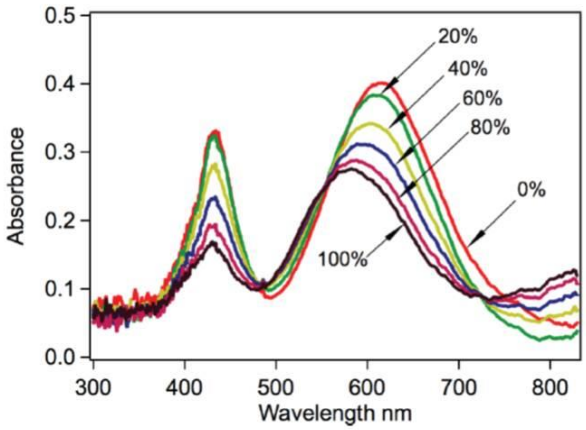

Figure 2.3 Absorption spectra of negative VRB electrolytes from 0% to 100% SOC, 1 M total V concentration. Figure from Tang et.al. [12].

However, the spectra of V^{+4}/V^{+5} mixtures are more complicated. Figure 2.4 taken from Reference [12] shows the absorption spectra for $V^{+4/}V^{+5}$ mixtures for different SOC, where SOC = 0% is pure V^{+4} and SOC = 100% is pure V^{+5}. The total V concentration was 0.5 M and the path length for the measurement was 1.0 mm. The spectra for SOC between 20% and 80% cannot be reproduced by a linear combination of the V^{+4} and V^{+5} spectra. The anomalous absorption observed by Tang *et. al*. has been observed by other researchers [13,14] and is believed to be due to the formation of a mixed-valence cation-cation complex between V^{+4} and V^{+5} ions.

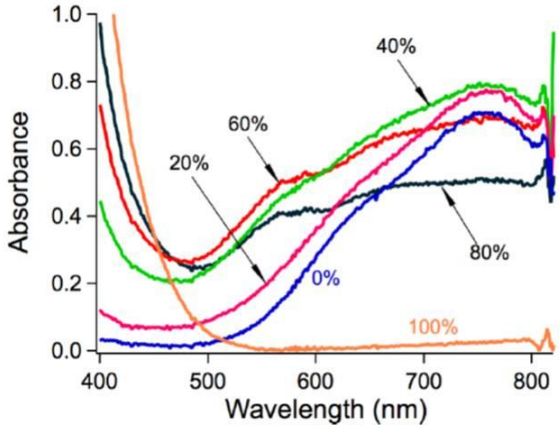

Figure 2.4 Absorption spectra of positive VRB electrolyte from 100% SOC (100% V^{+5}) to 0% SOC (100% V^{+4}). 0.5 M total V concentration. Figure from Tang et. al. [12].

The formation of a cation-cation complex is less likely at lower concentrations, so the absorption spectra at lower (<0.1 M) concentrations was investigated for this thesis. Samples of V^{+4}/V^{+5} mixtures with 0.07 M total V concentration and V^{+4} content varying between 20% and 80% were prepared and the samples were measured using a Milton Roy Spectronic 3000 spectrometer with 1 cm path length cuvettes. The resulting spectra are shown in Figure 2.5 (a). Analysis of the spectra shows that the absorption from 380 to

400 nm is proportional to the V^{+5} content and the absorption from 750 to 780 is proportional to the V^{+4} content. The spectra of the mixtures were then fit with a linear combination of the spectra from pure V^{+4} and V^{+5} samples. The composite spectra fit to the mixture spectra are shown in Figure 2.5 (b). Comparison of the measured and the combination spectra show that at low concentrations (<0.1 M) the composition of V^{+4}/V^{+5} mixtures can be determined by fitting the absorption spectra of the mixture using reference spectra from pure V^{+4} and V^{+5} samples.

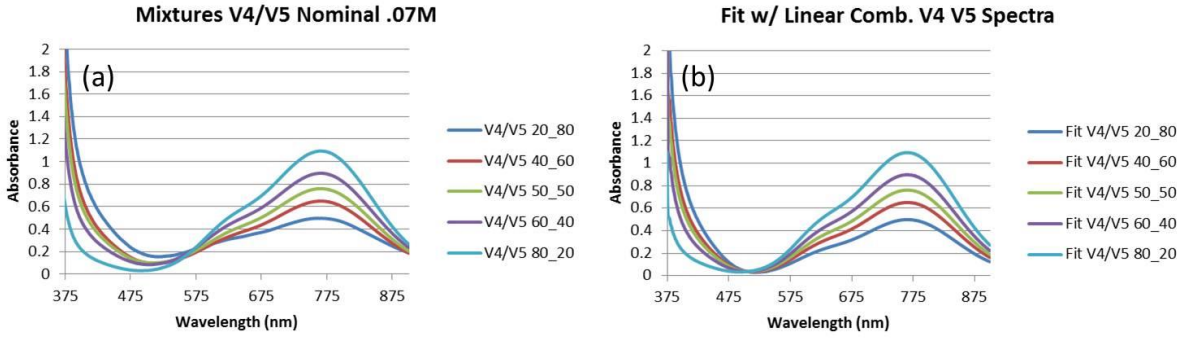

Figure 2.5 (a) Absorption spectra V^{+4}/V^{+5} mixtures with total V concentration 0.07 M. Nominal V^{+4} content 20% through 80%. (b) Spectra of linear combination of V^{+4} and V^{+5} spectra fit to spectra shown in (a).

2.3 ANALYSIS OF VRB ELECTROLYTE SAMPLES

In this section the methods discussed in the previous section for calculating the specific concentration of mixtures composed of two different ionization states of vanadium are used to analyze mixtures which are relevant to VRB's. The negative and positive electrolyte solutions of the VRB are the most common type of mixture encountered. The negative electrolyte is a mixture of V^{+2} and V^{+3}, with the ratio of V^{+2} to V^{+3} determined by the SOC of the cell, with 100% SOC corresponding to pure V^{+2} and 0% SOC corresponding to V^{+3}. Similarly, the positive electrolyte is a mixture of V^{+4} and V^{+5}, with 100% SOC corresponding to pure V+5 and 0% SOC corresponding to pure V^{+4}.

The only other combination of vanadium ions species which is stable is V^{+3} and V^{+4}. The doubly charged species V^{+2} will always be oxidized when in the presence of V^{+4} or V^{+5}. Similarly V^{+5} will always be reduced when combined with either V^{+2} or V^{+3}.

As discussed in the previous section, absorbance measurements at two wavelengths are sufficient to determine the composition of a two component vanadium mixture. However, absorbance data from a spectrometer system is often shifted by a constant offset. This offset can be due to drift in the spectrometer electronics or thermal effects as the spectrometer light source warms up. Therefore, three wavelengths are used to determine the composition of a two component mixture. The absorbance data from the third wavelength allows the determination of the constant (DC) offset. The set of equations to be solved in this case is:

$$\begin{aligned} A(\lambda_1) &= A_\alpha(\lambda_1)\frac{c_\alpha}{c_\alpha^{ref}} + A_\beta(\lambda_1)\frac{c_\beta}{c_\beta^{ref}} + C_{offset} \\ A(\lambda_2) &= A_\alpha(\lambda_2)\frac{c_\alpha}{c_\alpha^{ref}} + A_\beta(\lambda_2)\frac{c_\beta}{c_\beta^{ref}} + C_{offset} \\ A(\lambda_3) &= A_\alpha(\lambda_3)\frac{c_\alpha}{c_\alpha^{ref}} + A_\beta(\lambda_3)\frac{c_\beta}{c_\beta^{ref}} + C_{offset} \end{aligned} \tag{2.9}$$

where C_{offset} is the DC offset.

The choice of wavelengths λ_1, λ_2, and λ_3 depends on the shape of the spectra of the component species. Examination of Figure 2.2 shows that the absorption of V^{+5} increases strongly at the blue end of the spectrum while the absorption for V^{+4} peaks near 750 nm. (Note: the noise in Figure 2.2 (a) at wavelengths less than 400 nm is due to the limitations of the light source, the actual absorbance continues to rise as wavelength is decreased). The absorption of both species is weak near 480 nm, so a good choice of wavelengths to determine the concentration of V^{+4}, V^{+5}, and the DC offset for V^{+4}/V^{+5} combinations is 390, 480, and 750 nm. Table 2.1 lists the wavelengths used to determine

the concentrations of the component species (relative to the reference concentrations) and the DC offset for V^{+4}/V^{+5}, V^{+3}/V^{+4}, and V^{+2}/V^{+3} mixture combinations.

Table 2.1 Wavelengths to determine vanadium mixture composition for specific ion combinations.

	V2-V3	V3-V4	V4-V5
WL_1	380	390	390
WL_2	580	480	480
WL_3	825	750	750

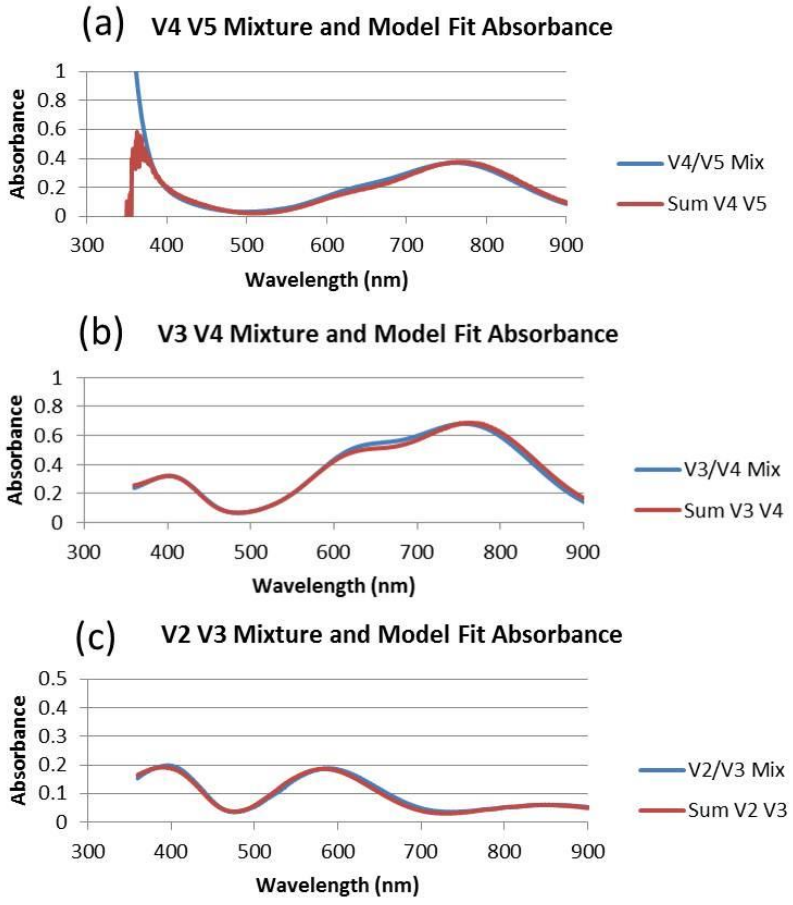

Figure 2.6 Sample mixture spectra and fit to reference spectra (labeled "Sum V4 V5" etc) for (a) V^{+5}/V^{+4} (b) $V^{+4/}V^{+3}$ and (c) V^{+3}/V^{+2} mixtures.

Figure 2.6 shows the absorbance spectra of V^{+4}/V^{+5}, V^{+3}/V^{+4}, and V^{+2}/V^{+3} mixtures typical of the samples measured in this thesis. The spectrum shown in Figure 2.6 (a) is from a sample in which V^{+4} and V^{+5} ions diffused from the positive electrolyte of a VRB through an ion exchange membrane and were collected in sulfuric acid. Also plotted in Figure 2.6 (a) is the representation of the mixture spectrum using a combination of reference V^{+4} and V^{+5}spectra. Similarly, Figure 2.6 (b) and (c) show the spectra of mixtures of V^{+3}/ V^{+4}, and V^{+2}/V^{+3}, collected in a similar manner, along with the representations of the mixture spectra using reference spectra. In all cases the linear combinations of the reference spectra provide an accurate representation of the mixture spectra. Using the absorbance spectra of the 0.1 M samples shown in Figure 2.2 to calibrate the reference absorbance data, the composition of the mixtures whose spectra are shown in Figure 2.6 were calculated using Equation (2.9) and are tabulated in Table 2.2:

Table 2.2 Ionic concentrations determined from spectra from Figure 2.6 using reference spectra from Figure 2.2.

	V4-V5 Mix	V3-V4 Mix	V2-V3 Mix
V5	0.013		
V4	0.019	0.034	
V3		0.026	0.012
V2			0.025

The uncertainty in the absolute values of the concentrations shown in Table 2.2 is approximately 20%, mainly due to uncertainty in the concentration of the reference samples. However, as will be shown later, the determination of vanadium ion transport coefficients depends on the ratio of vanadium concentrations in the different chambers of the experimental cell, so the uncertainty in the calibration coefficients does not lead to significant error in the vanadium transport coefficients.

2.4 CALCULATION OF MEMBRANE TRANSPORT COEFFICIENTS

In the preceding section it was shown that the composition of dilute (<0.1 M) mixtures of vanadium ions can be determined by absorption spectroscopy of the solutions. Higher concentration vanadium ion solutions (~ 1 to 2 M) are easily analyzed by diluting the samples by a factor of 10 to 20 to reduce the sample concentration to 0.1 M or less. Using this method the composition any mixtures of V^{+2}/V^{+3}, V^{+3}/V^{+4}, or V^{+4}/V^{+5} encountered in VRB experiments can be analyzed. In this section the calculation of membrane transport coefficients from absorption data is discussed in detail for a typical experiment using the XO cell.

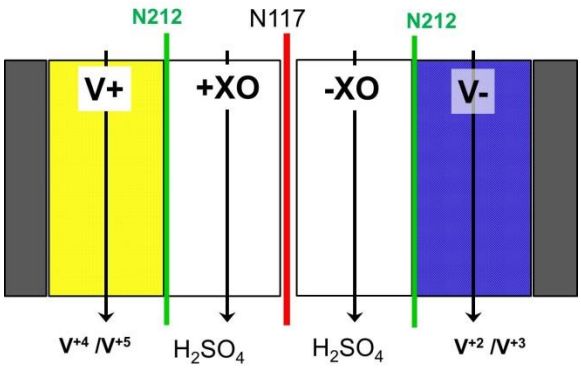

Figure 2.7 Experimental setup for a vanadium membrane transport experiment.

A schematic of the experimental arrangement is shown in Figure 2.7. In the chamber labeled V+, a mixture of V^{+4}/V^{+5} is circulated using an external pump and reservoir. An ion exchange membrane (Nafion N212) separates the V+ chamber from the neighboring chamber labeled +XO. A solution of sulfuric acid (with sulfate concentration matching the sulfate concentration of the V+ solution) is pumped through the +XO chamber. A second membrane (Nafion N117) separates +XO from the next chamber, labeled –XO. A solution of sulfuric acid identical to that pumped through +XO is

pumped through –XO. A third membrane (N212) separates –XO from the chamber labeled V-. A mixture of V^{+2}/V^{+3} circulates through the V- chamber. The total vanadium concentrations and sulfate concentrations of the V+ and V- solutions match. Graphite felt porous electrodes fill the flow regions of all four chambers.

In this experiment, no current is flowing through the cell. Transport of V^{+4} and V^{+5} will occur between the V+ and +XO chambers driven by the concentration gradient across the N212 membrane. Similarly transport of V^{+2} and V^{+3} will occur across the N212 membrane separating the V- and –XO chambers. The transport between the V+ or V- chambers and the adjacent +XO or –XO chamber will be much greater than any transport between the –XO and +XO chambers because the vanadium concentration difference across the outer N212 membranes (of order 1 M) is much greater than the concentration difference across the center N117 membrane (of order 0.01 M).

The experiment is initiated by pumping sulfuric acid solution through the +XO and –XO chambers while a mixture of V^{+4}/V^{+5} is pumped through V+ and V^{+2}/V^{+3} is pumped through V-. The transport of vanadium ions across the ion exchange membrane is modeled as a diffusion process, with the ion flux being described by Fick's law:

$$N_i = -D_i \nabla c_i \tag{2.10}$$

In the above expression N_i is the ion flux (in moles/cm^{2}sec) of species i through the membrane, D_i is the diffusion coefficient for species i, and ∇c_i is the concentration gradient across the membrane. The following analysis is made with regards to transport from the V+ chamber to the +XO chamber, the analysis for transport between V- and –XO is analogous. With the assumption that the concentration on the V+ side of the membrane is much greater than the concentration on the +XO side, the concentration gradient can be approximated as:

$$-\nabla c_i \approx \frac{c_i^{V+}}{l} \tag{2.11}$$

where c_i^{V+} is the concentration of species i in the V+ chamber and l is the membrane thickness. If the area of the membrane is A and the time of the experiment is T, then n_i, the number of moles of species i which accumulate in chamber +XO, is:

$$n_i = N_i AT \approx \frac{D_i ATc_i^{V+}}{l} \tag{2.12}$$

The number of moles n_i is also equal to the product of Q, the volume of the electrolyte solution circulating through +XO, and c_i^{+XO}, the concentration of species i in the +XO reservoir measured at the end of the experiment. By equating the two expressions for n_i, the diffusion coefficient D_i can be expressed in terms of the experiment parameters l, Q, A, T and the +XO and V+ concentrations as:

$$D_i \approx \frac{lQc_i^{+XO}}{ATc_i^{V+}} \tag{2.13}$$

Note that the result depends upon the ratio of the concentration of i in the +XO reservoir to the concentration in the V+ reservoir. Therefore, any uncertainty in the concentrations due to uncertainty in the absolute calibration of the reference sample spectra will cancel out as long as both measurements are made with respect to the same reference spectrum.

In many experiments the concentration of species i in the V+ chamber varies as the cell is charged or discharged. In that case $\left\langle c_i^{V+} \right\rangle$, the average value of the concentration of species i in V+, is used in the expression for the diffusion coefficient:

$$D_i \approx \frac{lQc_i^{+XO}}{AT\left\langle c_i^{V+} \right\rangle} \tag{2.14}$$

For constant current experiments, the average value can be calculated from the average of the initial and final value of c_i^{V+}.

A useful quantity for comparing ion cross-over rates for different membrane types and thickness is the mass transfer coefficient m, which is the proportionality constant relating the flux of species i to the difference in concentrations across the membrane. For of cross-over between V+ and +XO chambers, the flux is $N_i = m_i(c_i^{V+} - c_i^{+XO})$. With the assumption that $c_i^{V+} \gg c_i^{+XO}$, and using equations (2.10) and (2.11), the mass transfer coefficient m_i can be expressed in terms of terms of the experimentally measured concentrations in the V+ and +XO reservoirs as:

$$m_i = \frac{D_i}{l} = \frac{Qc_i^{+XO}}{AT\left\langle c_i^{V+}\right\rangle} \tag{2.15}$$

Given m_i, the cross-over flux from V+ to +XO is easily calculated as $N_i = m_i c_i^{V+}$.

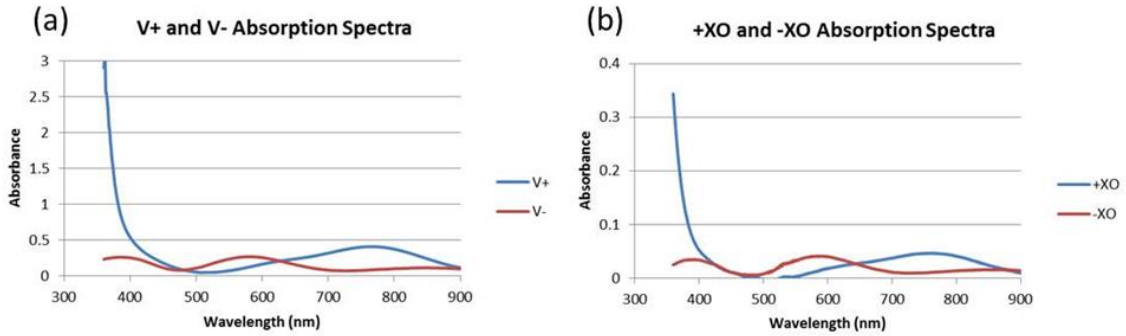

Figure 2.8 (a) V+ and V- Absorption Spectra (b) +XO and -XO Absorption Spectra, XO cell with no current flow.

One mL samples of V+ and V- were collected before the experiment was run and diluted by a factor of 10 to determine the initial vanadium concentrations. The vanadium and sulfuric acid solution were then pumped through the cell for 3600 seconds, after which samples of +XO and –XO solutions collected. Figure 2.8 shows the absorption spectra of the V+, V-, +XO, and –XO samples. It is clear from Figure 2.8 that the spectra

of the +XO and –XO electrolytes closely resemble the spectra of V+ and V- samples respectively.

Table 2.3 Experimental parameters, measured vanadium concentrations, and calculated diffusion and mass transfer coefficients for zero current experiment.

Experimental Parameters			
Membrane Area	A	2	cm^2
XO Vol	Q	33	cm^3
Time	T	3600	sec
Thickness	l	0.005	cm
V+/V- Dilution		10	

	Concentrations		m	D
Species	V+	+XO	(cm/sec)	(cm^2/sec)
V+5	0.353	0.00418	5.44E-05	2.72E-07
V+4	0.204	0.00283	6.38E-05	3.19E-07
	V-	-XO		
V+3	0.131	0.00170	5.92E-05	2.96E-07
V+2	0.345	0.00629	8.35E-05	4.18E-07

Table 2.3 lists the experimental parameters, the measured vanadium concentrations (M), and the calculated diffusion and mass transfer coefficients for the four vanadium ion species for this experiment. The calculation procedure discussed above for determining the transport coefficients from absorption data for this simple experiment is utilized for all of the experiments reported in this thesis. In most of the experiments to be discussed later, current is flowing through the cell, and the compositions of the V+ and V- electrolytes change during the experiment. In this case the diffusion coefficient is calculated using (2.14) instead of (2.13). Also, as will be discussed later in greater detail, the mechanism for transport is no longer purely diffusive; electric field effects play an important role in determining transport rates when current is present.

2.5 SUMMARY OF OPTICAL MEASUREMENT OF VANADIUM ION CONCENTRATIONS AND TRANSPORT COEFFICIENTS

In this chapter, it was shown that absorption spectroscopy could be used to determine the composition and concentration of vanadium ion mixtures encountered when analyzing vanadium flow battery electrolytes. Problems in analyzing V^{+4}/V^{+5}

mixtures which had been identified by other researchers were shown to be alleviated by diluting the mixtures sufficiently. It was shown that, with the use of reference spectra of known concentration samples of vanadium ions, measurements at three different wavelengths provided sufficient information to decompose the spectrum of any vanadium ion mixture and to determine the concentration of the different components. A formalism was developed to calculate the diffusion and mass transfer coefficients of vanadium ions across an ion exchange membrane using the concentrations determined from the absorption spectra.

Chapter 3: Cross-over Measurements using the Triple Membrane VRB Cell

3.1 Vanadium Redox Flow Battery Operation

Initial experiments were performed with the VRB cell shown in Figure 3.1. This cell had a Nafion N117 membrane with 5 mm carbon felt porous electrodes. The cross sectional area of the cell was 22.3 cm^2. Flat Viton gaskets 1.5 mm thick sandwiched the Nafion membrane and provided the sealing surfaces for the PVC frames. The entire assembly was bolted together with machine screws and an external clamping assembly provided pressure on the graphite current collectors which compressed the porous electrodes to approximately 4 mm thickness when assembled. Brass plated external electrodes placed between the back of the graphite current collectors and the clamping plates provided an attachment for the external power supplies. In later experiments, the brass-plated electrodes were replaced with electrodes cut from 3 mm graphite stock to avoid corrosion problems due to leaking electrolytes. This cell was used to prepare the V^{+5} and V^{+2} electrolytes from V^{+4} electrolyte using the process described in Chapter 2.

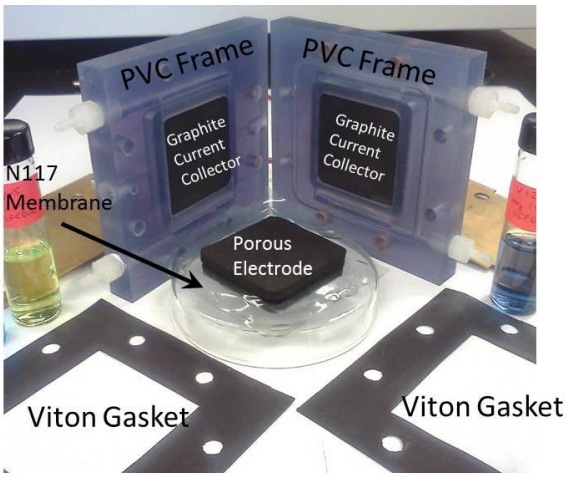

Figure 3.1 VRB Cell for initial experiments. N117 Membrane, no current defining aperture.

Figure 3.2 shows current-voltage and power density data for the cell with the original N117 membrane and a subsequent experiment in which a N212 ion exchange membrane was used. A potentiostat (Princeton Applied Research PAR 2273 with current booster) was used to apply a slow current ramp from zero to 8 amps over 400 seconds. Electrolyte solutions with 1 M total vanadium concentration and 4 M total sulfate concentration were used in these experiments. The data in Figure 3.2 (a) shows that the output voltage at the highest currents was slightly higher with the N212 membrane compared to the N117 data, which was due to the lower series resistance of the thinner N212 material (50 microns) compared to N117 (180 microns). Figure 3.2 (b) shows the power density versus current density curves derived from the data in Figure 3.2 (a). The peak power achieved by the cell with the N212 membrane was 261 mW/cm^2 at a current density of 342 mA/cm^2.

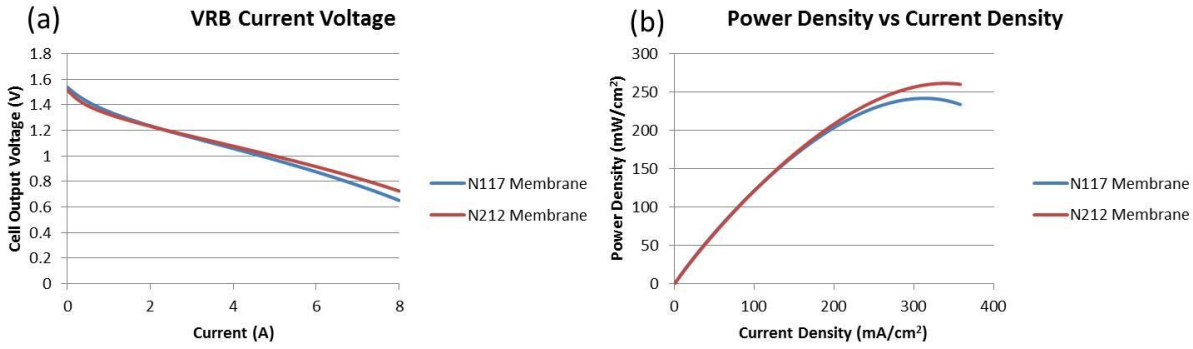

Figure 3.2 (a) Current vs Voltage (b) Power Density vs Current Density for VRB with N117 and N212 membranes

3.2 TRIPLE MEMBRANE (XO) CELL

The motivation for the development of the triple membrane, or XO cell, was discussed in Chapter 1. The XO cell is a modified VRB cell identical to the one used in the initial experiments described in the previous section, with two additional flow

chambers added. The original 1.5 mm Viton gaskets were replaced with 3 mm thick gaskets, sandwiching the center N117 membrane. The cut-outs in the 3 mm gaskets were filled with 3 mm graphite felt, and an additional ion exchange membrane was placed over each felt spacer. Teflon current defining gaskets with 2 cm^2 apertures were placed over the ion exchange membranes. The current defining apertures allowed operation of the cell at much higher current densities than could be achieved otherwise. The 3 mm thick gaskets were thick enough to provide passages to allow connections to external sulfuric acid flow circuits. Figure 3.3 shows an exploded schematic diagram of the XO cell showing the arrangement of the ion exchange membranes, current defining apertures, and the carbon felt spacers. Figure 3.4 (a) shows a photograph of the assembled XO cell with the input and output connections for the electrolytes highlighted and (b) shows a photo of a charge exchange membrane covered with a Teflon 2 cm^2 current defining aperture.

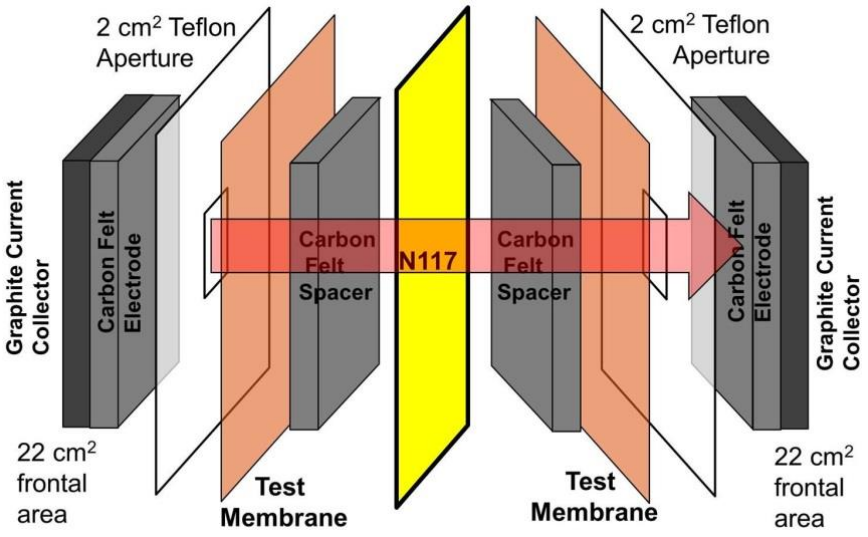

Figure 3.3 Exploded view of Triple membrane (XO) Cell

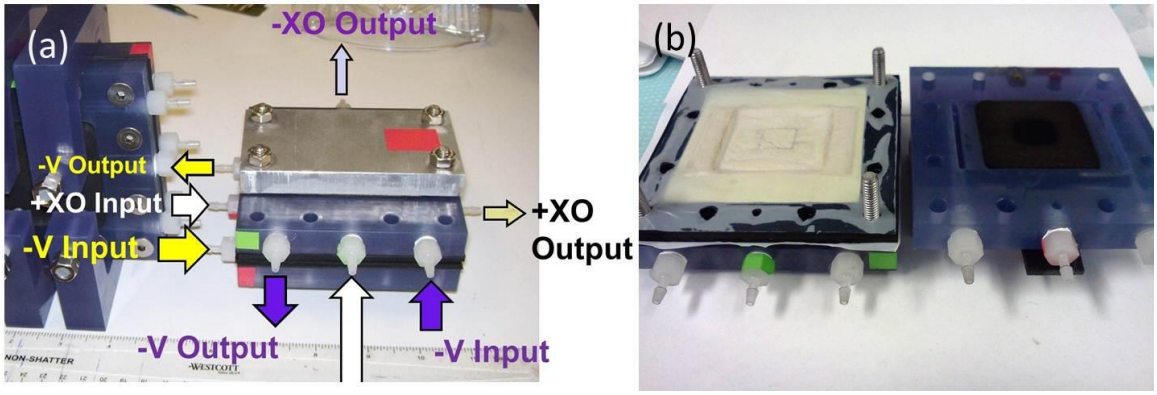

Figure 3.4 (a) XO Cell showing electrolyte inputs and outputs (b) internal view showing a white ion exchange membrane separating the V- chamber from the –XO chamber and the 2 cm^2 Teflon current defining aperture.

The assumption made when the XO cell was designed was that no electrochemical reactions would occur within either the +XO or –XO chambers of the cell. In principle, the graphite felt spacers in the XO chambers were meant to be electrically isolated, with no path for electrons to be sourced or sinked from the spacers. In practice, the spacers do contact the ion exchange membranes, which provide an electrical connection to the porous electrodes in the V+ and V- regions of the cell. Although the connection between through the ion exchange membrane is highly resistive, electrochemical side reactions are possible within either of the XO chambers. The occurance of un-intended oxidation reactions of vanadium ions collected in the XO chambers will be discussed in a later section of this thesis.

3.4 FULL CELL MODE XO EXPERIMENTS

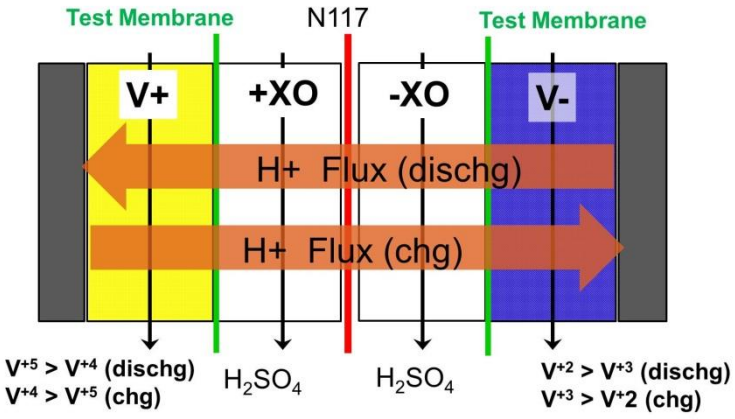

Figure 3.5 XO running as a VRB showing current flow during charge and discharge.

The XO cell is capable of running as a VRB with V+ electrolyte consisting of V^{+4}/V^{+5} and V- electrolyte consisting of V^{+2}/V^{+3}. The direction of the flow of current through the +XO and –XO chambers depends upon the mode of operation of the cell, with the flux of H^{+} ions from V+ to V- during charging and from V- to V+ during discharge, as shown in Figure 3.5. During full cell mode operation the transport properties of all four vanadium ion species can be determined with the XO cell.

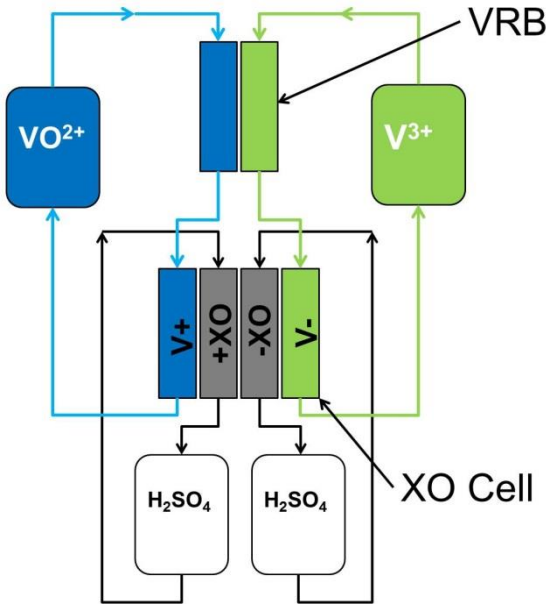

Figure 3.6 Experimental Arrangement for XO Cell Measurements.

Figure 3.6 shows the experimental layout for full cell mode cross-over experiments with the XO cell. A Gilson Minipuls 3 peristaltic pump with four separate flow channels provided circulation for the V+, V-, +XO, and –XO flow circuits. All the reservoirs were purged with an inert Argon atmosphere to prevent unintended oxidation of the vanadium ions. A conventional VRB shared the V+ and V– flow circuits. If the XO cell was run as a conventional VRB, the second VRB cell was used to measure the open circuit voltage (OCV) which gave an indication of the SOC of the vanadium electrolyte solutions. Alternatively, the second VRB could be used to run a charge or discharge cycle while the XO cell was run with zero current. In this manner the effect of current flow on vanadium transport could easily be isolated from that of V+/V– electrolyte composition changes due to SOC changes.

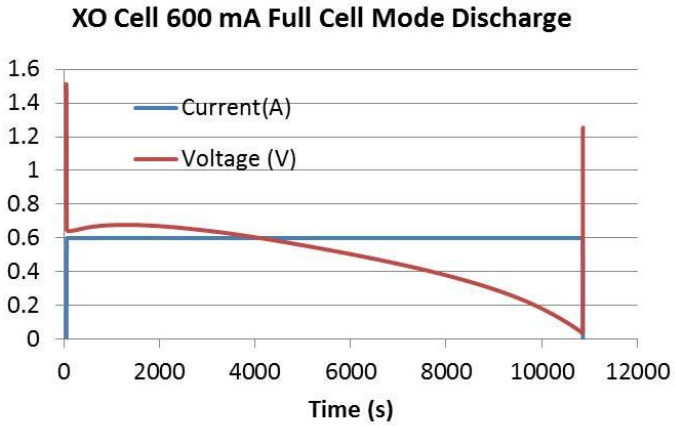

Figure 3.7 Full Cell Mode I-V curve for XO cell operating as a VRB.

Figure 3.7 shows the current-voltage curve for a full cell mode experiment in which the XO cell was running a 600 mA discharge for 10800 seconds. An Arbin BT-2000 battery tester was used to control the current and log the data. The voltage dropped from 1.5 V to 0.65 V when the current flow was initiated. At the end of the experiment the output voltage had dropped to below 0.1 V. When the current flow was interrupted an open circuit voltage of 1.25 V was measured. The total vanadium concentration of the anolyte and catholyte was 0.7 M and the total sulfate concentration was 3.7 M. The +XO and –XO reservoirs were filled with 30 mL each of fresh 4 M sulfuric acid before the start of the experiment. A trapped volume of 3 mL was assumed for each XO chamber and was added to the total volume of liquid contained in the +XO and –XO reservoirs when mass transfer coefficients were calculated from the raw data.

The initial and final SOC of the electrolytes in the V+ and V- chambers was determined by taking 1 mL samples of the anolyte and catholyte at the beginning and end of the experiment. The samples were diluted 10:1 and then analyzed using the UV/VIS absorption spectroscopy method discussed earlier. Samples of the +XO and –XO

reservoirs were collected at the end of the discharge. The vanadium concentration of the +XO and –XO electrolytes was well below 0.05 M so these samples were analyzed at full strength.

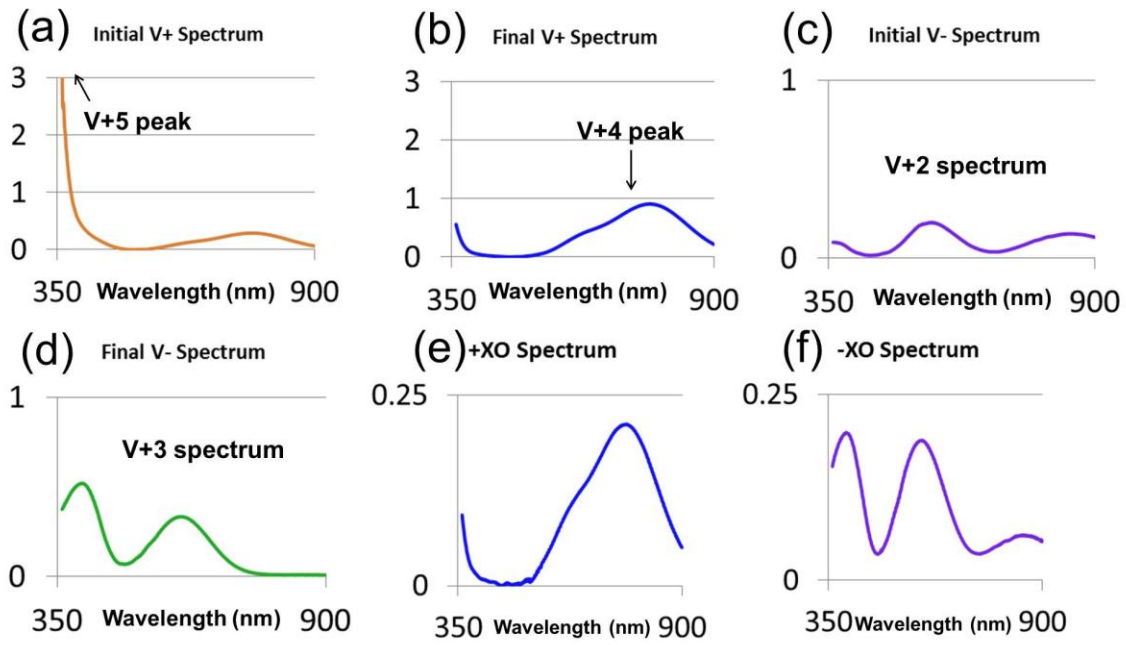

Figure 3.8 Absorption spectrographs for XO cell electrolytes collected during a full cell mode 600 mA experiment. (a) Initial V+ (b) Final V+ (c) Initial V- (d) Final V- (e) +XO (f) -XO.

Figure 3.8 shows the absorption spectra data of the initial and final samples of the catholyte and anolyte and the +XO and –XO electrolyte. The V+ reservoir initially contained 180 mL of a mixture of V^{+4}/V^{+5} at 75% SOC. The V– reservoir contained 125 mL of nearly 100% V^{+2}. After a 10800 second 600 mA discharge the SOC of the V+ electrolyte was 15% SOC and the SOC of the V– electrolyte was close to 0%. The initial spectrum of the V+ electrolyte shown in Figure 3.8 (a) had very strong absorption at the blue end of the spectrum, characteristic V^{+5}, while the spectrum in Figure 3.8 (b) showed a strong peak at 760 nm, characteristic of V^{+4}.

The initial V– spectrum shown in Figure 3.8 (c) is characteristic of pure V^{+2} and the spectrum at the end of the discharge shown in Figure 3.8 (d) is that of pure V^{+3}. The XO reservoirs of the cell were initially filled with 30 mL of 4 M H_2SO_4 solution. During the discharge the +XO and –XO chambers accumulated vanadium which crossed over from the V+ and V– chambers. At the end of the experiment the XO samples were analyzed in the spectrometer. Figure 3.8 (e) shows the spectrum of the +XO solution and Figure 3.8 (f) shows the spectrum of the –XO solution. It can be seem from the figures that the spectrum of the +XO sample is a linear combination of the V^{+4} and V^{+5} spectra while the –XO sample spectra is a combination of V^{+2} and V^{+3} spectra.

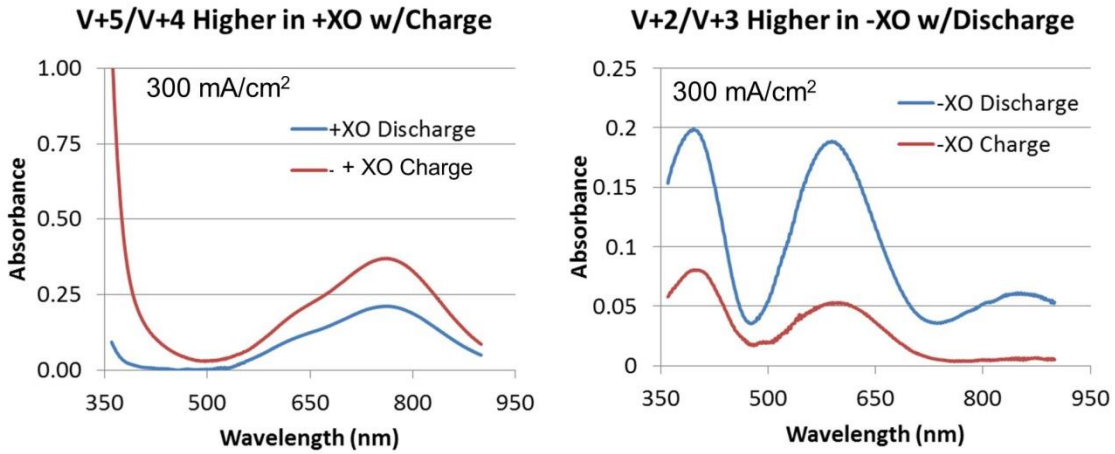

Figure 3.9 Effect of current flow direction on +XO and -XO spectra.

At the end of the experiment the XO chambers of the cell were flushed with deionized water to remove any trances of vanadium and the XO reservoirs were refilled with 30 mL of fresh H_2SO_4 solution. The cell was then run in the charge mode with the same magnitude of current and time duration. At the end of the experiment the V+ and V– electrolytes were restored to nearly their original state and the samples from the +XO

and –XO reservoirs were collected for analysis. Figure 3.9 compares the spectra for the +XO and –XO solutions for the charge and discharge experiments.

It can be seen from Figure 3.9 that the absorption, and hence vanadium concentration, in the +XO electrolyte was higher during charge than discharge, while the reverse was true in the –XO electrolyte. During charge mode, the H^+ flux was in the V+ to V– direction, so the H^+ flux and the electric field were parallel with the direction of concentration gradient driven flux of V^{+4}/V^{+5} into the +XO chamber and opposite to the direction of the concentration gradient driven flux of V^{+2}/V^{+3} from the V– chamber into the –XO chamber. Transport was enhanced when the electric field and the concentration gradient were in the same direction and suppressed when the electric field was in the opposite direction. The changes in vanadium transport with current direction observed in this experiment are in agreement the results reported in [9] from the mixed V/Fe flow battery experiments.

3.5 ELECTRIC FIELD EFFECT ON TRANSPORT COEFFICIENTS

At the end of Chapter 2, the calculation of membrane transport coefficients was described for an experiment in which the XO cell was run without current. For the zero current case the flux of ions of species *i* was assumed to be due to diffusion alone:

$$N_i = -D_i \nabla c_i \tag{3.1}$$

The general expression for the flux of ions of species *i* due to diffusion and electro-migration is given by the Nernst-Planck equation [15]:

$$N_i = -D_i \nabla c_i - z_i \mu_i c_i \nabla \phi \tag{3.2}$$

where z_i is the charge number, μ_i is the mobility, and $\nabla\phi$ is the gradient of the electrostatic potential. At the end of Chapter 2, it was shown that a suitable

approximation to the diffusive component of Equation (3.2) when considering transport of species *i* from V+ to +XO across a membrane is:

$$-D_i \nabla c_i \approx D_i \frac{c_i^{V+}}{l} \tag{3.3}$$

If the assumption is made that the gradient of the potential across the membrane can be approximated by the Ohmic voltage drop divided by the membrane thickness, then the electro-migration term can be written as:

$$\begin{aligned} -z_i \mu_i c_i \nabla \phi &\approx z_i \mu_i c_i \frac{IR_{mem}}{l} \\ &\approx z_i \mu_i c_i \frac{I(\rho_m l / A)}{l} \\ &\approx z_i \mu_i c_i \frac{I \rho_m}{A} = z_i \mu_i k c_i^{V+} J_e \rho_m \end{aligned} \tag{3.4}$$

In Equation (3.4) ρ_m is the membrane resistivity, J_e is the current density, and the partition coefficient *k* has been introduced which relates c_i , the concentration of species *i* inside the membrane, to c_i^{V+}, the concentration in the V+ chamber of the cell. An effective diffusion coefficient D^* can be defined which combines the effects of diffusion and electro-migration:

$$D_i^* = (D_i + z_i \mu_i k l \rho_m J_e) \tag{3.5}$$

Equation (3.5) implies that the transport due to diffusion will either be suppressed or enhanced, depending upon the direction of the current relative to the concentration gradient. Similarly, an effective mass transport coefficient m_i^* can be defined as:

$$m_i^* = \frac{D_i^*}{l} = (m_i + z_i \mu_i k \rho_m J_e) \tag{3.6}$$

Comparing Equation (3.6) against Equation (1.8), it is apparent the electro-migration coefficient k_i defined earlier is equal to $z_i \mu_i k \rho_m$.

The absorption spectrographs from the full cell 600 mA/cm^2 discharge and charge experiments with the XO cell can be analyzed using the same method as described at the end of Chapter 2, but the transport coefficients D_i and m_i which are calculated using Equations (2.14) and (2.15) should be interpreted as an effective diffusion coefficient D_i^* and m_i^* with the effects of electro-migration combined with concentration gradient driven transport. The absorption spectrographs shown in Figure 3.8 were analyzed by fitting the spectra to reference sample spectra to determine the composition of the samples in terms of V^{+2}, V^{+3}, V^{+4} and V^{+5} concentrations. The effective transport coefficients for the 600 mA discharge experiment are listed in Table 3.1.

Table 3.1 Effective diffusion and mass transfer coefficients (600 mA Discharge)

Experimental Parameters			
Membrane Area	A	2	cm^2
XO Vol	Q	33	cm^3
Time	T	10800	sec
Thickness	l	0.005	cm
V+/V- Dilution		10	
Current (Discharge)	I	600	mA

	Concentrations				m	D
Species	V+ Init	V+ Fin	Avg V+	+XO	(cm/sec)	(cm^2/sec)
V+5	0.339	0.045	0.192	0.00078	6.20E-06	3.10E-08
V+4	0.167	0.481	0.324	0.01114	5.25E-05	2.63E-07
	V- Init	V- Fin	Avg V-	-XO		
V+3	0.000	0.429	0.215	0.01219	8.68E-05	4.34E-07
V+2	0.469	0.064	0.267	0.02247	1.29E-04	6.44E-07

Figure 3.9 shows that the amount of V^{+4} and V^{+5} transport into the +XO chamber increased when the cell was run in charge mode, while V^{+2} and V^{+3} transport into the –XO chamber decreased. The effective transport coefficients for the 600 mA charge experiment listed in Table 3.2 and show that transport is greater for V^{+4} and V^{+5} and smaller for V^{+2} and V^{+3} when the cell is run in charge mode compared to discharge mode.

Table 3.2 Effective diffusion and mass transfer coefficients (600 mA Charge)

Experimental Parameters			
Membrane Area	A	2	cm^2
XO Vol	Q	33	cm^3
Time	T	10800	sec
Thickness	l	0.005	cm
V+/V- Dilution		10	
Current (Charge)	I	600	mA

	Concentrations				m	D
Species	V+ Init	V+ Fin	Avg V+	+XO	(cm/sec)	(cm^2/sec)
V+5	0.045	0.332	0.188	0.01242	1.01E-04	5.04E-07
V+4	0.481	0.157	0.319	0.01889	9.05E-05	4.53E-07
	V- Init	V- Fin	Avg V-	-XO		
V+3	0.429	0.000	0.215	0.00639	4.55E-05	2.28E-07
V+2	0.064	0.450	0.257	0.00254	1.51E-05	7.53E-08

In Figure 3.10 the effective mass transfer coefficients for V^{+5}, V^{+4}, V^{+3}, and V^{+2} are plotted as a function of mode of operation (charge, zero current, or discharge). It is clear from Figure 3.10 that the simple linear variation in m^* with current density implied by Equation (3.6) is an oversimplification, since nonlinearities are apparent in the changes in transport of V^{+4}, V^{+3}, and V^{+2} with current, and that extrapolating the linear variation observed in the V^{+5} transport would rapidly lead to a negative transport coefficient. The measurement in the variation in m^* over a wider range of current densities is the topic of Chapter 4, but it is clear that complicated behaviors are seen, which lead to a more complicated picture of the interplay of diffusion and electro-migration effects.

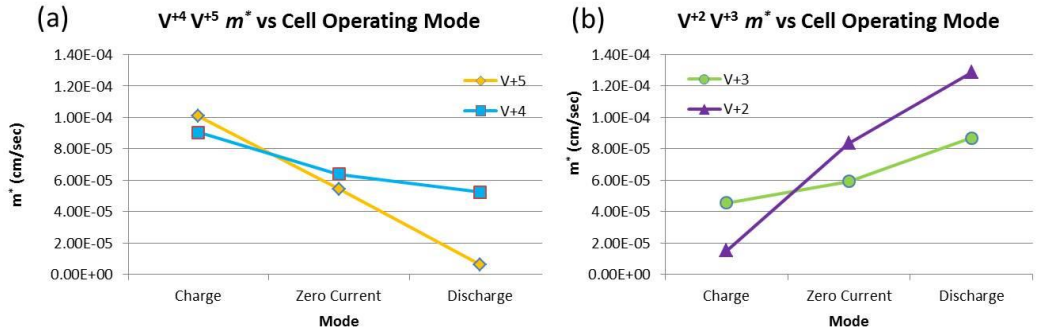

Figure 3.10 Effective mass transfer coefficients for (a) V^{+4} and V^{+5} and (b) V^{+2} and V^{+3} versus cell operation mode.

3.6 HALF CELL MODE XO EXPERIMENTS

Although the XO cell can be run as a VRB with V^{+4}/V^{+5} and V^{+2}/V^{+3} electrolyte mixtures in the V+ and V- flow circuits, for many of the experiments reported in this thesis, the XO cell was run half cell mode, in which both the V+ and V- sides of the cell run the same redox reaction, with one side running the reaction in the oxidation direction and the other in the reduction direction. Operation with just the V^{+4}/V^{+5} mixture

simplifies operation of the cell, removing the requirement to provide an inert atmosphere purge in the V- reservoir to avoid oxidation of V^{+2} by atmospheric oxygen. Another advantage of operation in half cell mode is that simultaneous measurement of the effect of current flow in both the co- and counter directions to the gradient driven ion flux can be performed in a single run.

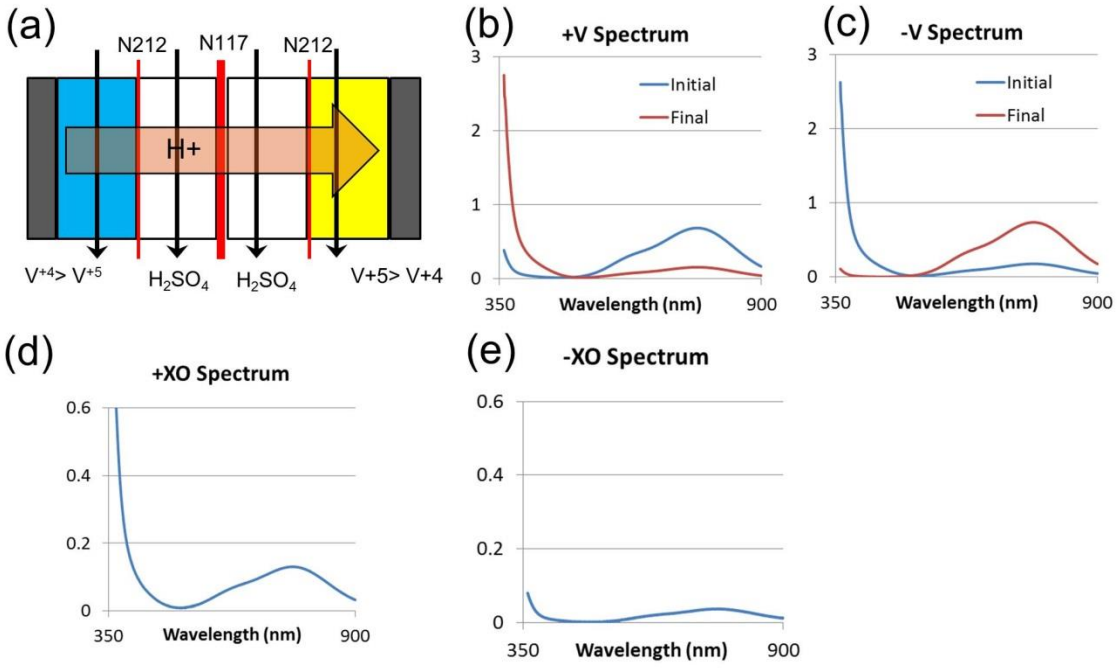

Figure 3.11 (a) Experimental arrangement for V^{+4}/V^{+5} half cell mode experiments (b) V+ absorption spectra (c) V– spectra (d) +XO spectrum (e) –XO spectrum.

Figure 3.11 shows the experimental arrangement and the absorption data spectra for the XO cell running a 1200 mA charge cycle with the V+ electrolyte initially consisting of nearly 100% V^{+4} and the V– electrolyte with nearly 100% V^{+5}. Figure 3.11 (a) shows the cell reactions and the direction of current flow through the cell. An Arbin BT-2000 battery tester was used to drive the oxidation reaction $V^{+4} \rightarrow V^{+5}$ on the V+ side and the reduction reaction $V^{+5} \rightarrow V^{+4}$ on the V– side. The H^{+} flux was from V+ chamber to the V– chamber. After one hour of operation samples of electrolytes were

collected and the spectra measured. The spectra in Figures 3.11 (b) and (c) show that V+ electrolyte was nearly 100% converted to V^{+5} and the reverse was true of the V– electrolyte. The XO samples both show absorption spectra which are linear combinations of V^{+4} and V^{+5} spectra but the +XO absorption was significantly larger than the –XO absorption. This result is consistent with the result seen with the full cell experiment, in which the vanadium transport was enhanced when the H^+ flux is in the direction of the concentration gradient flux and suppressed with the H^+ flux opposed the concentration gradient flux.

Table 3.3 Effective diffusion and mass transfer coefficients (1200 mA V^{+4}/V^{+5} Half Cell Mode)

Experimental Parameters			
Membrane Area	A	2	cm^2
XO Vol	Q	33	cm^3
Time	T	3600	sec
Thickness	l	0.005	cm
V+/V- Dilution		10	
Current (Charge)	I	1200	mA

	Concentrations				*m*	*D*
Species	V+ Init	V+ Fin	Avg V+	+XO	(cm/sec)	(cm^2/sec)
V+5	0.031	0.301	0.166	0.01045	2.88E-04	1.44E-06
V+4	0.356	0.083	0.220	0.00702	1.46E-04	7.32E-07
	V- Init	V- Fin	Avg V-	-XO		
V+5	0.281	0.001	0.141	0.00083	2.70E-05	1.35E-07
V+4	0.095	0.386	0.240	0.00194	3.70E-05	1.85E-07

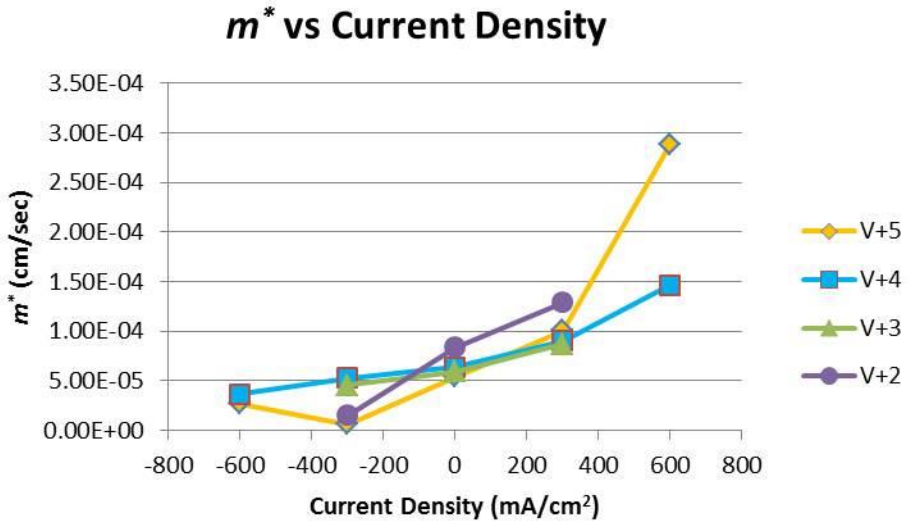

Figure 3.12 Effective mass transfer coefficient vs. current density, XO cell experiments.

Figure 3.12 shows the effective mass transfer coefficient as a function of current density for all of the experiments discussed so far (full cell mode 600 mA charge and discharge, full cell mode zero current, half cell mode V^{+4}/V^{+5} 1200 mA charge). Positive current density corresponds to the direction of current flow in the same direction of the concentration gradient driven flux (from V+ to +XO or V- to –XO), and negative current density corresponds to current flow in the direction opposite to the concentration driven flux. This convention is used for all of the data presented in the remainder of this thesis. In all cases the transport parameters increase when the current is in the same direction as the concentration driven flux and decrease when the current is in the opposite direction. In the next chapter, results for experiments with a greater range of currents and for different types of ion exchange membranes will be presented.

Chapter 4: The Effects of Current Density on Vanadium Cross-over

The use of the XO cell to measure the effective transport coefficients for vanadium ion cross-over through Nafion N212 charge exchange membranes was discussed in the previous chapter. The XO cell can be used in full cell mode in which both the V^{+4}/V^{+5} and V^{+2}/V^{+3} redox couples are used, or in the half cell mode in which a single redox couple is used. The half cell mode was shown to be useful for facilitating the measurement of the effective diffusion coefficients for the ions of the redox couple with the current in both co- and counter directions in a single charge or discharge run. Also, purging of the electrolyte reservoirs with inert gas is not required if the V^{+2} species is not part of the redox couple being used. Hence, much of the data reported in this chapter was collected using the XO cell in the half cell mode.

4.1 Cross-Over experiments with N212 Membranes 0.7 M Solutions

The initial set of experiments using the XO cell to study cross-over as a function of current density were made with N212 membranes separating the XO chambers of the cell from the V+ and V- chambers of the cell. A N117 membrane separated the +XO from the –XO chamber.

As mentioned in Chapter 1, Vanadyl sulfate, formula $VOSO_4 \cdot xH_2O$, has a variable number of water atoms which form a complex with each $VOSO_4$ molecule. During preparation of what was meant to be 1 M V^{+4} /3 M H_2SO_4 solution, the molar weight of the Vanadyl sulfate was assumed to be 163 gm/mole, which neglected the contribution of the water molecules. Subsequent coulometric analysis of the current-time data taken during the electrolysis process of preparing V^{+5} and V^{+2} from the V^{+4} solution revealed that the actual vanadium concentration of the solutions prepared was 0.7 M. The

value of x, the number of water molecules associated with each $VOSO_4$ molecule, was deduced to be 3.75. This value was used in subsequent preparations of V^{+4} solutions.

Half cell mode experiments using V^{+4}/V^{+5} or V^{+2}/V^{+3} redox couples and full cell mode experiments using V^{+2}/V^{+3} and V^{+4}/V^{+5} were performed using the 0.7 M strength anolyte and catholyte solutions.

Half Cell Mode Experiments with V^{+4}/V^{+5}

A large range of current densities were explored with half cell mode experiments with the V^{+4}/V^{+5} redox couple. For each experiment 1 mL samples of the V+ and V- electrolyte were taken before and after each charge or discharge run. The samples were diluted 10:1 before measurement of the absorption spectrum. At the end of the run 10 mL samples of the +XO and –XO electrolyte were collected for absorption measurements at full strength. The XO cell was run at currents up to 1800 mA for experiments with the V^{+4}/V^{+5} redox couple, for an effective current density of 900 mA/cm^2, which is comparable to the highest current densities that have been achieved in experimental VRB cells [10,19]. The absorption spectra were analyzed using the method illustrated in the examples discussed in Chapter 3. Figure 4.1 shows the variation in m^* as a function of current density for these experiments.

The effective mass transfer coefficients for V^{+4} and V^{+5} both decrease as current density becomes more negative, dropping to about a third of the zero-current value at -900 mA/cm^2. They both increase as the current density is increased from zero to 300 mA/cm^2, but surprisingly m^* for V^{+4} saturates while m^* for V^{+5} increases dramatically at current densities higher than 300 mA/ cm^2. The apparent divergence in V^{+4}/V^{+5} values of m^* at high current densities was reproduced during subsequent experiments with other types of ion exchange membranes and higher vanadium electrolyte concentrations.

Reasons for this behavior and the results of additional experiments to determine if the transport difference was real or an artifact of the measurement technique will be discussed in later sections.

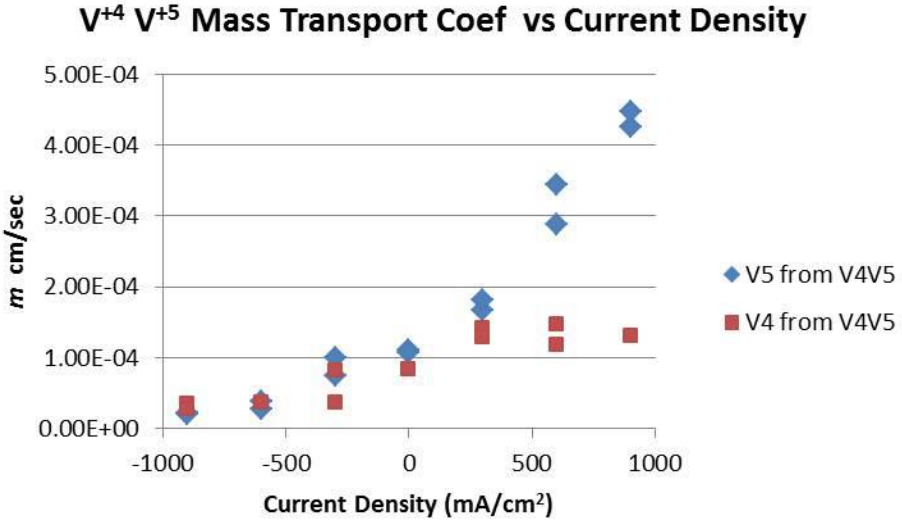

Figure 4.1 V^{+4} and V^{+5} m^* vs current density, N212 Membrane 0.7 M V concentration, Half cell mode.

Half Cell and Full Cell Experiments with V^{+2}/V^{+3}

A limited number of experiments with the V^{+2}/V^{+3} redox couple were performed with the N212 membrane and the 0.7 M V electrolytes. Complications due to the sensitivity of V^{+2} to oxidation from atmospheric oxygen limited the amount of data collected using the V^{+2}/V^{+3} couple; as such, half cell and full cell experiments were conducted at current densities up to 600 mA/cm^2. In addition to purging of the V^{+2}/V^{+3} reservoirs with inert gas, the sulfuric acid used in the XO reservoirs needed to be de-oxygenated in order to preserve any V^{+2} collected during experiments. Oxidation of V^{+2} by dissolved oxygen leads to an underestimation of m^* for V^{+2} and overestimation of m^* for V^{+3} in a given experiment. Figure 4.2 shows m^* as a function of current density for

V^{+2} and V^{+3} for both half cell and full cell mode experiments. The large amount of scatter in the data is partly due to oxidation of V^{+2} to V^{+3} after collection.

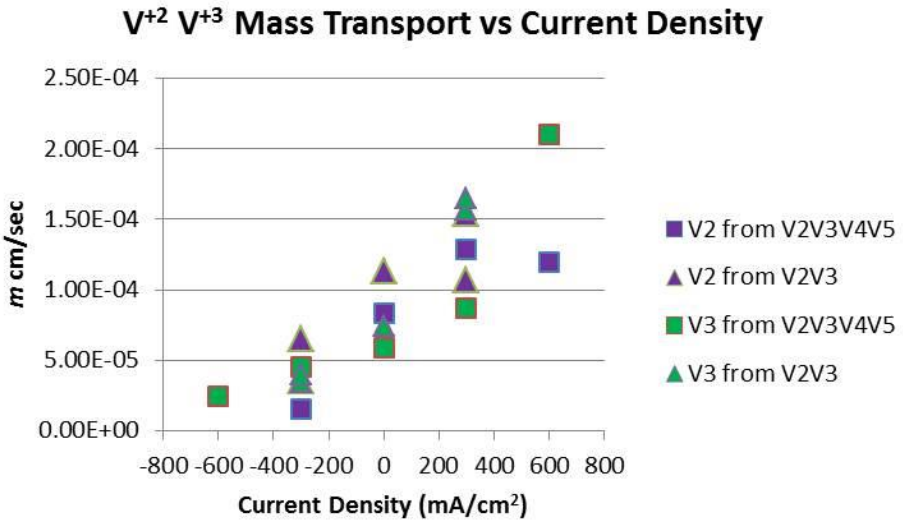

Figure 4.2 V^{+2} and V^{+3} m^* vs current density, N212 Membrane 0.7 M V concentration. Half cell ('V2V3') and full cell ('V2V3V4V5') mode experiments.

Combined V^{+2}/V^{+3} and V^{+4}/V^{+5} Mass Transfer Coefficients

Since un-intended oxidation of V^{+2} artificially suppressed m^* for V^{+2} and enhanced m^* for V^{+3}, the calculation of a combined V^{+2}/V^{+3} m^* by combining the measured concentrations of V^{+2} and V^{+3} has the potential to reduced the scatter in the measurements. The formula used to calculate the combined mass transfer coefficient for V^{+2} and V^{+3} transport between V- and –XO is:

$$m^*_{V^{+2}/V^{+3}} = \frac{Q(c^{-XO}_{V^{+2}} + c^{-XO}_{V^{+3}})}{AT(\langle c^{V-}_{V^{+2}} \rangle + \langle c^{V-}_{V^{+3}} \rangle)} \tag{4.1}$$

Figure 4.3 shows that the combined V^{+2}/V^{+3} m^* varies linearly with current density, in agreement with the prediction of the simple model result given by Equation (3.6), and the amount of scatter in the data is less than that observed in Figure 4.2.

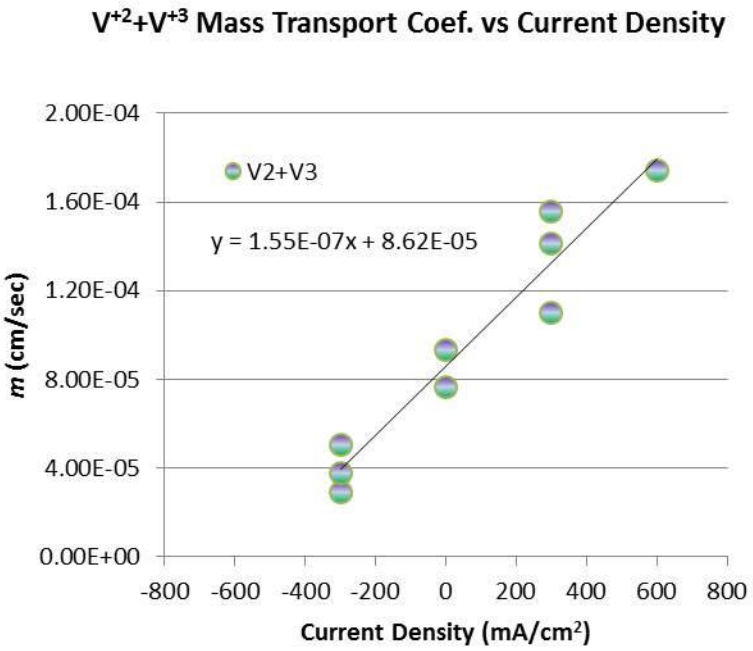

Figure 4.3 Combined V^{+2}/V^{+3} mass transport coefficient vs current density.

In the same way that un-intended oxidation of V^{+2} by dissolved oxygen affected V^{+2} and V^{+3} mass transport calculations, un-intended side reactions were thought to be present during higher current experiments with the V^{+4}/V^{+5} redox couple. The saturation of the mass transport coefficient for V^{+4} for current densities greater than 300 mA/cm^2, as seen in Figure 4.1, implies that oxidation of V^{+4} to V^{+5} occurred after it had been collected in the +XO reservoir. A combined V^{+4}/V^{+5} mass transport coefficient can be defined using a formula analogous to Equation (4.1), and the results of that calculation are shown in Figure 4.4. The combined mass transport coefficient for V^{+4}/V^{+5} increases linearly for current densities greater than zero, consistent with Equation (3.6). The combined V^{+4}/V^{+5} mass transport coefficient approaches a limiting value as current densities become more negative.

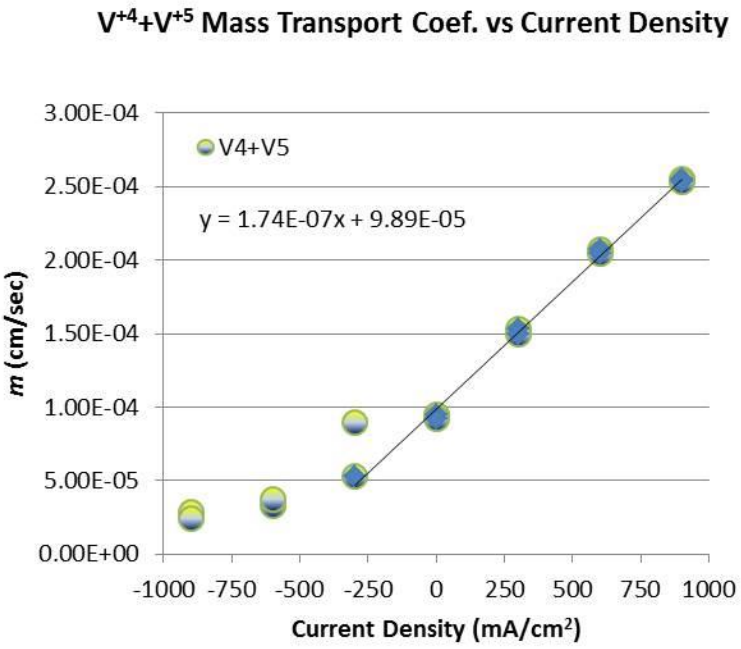

Figure 4.4. Combined V^{+4}/V^{+5} mass transport coefficient vs current density.

4.2 PREDICTING CELL IMBALANCE FROM MASS TRANSFER COEFFICIENTS

One of the deleterious consequences of electrolyte cross-over in a VRB is cell imbalance, which will cause loss of capacity. Cell imbalance results when there is a net transfer of vanadium from one side of the cell to the other over a number of charge and discharge cycles. In this section a simple model is presented which quantifies how an imbalance in the cross-over results in an imbalance in the electrolyte concentration between the V+ and V- sides of the cell. Next, the results of an experiment are presented in which the XO cell was run through several discharge/charge cycles and the net cross-over was determined by measuring the amount of vanadium accumulated in the +XO and –XO reservoirs.

Prediction of Cell Imbalance from V^{+2}/V^{+3} and V^{+4}/V^{+5} mass transfer coefficients

A simple model was built to demonstrate the imbalance in V+ and V- concentrations which results from differences between V^{+2}/V^{+3} and V^{+4}/V^{+5} transport rates. The model calculates the change in vanadium concentration over a series of discharge and charge steps of time duration T with constant current I. The total vanadium concentration of the V+ electrolyte at step i is denoted as c_i^+, similarly the total vanadium concentration of the V- electrolyte at step i is c_i^-. At step i+1, the vanadium concentrations are given by:

$$\begin{aligned} c_{i+1}^+ &= c_i^+ - (m^+ c_i^+ - m^- c_i^-)AT/Q \\ c_{i+1}^- &= c_i^- - (m^- c_i^- - m^+ c_i^+)AT/Q \end{aligned} \tag{4.2}$$

where A is the membrane cross sectional area and Q is the volume of the electrolyte. The mass transfer coefficients m^+ and m^- vary depending if i is a charge or discharge step. Values for m^+ and m^- can be estimated using the combined V^{+4}/V^{+5} and V^{+2}/V^{+3} mass transfer coefficients shown in Figures 4.4 (for m^+) and 4.3 (for m^-). During a charging step, m^+ is calculated assuming a positive current density $J = I/A$, and m^- is calculated for negative current density $J = -I/A$. During a discharge step the current direction reverses and m^+ is calculated for $J = -I/A$ and m^- for $J = I/A$.

Table 4.1 lists the parameters for a sample calculation. Initially both sides of the cell have 1 M vanadium concentration and are at 10% SOC. The cell is cycled between 10% SOC and 90% SOC at a constant charge/discharge current density of 300 mA/cm^2. After one charge/discharge cycle the V+ electrolyte has lost 0.62% of its vanadium concentration. The iteration formula given by Equation (4.2) is repeated for 50 charge/discharge cycles to generate the results shown in Figure 4.5. A steady state imbalance in V+ and V- concentrations results when the concentration imbalance compensates for the difference in transport coefficients. The steady state ratio of V+ to

V- total vanadium concentrations can be shown to be equal to the inverse ratio of the sum of the mass transfer coefficients during charge and discharge:

$$\frac{c_{SS}^{+}}{c_{SS}^{-}} = \frac{m_{Chg}^{-} + m_{DChg}^{-}}{m_{Chg}^{+} + m_{DChg}^{+}} \tag{4.3}$$

In the example shown in Figure 4.5, the V+ side of the cell increases in concentration and the V- side decreases in concentration until the flux rates, integrated over a charge/discharge cycle, balance. This simple model does not account for the self discharge reactions listed in Table 1.1 that occur when the vanadium ions cross-over to the other side of the cell. Much more detailed models of cross-over effects on cell capacity have been produced by Knehr [16] and Tang [4]. These models take into account side reactions and water transport, as well as treating all four vanadium species separately, but both predict the establishment of a steady state imbalance when side reactions are not significant.

Table 4.1 Parameters for Electrolyte Imbalance Model.

Current Density	300	mA/cm^2	Mass Trans. Coef Charge	During Charge	During Discharge
Vol	100	cm^3	m^+ (cm/sec)	1.51E-04	5.07E-05
Area	10	cm^2	m^- (cm/sec)	3.97E-05	1.33E-04
Initial V+	1	Mole/L	Initial V-	1	Mole/L
Init SOC	10%		Chg Time	2569	sec
Final SOC	90%		Dschg Time	2569	sec
Imbalance after 1 cycle			V+ (1 cycle)	0.9938	Mole/L
V+ Change		-0.62%	V- (1 cycle)	1.0062	Mole/L

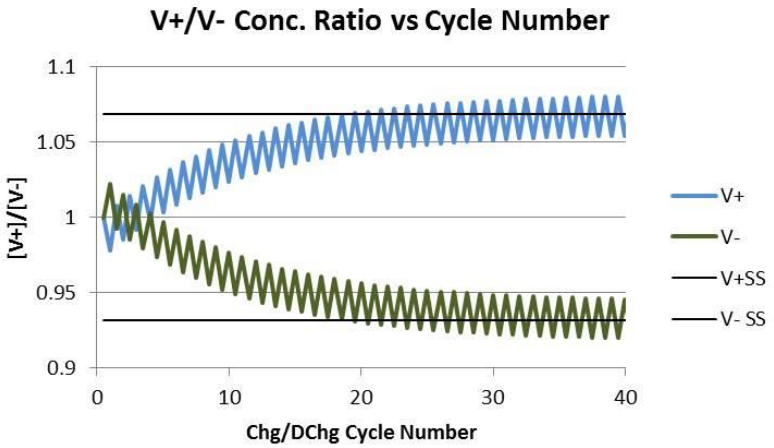

Figure 4.5 Development of steady state imbalance in vanadium concentration due to differences in transport rates. Parameters as listed in Table 4.1.

Experimental Measurement of Cell Imbalance over two charge/discharge cycles

A method to experimentally measure the likelihood for electrolyte imbalance to occur is to compare the total cross-over into the +XO and –XO chambers over one or more complete discharge/charge cycles. This method was tested with the XO cell over a two discharge/charge cycle experiment. The experimental setup was identical to that of full cell mode cross-over experiments discussed in Section (3.4) and illustrated in Figure (3.5). The initially charged XO cell was discharged at 1200 mA for 1.5 h, then recharged at the same current for 1.5 h. One mL samples were collected from the V+ and V- reservoirs before the experiment started, after the first discharge, and after the first charge. During the second discharge/charge cycle samples of V+ and V- were not taken, with the assumption that the second discharge/charge cycle was identical to the first. The measured vanadium concentrations in V+ and V- electrolytes are shown in Figure 4.6.

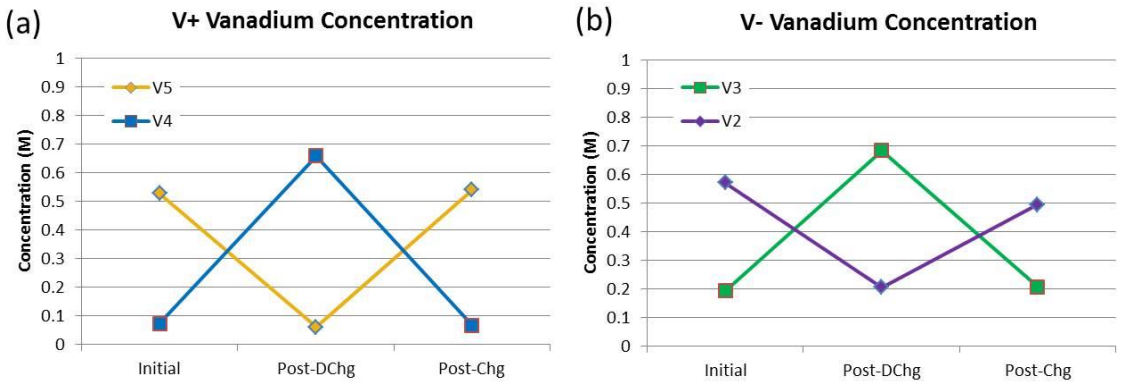

Figure 4.6 Vanadium concentrations in the (a) V+ and (b) V- electrolytes during the first discharge/charge cycle of a two cycle cross-over experiment.

The +XO and –XO reservoirs were initially filled with 30 mL of fresh 4.5 M H_2SO_4 solution. Samples were taken from the XO reservoirs after each discharge and charge step for measurement in an Ocean Optics USB-2000 UV/VIS spectrometer system and then returned to the reservoirs. The –XO reservoir was not flushed with inert gas since samples were to be collected and returned several times, hence V^{+2} oxidation to V^{+3} was expected.

The spectra for the +XO and –XO samples measured after each discharge and charge are shown in Figure 4.7. Since the first step of the experiment was a discharge step, the flux of H^+ ions was initially from V- to V+, hence as seen in Figure 4.7 (a) and (b) the +XO reservoir initially collected some V^{+4} and V^{+5} while the –XO reservoir collected a much larger amount of vanadium, all in the V^{+3} state. Due to the lack of inert gas purge in the –XO reservoir, all the V^{+2} collected was oxidized by dissolved oxygen. During the subsequent charge step, the +XO reservoir collected a significant amount of V^{+4} and V^{+5}, as is apparent from the spectrum in Figure 4.7 (c). The –XO spectrum in Figure 4.7 (d) was little changed, what change that did occur is mainly due to the

presence of V^{+4} in the –XO sample. The V^{+4} present is from cross-over of V^{+4} from the +XO chamber and also from V^{+5} which crossed over and was immediately oxidized to V^{+4} by V^{+3} in the –XO solution.

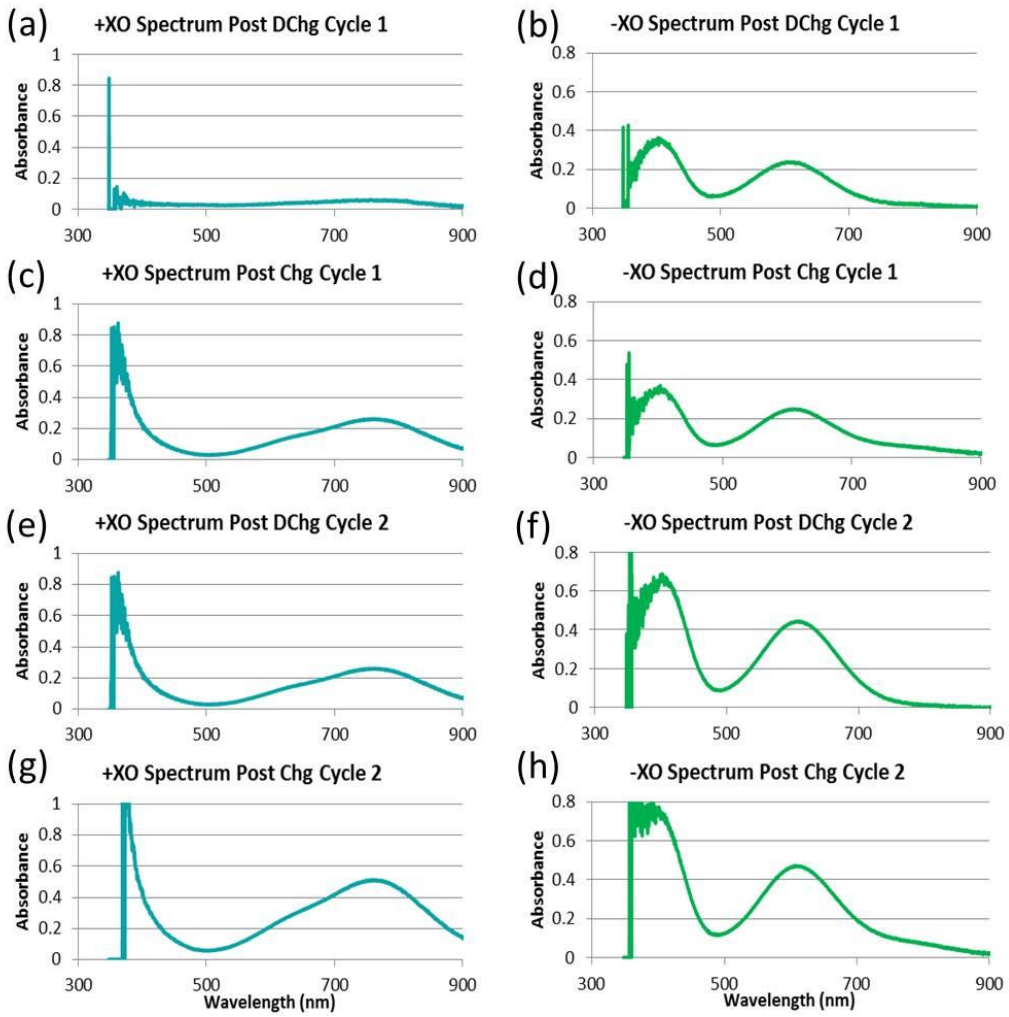

Figure 4.7 Spectra of samples from +XO in (a) (c) (e) and (g) and from –XO in (b) (d) (f) and (g) measured after each step of a two cycle discharge/charge cross-over experiment.

(a)

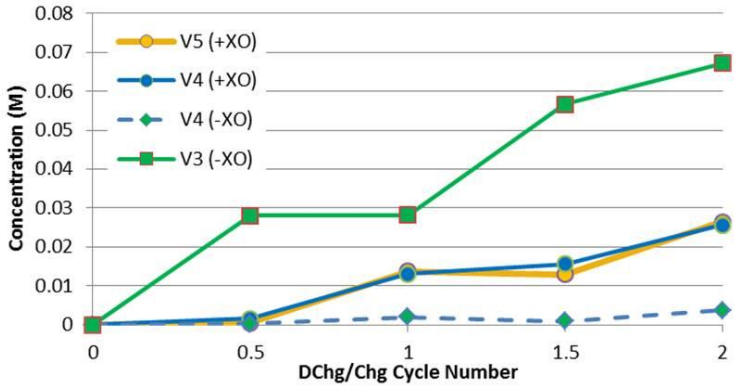

(b)

Time	21600	Seconds
Area	2	cm^2
Volume	33	cm^3
Avg V+ V^{+4}	0.364	M
Avg V+ V^{+5}	0.297	M
Final +XO V^{+4}	0.0257	M
Final +XO V^{+5}	0.0264	M
Avg V- V^{+3}	0.442	M
Final -XO V^{+3}	0.0671	M
m^* (V^{+4})	5.39E-05	cm/sec
m^* (V^{+5})	6.77E-05	cm/sec
m^* (V+ to +XO)	1.22E-04	cm/sec
m^* (V- to -XO)	1.16E-04	cm/sec
Ratio (m +/-)	1.05	

Figure 4.8 (a) Cumulative concentrations of vanadium collected in +XO and –XO reservoirs during two cycle cross-over experiment. (b) Mass transfer coefficients for V+ to +XO and V- to –XO averaged over two discharge/charge cycles.

Figure 4.8 (a) shows the concentrations of the V^{+3}, V^{+4}, and V^{+5} in the +XO and –XO reservoirs at the end of each step during the experiment. At the end of the second discharge step (cycle number 1.5 in Figure 4.8), the +XO chamber has lost a small amount of V^{+5} due to V^{+3} crossing over from the –XO chamber and reacting to form V^{+4}. The concentration of V^{+3} in –XO has doubled due the influx of V^{+2} and V^{+3} into the –XO chamber during the discharge step. At the end of the final charge step (cycle number 2 in Figure 4.8) the concentration of V^{+4} and V^{+5} in the +XO reservoir has nearly doubled due to the influx from the V+ chamber.

The concentration data in Figure 4.8 are used to calculate mass transfer constants for cross-over from V- to –XO and V+ to +XO averaged over two discharge/charge cycles. The results of these calculations are listed in Figure 4.8 (b). For this experiment the mass transfer coefficients for transfer from V+ to +XO and V- to –XO are relatively close,

only differing about 5%, which means in steady state the average vanadium concentration in a VRB cell would be about 5% less than on the V+ side compared to the V- side.

4.3 CROSS-OVER EXPERIMENTS WITH 1.5 M SOLUTIONS

Subsequent experiments with the XO cell were carried out with higher concentration solutions of the vanadium anolyte and catholyte. Solutions were prepared with 1.5 M vanadium concentration and 3.5 M H_2SO_4 concentration. Due to the higher concentration of the vanadium in the V+ and V- chambers of the cell, samples taken for spectroscopic analysis from these parts of the cell were diluted 20:1 before performing absorption spectrometry analysis.

Membrane comparison experiments

A series of experiments were undertaken to compare the cross-over performance of three different ion exchange membranes: Nafion N212, Nafion N117, and Fumatech FX-7050. The Nafion membranes differ primarily in thickness, with N212 being 50 μm thick and N117 180 μm thick. The Fumatech FX-7050 membrane is a per-fluorosulfonic acid cation exchange membrane, nominally 50 μm thick. Compared to the Nafion membrane, the Fumatech membrane has better dimensional stability, with very little swelling when wetted, and is more robust than equivalent thickness Nafion membranes.

The XO cell was run in half cell mode with the V^{+4}/V^{+5} redox couple. For all the experiments run, the center membrane separating the +XO from the –XO chamber was Nafion N117. The first set of experiments with 1.5 M concentration solutions were done with N212 membranes separating the XO chambers from the neighboring V+/V- chambers. N117 membranes were used in the second set of experiments, followed by a third set with FX-7050 membranes.

N212 Membrane Experiments with 1.5 M V solutions

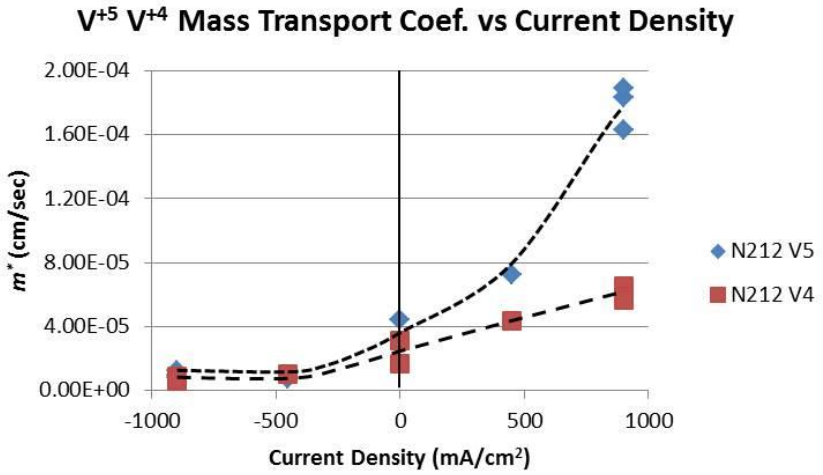

Figure 4.9 V^{+4} and V^{+5} m^* vs current density, N212 Membrane 1.5 M V concentration, Half cell mode.

Figure 4.9 shows the measured mass transport coefficient m^* for V^{+5} and V^{+4} as a function of current density for N212 experiments with 1.5 M total vanadium concentration. The mass transport coefficient for V+5 rises much faster than V+4 for current densities in excess of 450 mA/cm^2, similar to what was observed in Figure 4.1 at lower concentrations. Unexpectedly, the mass transport coefficients for the 1.5 M concentration experiments are much less than those measured at 0.7 M concentrations. A possible reason for the discrepancy is osmotic pressure differences present during the lower concentration experiments driving convective flows. More care was taken to match the sulfate concentration of the V+ and V- solutions to the sulfuric acid solutions used in the +XO and –XO chambers during the higher concentration experiments. A set of experiments in which sulfate concentration was deliberately mismatched was performed later and the results will be discussed in a later chapter of this thesis. Those experiments

did show that sulfate concentration mismatch across an ion exchange membrane greatly affects the amount of vanadium transport.

N117 Membrane Experiments with 1.5 M V solutions

Figure 4.10 shows the measured mass transport coefficient m^* for V^{+5} and V^{+4} as a function of current density for N117 experiments with 1.5 M total vanadium concentration. The effect of the thicker membrane was apparent only for current densities less than 450 mA/cm^2, where the N117 transport coefficients were about a factor of two less than those for N212. Cross-over rates at high current densities much more important for determining net cross over than those at very negative current densities, so there appears to be little advantage to using the thicker N117 membrane to mitigate cross over effects.

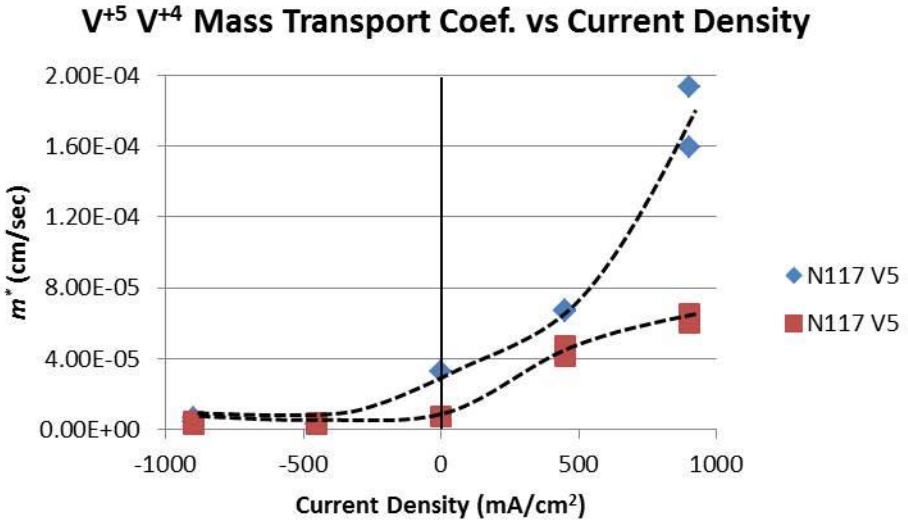

Figure 4.10 V^{+4} and V^{+5} m^* vs current density, N117 Membrane, 1.5 M V concentration. Half cell mode.

FX-7050 Membrane Experiments with 1.5 M V solutions

Figure 4.11 shows the measured mass transport coefficient m^* for V^{+5} and V^{+4} as a function of current density for experiments with FX-7050 membranes with 1.5 M total vanadium concentration. The effect of the Fumatech FX-7050 membrane is profound, mass transport coefficients for V^{+4} and V^{+5} are reduced by a factor of three or more compared to either Nafion membrane for all current densities tested. However, it was noted that higher voltage was required to drive the equivalent current through the cell when the FX-7050 membranes were in place, which indicates that the conductivity of the Fumatech membrane was lower than that of the Nafion membranes. Quantitative measurements of the difference in conductivity were not attempted due to corrosion on the external clips connecting the cell to the battery test equipment causing variable contact resistance run to run.

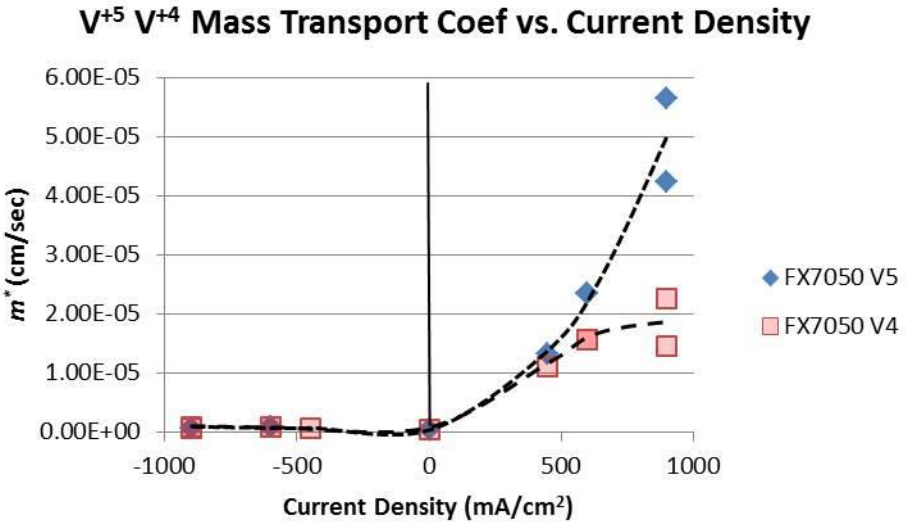

Figure 4.11 V^{+4} and V^{+5} m^* vs current density, FX-7050 Membrane, 1.5 M V concentration. Half cell mode

Direct Comparison of N212, N117, and FX-70450 Combined V^{+4}/ V^{+5} Transport Coefficients

Figure 4.12 shows the combined V^{+4}/V^{+5} mass transfer coefficient for all three types of membranes on the same scale. Figure 4.12 (a) shows the entire range of current densities while (b) shows the range from -1000 mA/cm^2 to 0 mA/cm^2. The difference between the thicker (N117) and thinner (N212) Nafion membranes is apparent only at current densities less than 450 mA/cm^2. Figure 4.12 (b) shows in greater detail the differences in cross-over for zero and negative current densities. Differences between the two thickness of Nafion are readily apparent for negative current densities. Figure 4.12 (b) also shows the extremely low amount of cross-over for the Fumatech FX-7050 membranes at zero and negative current densities, about a factor of five less than N117 and more than a factor of ten less than N212. At the peak positive current densities cross-over for FX-7050 is a factor of three less than that of the Nafion membranes.

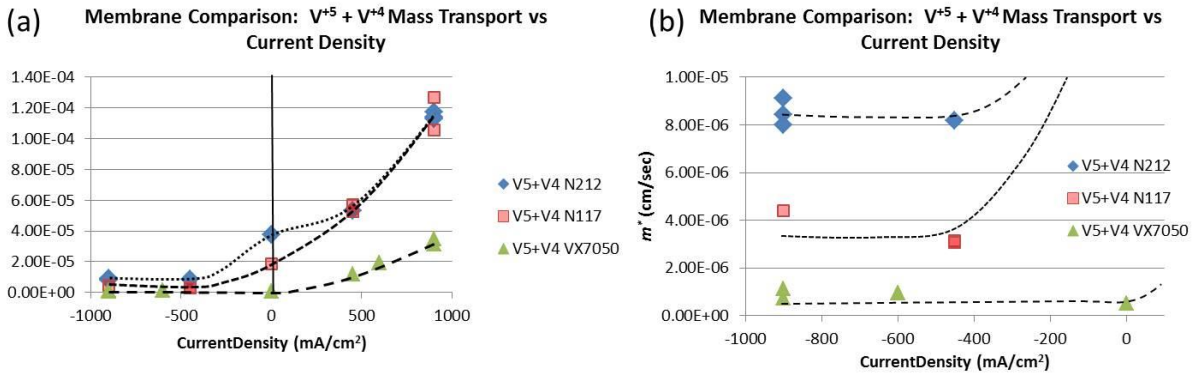

Figure 4.12 (a) Combined V^{+4} and V^{+5} transport coefficient vs current density for N212, N117, and FX-7050 Membranes -1000 to 1000 mA/cm^2 (b) -1000 to 0 mA/cm^2 x-axis.

4.4 EVIDENCE OF OXIDATION OF V^{+4} TO V^{+5} IN XO CELL

As reported in earlier sections of this thesis, the mass transfer coefficient m^* for V^{+4} appears to saturate for current densities ≥ 450 mA/cm^2, while m^* for V^{+5} increases rapidly. At current densities below this value m^* for V^{+4} and V^{+5} track together. One possible explanation for this observation is that the V^{+4} collected in the +XO electrolyte is being oxidized to V^{+5}. The +XO and –XO chambers of the XO cell are both filled with carbon felt electrodes, and redox reactions could occur in the cross-over chambers if there is a source or sink of electrons. When considering the oxidation of V^{+4} to V^{+5} in the +XO chamber when the current density is positive (ie H^+ flux flowing from V+ through the ion exchange membrane to +XO), if there is sufficient membrane electronic conductivity electrons could flow from the +XO porous electrode through the ion exchange membrane to the V+ porous electrode and then into current collector. In this way V^{+4} in the +XO electrolyte could be oxidized to V^{+5}. Figure 4.13 (b) illustrates the current pathway for this reaction.

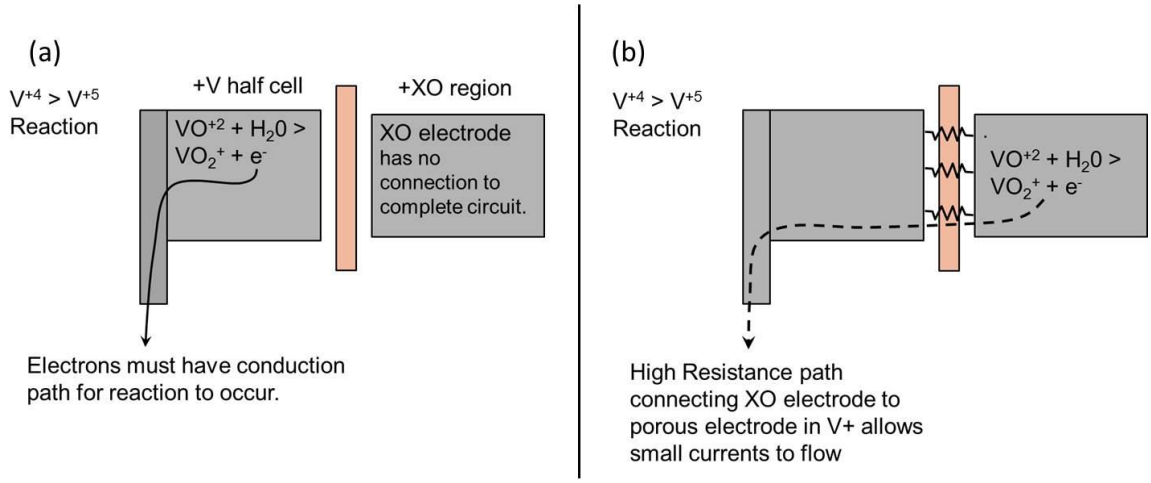

Figure 4.13 (a) XO electrode without leakage path cannot support V^{+4} oxidation. (b) Leakage path through membrane allows V^{+4} oxidation reaction to occur.

Cross-over Experiments with Vanadium solutions in the +XO reservoir

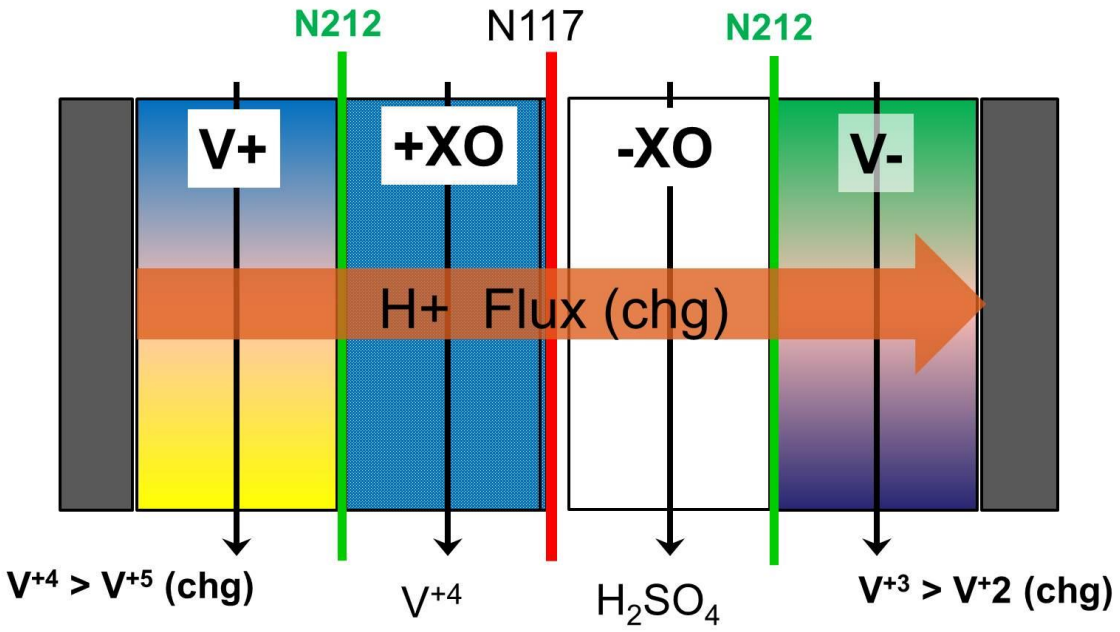

Figure 4.14 Experimental configuration with V electrolyte (V^{+4} this illustration) in +XO reservoir and sulfuric acid in -XO reservoir. Experiments conducted with V^{+5} and V^{+4}in +XO.

A new experimental arrangement was devised to try to prevent the occurrence of the situation depicted in Figure 4.13 (b). Figure 4.14 shows the configuration used for a series of experiments in which one of the XO reservoir was filled with a solution of either V^{+4} or V^{+5} and the other reservoir was filled with sulfuric acid. The V+ reservoir was filled with the usual V^{+5}/V^{+4} mixture and the V- reservoir was filled with V^{+2}/V^{+3} mixture. When the cell was being charged, V^{+4} oxidation occurred in the V+ chamber and V^{+3} reduction occurred in the V- chamber. A flux of H^{+} flowed from V+ through the XO chambers and into the V- chamber.

The composition of the vanadium solution in the +XO electrolyte was largely unchanged throughout the experiment, while the –XO electrolyte collected V^{+4} which crossed over from the +XO electrolyte due to diffusion and migration. The possibility of

oxidation of V^{+4} to V^{+5} occurring in the –XO chamber was decreased, since electrons would have to pass through two ion exchange membranes to reach the V+ current collector to complete the reaction. A 2 cm^2 Teflon aperture identical to the Teflon apertures installed between the +XO/-XO chambers and the V+/V- chambers was installed over the center N117 membrane to confine the proton flux to the same density as that passing through the outer membranes.

Solutions of 0.7 M V^{+4} or 0.8 M V^{+5} with 4 M H_2SO_4 were used for the +XO solutions and 4.5 M H_2SO_4 were used for –XO solutions. In preparation for an experiment run the XO flow circuits were flushed with de-ionized water while the V+ and V- electrolyte mixtures were discharged using another VRB cell. Fresh H_2SO_4 (30 mL) was loaded into the XO reservoirs just before the experiment was run. During the experiment the charging reactions were run in the V+ and V- chambers of the XO cell which provided a flux of H+ passing from the +XO to the –XO cell. After each run the XO chambers were flushed with de-ionized water while the V+ and V- electrolytes were discharged with the second VRB cell.

Figure 4.15 shows the measured V^{+4} and V^{+5} mass transfer coefficients as a function of current density for the experiments run using the configuration shown in Figure 4.14. Mass transfer coefficients for V^{+4} and V^{+5} follow the same trend as current density was varied from 150 to 750 mA/cm^2. The range of values for the mass transfer coefficients are in similar to those shown in Figure 4.4. The results shown in Figure 4.15 show that the divergence at high (>300 mA/cm^2) current densities between V^{+4} and V^{+5} mass transfer coefficients observed in Figures 4.1, 4.9, 4.10, and 4.11 is likely an artifact due to un-intended oxidation of V^{+4} after it had crossed over into the +XO or –XO chamber from the neighboring V+ or V- chamber.

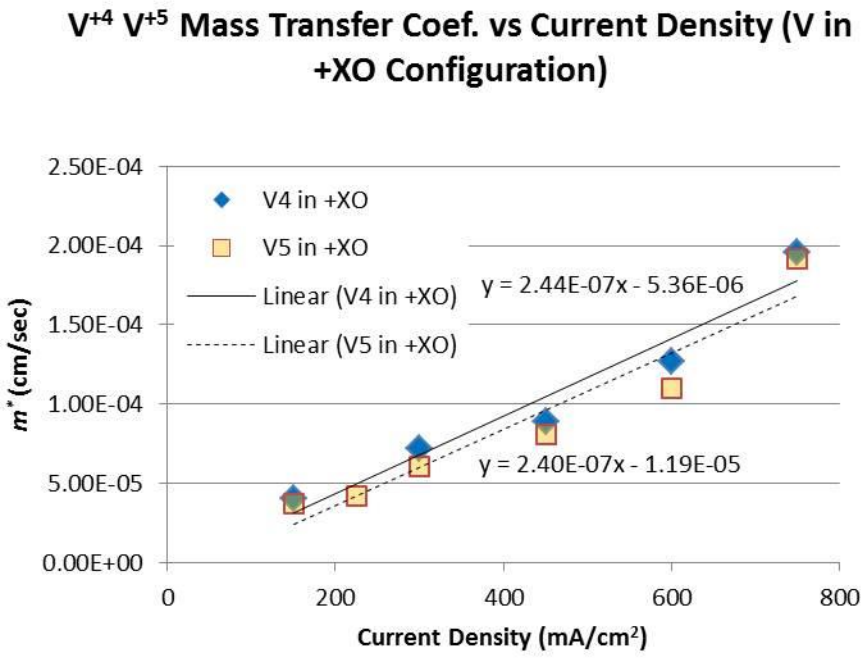

Figure 4.15 V^{+4} and V^{+5} mass transfer coefficients obtained using the cell configuration of Figure 4.14. 0.7 M V^{+4} or 0.8 M V^{+5} solutions in +XO.

4.5 COMPARISON OF EXPERIMENTAL RESULTS WITH PREVIOUS MEASUREMENTS

The experiments described in the preceding sections of this thesis determined the mass transfer coefficient for vanadium ions passing through various ion exchange membranes at different current densities. In most cases the result of the experiments was a plot of the effective mass transfer coefficient m_i^* for species *i* versus current density *J*. The results can be expressed in the form

$$m_i^* = (m_i + k_i J) \tag{4.4}$$

where m_i is the mass transfer coefficient at zero current and k_i is the electro-migration coefficient, which quantifies the degree of enhancement or suppression of the mass transfer depending upon the direction and magnitude of the current. In this section, the

values of m_i and k_i determined from the experiments with the XO cell will be compared against results reported in the literature.

Table 4.2 lists the values of m_i from References [8] and [9] (and as shown in Tables 1.1 and 1.2) and the values of m_i from the experimental results reported in sections 4.1,4.3, and 4.4 of this thesis. Also listed in Table 4.2 is the diffusion coefficient D_i which is calculated by multiplying the mass transfer coefficient m_i by the membrane thickness l. The diffusion coefficient is calculated to allow comparison of the experimental results against the literature values, since three different thickness of Nafion membrane are represented in the previous results and the experimental data. Figure 4.16 shows the diffusion coefficient data listed in Table 4.2 plotted on a logarithmic scale.

Table 4.2 Comparison of m_i and D_i from previous results and experimental results.

Values from Literature				Values from Chapter 4 Sections 4.1, 4.3, 4.4				
	m_i (cm/sec)			V Conc	0.7M	1.5M	1.5M	1.5M
Species	N115			Membrane	N212	N212	N117	FX7050
V^{+2}	7.01E-06	7.55E-06	7.28E-06	V^{+2}	8.34E-05			
V^{+3}	2.58E-06	1.16E-05	7.09E-06	V^{+3}	6.70E-05			
V^{+4}	5.46E-06	3.56E-06	4.51E-06	V^{+4}	8.34E-05	2.41E-05	7.21E-06	5.44E-07
V^{+5}	4.72E-06	1.92E-06	3.32E-06	V^{+5}	1.09E-04	4.42E-05	3.24E-05	5.18E-07
Mem Thickness	0.0125			cm	0.005	0.005	0.01778	0.005
Species	D_i (cm^2/sec)			Membrane	N212	N212	N117	FX7050
V^{+2}	8.76E-08	9.44E-08	9.10E-08	V^{+2}	4.17E-07			
V^{+3}	3.23E-08	1.45E-07	8.86E-08	V^{+3}	3.35E-07			
V^{+4}	6.83E-08	4.45E-08	5.64E-08	V^{+4}	4.17E-07	1.21E-07	1.28E-07	2.72E-09
V^{+5}	5.90E-08	2.40E-08	4.15E-08	V^{+5}	5.45E-07	2.21E-07	5.76E-07	2.59E-09

The diffusion coefficient data shows the experimental results for the Nafion membranes are larger than the results from References [8] and [9], by up to a factor of ten. Such large differences could indicate a systematic problem in the measurements,

such as a leak which allowed electrolytes to bypass the membrane. However, cross-over rates with the Fumatech FX-7050 membrane, obtained with exactly the same cell configuration as the Nafion membrane results, were up to two orders of magnitude less. This provides confidence that the transport measured was through the membranes tested and there was no side channel for ionic transfer.

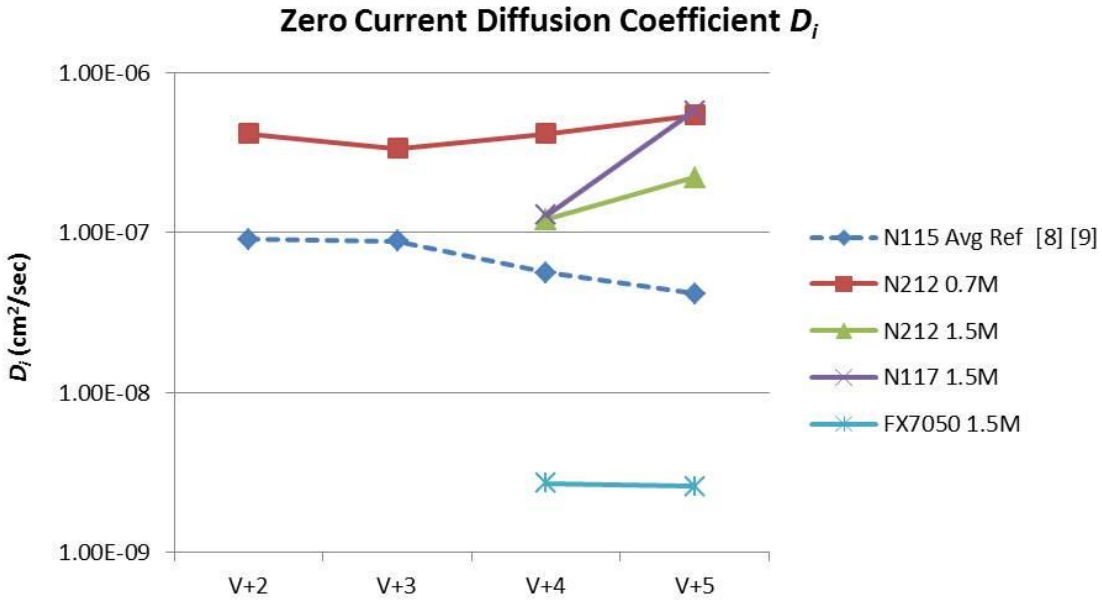

Figure 4.16 Diffusion coefficient data from Table 4.2.

The other parameter which can be obtained from the experiments is k_i, the electro-migration coefficient which describes the change in mass transport rate as function of the applied current density. Experimental values of k_i were obtained by applying linear regression to the parts of the m^* vs J curves in which linear behavior was observed. Because of issues with oxidation of V^{+2} and V^{+4}, the combined V^{+2}/V^{+3} or V^{+4}/V^{+5} mass transport coefficient data were analyzed to determine k_i from the experimental results reported in Sections 4.1 and 4.3. There were no unintended oxidation reactions occurring during the experiments reported in Section 4.4, so k_i for V^{+4} and V^{+5} could be calculated from the results of those experiments for each species separately. Table 4.3 gives a

compilation of the k_i values obtained from the experiments described in this chapter and the values of k_i from Reference [9]. Aside from the value of k_i for V^{+5} from Reference [9], all of the k_i values from the experiments and the literature are within a factor of 2.5 of each other. It should be noted that the maximum current density used in the experiments described in Reference [9] was 50 mA/cm^2, while the maximum current densities for the experiments in this thesis were in excess of 750 mA/cm^2. The fact that the values of k_i from the literature and this thesis agree despite the huge difference in the range of current densities investigated lends confidence in the results.

Table 4.3 Electro-migration coefficient k_i from Reference [9] and the experiments described in this thesis.

<table>
<tr><td colspan="2">Values from Ref [9]</td><td colspan="6">Values from Chapter 4 Sections 4.1, 4.3, 4.4 Data</td></tr>
<tr><td></td><td>Table 4.2</td><td>V Conc.</td><td>0.7 M</td><td>1.5 M</td><td>1.5M</td><td>1.5M</td><td>0.75M</td></tr>
<tr><td>Species</td><td>k_i (cm^3/sec-mA)</td><td>Membrane</td><td>N212</td><td>N212</td><td>N117</td><td>FX7050</td><td>N117</td></tr>
<tr><td>V^{+2}</td><td>1.05E-07</td><td></td><td rowspan="2">1.55E-07</td><td></td><td></td><td></td><td></td></tr>
<tr><td>V^{+3}</td><td>1.48E-07</td><td></td><td></td><td></td><td></td><td></td></tr>
<tr><td>V^{+4}</td><td>1.10E-07</td><td></td><td rowspan="2">1.74E-07</td><td rowspan="2">1.37E-07</td><td rowspan="2">1.36E-07</td><td rowspan="2">4.65E-08</td><td>2.44E-07</td></tr>
<tr><td>V^{+5}</td><td>3.50E-08</td><td></td><td>2.40E-07</td></tr>
<tr><td colspan="3"></td><td>V^{+2}/V^{+3}
V^{+4}/V^{+5}</td><td colspan="3">Combined V^{+4}/V^{+5}</td><td></td></tr>
</table>

4.6 CONCLUSIONS FOR CURRENT DENSITY SCALING STUDY EXPERIMENTS

Common amongst all of the experimental results reported in this thesis is the powerful effect current density magnitude and direction has on the cross-over rates of vanadium ions through ion exchange membranes. Cross-over rates vary by up to several decades in magnitude as current is varied from -900 to 900 mA/cm^2, which are current regimes relevant to the state of the art VRB cells being developed. Surprisingly, the difference between thick and thin Nafion membranes (N117 vs N212) disappeared at the highest current densities tested. The Fumatech FX-7050 membrane was the best

performing membrane from a cross-over perspective, with cross-over rates at large positive current densities less than one third that of the Nafion membranes. At negative current densities cross over rates for the Fumatech membrane were a factor of twenty less than N212 and almost a factor of ten less than N117.

Electrolyte imbalance was shown to result when cross-over rates between the two sides of a VRB are not equal. A simple model was constructed which demonstrates that small (< 1%) electrolyte imbalances present over a single charge/discharge cycle will grow over many cycles and can eventually lead to a steady state electrolyte imbalance situation. A method to directly measure the net cross-over in the XO cell by running the cell over several discharge/charge cycles was described and the results from an experiment showed the feasibility of this method.

Comparison of results with low (~ 0.7 M) and high (~ 1.5 M) concentration vanadium solutions with the same membrane (N212) showed a factor of two difference in the measured cross-over rates, with the rate for the lower concentration being higher. A possible cause for this discrepancy may be the presence of convective flows which provide an additional transport mechanism for ions to move across a membrane. A set of experiments will be described in the next chapter which quantifies the effect of convective flows on vanadium cross-over.

The absolute value of the diffusion coefficient measured for Nafion membranes in the experiments described in this thesis was approximately one order of magnitude higher than those measured by other researchers. However, the diffusion coefficient for Fumatech FX-7050 membrane material was two orders of magnitude less than the value measured for Nafion membranes, which indicates that the experimental technique used in this thesis was sound and the transport measured was through the membrane and leakage around the membrane was not likely to have occurred. The experimentally determined

electro-migration coefficient for Nafion membranes measured in this thesis agreed with the value reported in the literature within a factor of 2.5, despite the large difference in current densities between the previous results and this thesis.

Chapter 5: Convective Flow Effects on Cross-over

5.1 CONVECTIVE FLOW EFFECTS ON MASS TRANSPORT

In addition to diffusion and migration, convective flow is an important effect to consider when analyzing mass transport. The expression for the flux of species *i* taking into account diffusion, electro-migration, and convection is:

$$N_i = -D_i \nabla c_i - z_i \mu_i c_i \nabla \phi + c_i V \tag{5.1}$$

Equation (5.1) differs from Equation (3.1) only in the addition of the convective term $c_i V$, where V is the bulk fluid velocity. The addition of the convection term adds an additional term to the expression for the effective mass transfer coefficient m^*:

$$m^* = (m_i + z_i \mu_i k \rho_m J_e + kV) \tag{5.2}$$

In Equation (5.2) the factor k in the convective term is the partition coefficient which was first introduced in Equation (3.6) and takes into account the drop in the vanadium concentration across the membrane to electrolyte interface.

As mentioned at the conclusion of the previous chapter, an unresolved issue from the experimental results is the discrepancy between measurements of m^* obtained with experiments with low (~ 0.7 M) and high (~ 1.5 M) concentration vanadium solutions using the same membrane (Nafion N212). Convective flow effects provide a possible explanation for this discrepancy. A set of experiments was designed to deliberately introduce convective flow variations and to quantify their effect on vanadium cross-over.

5.2 CONVECTIVE FLOW/ VARIABLE SULFATE CONCENTRATION CROSS-OVER EXPERIMENTS

Experiment Configuration

Convective flow variations were created by varying the difference in total ionic strength across the membrane. The experimental arrangement for these experiments is shown in Figure 5.1.

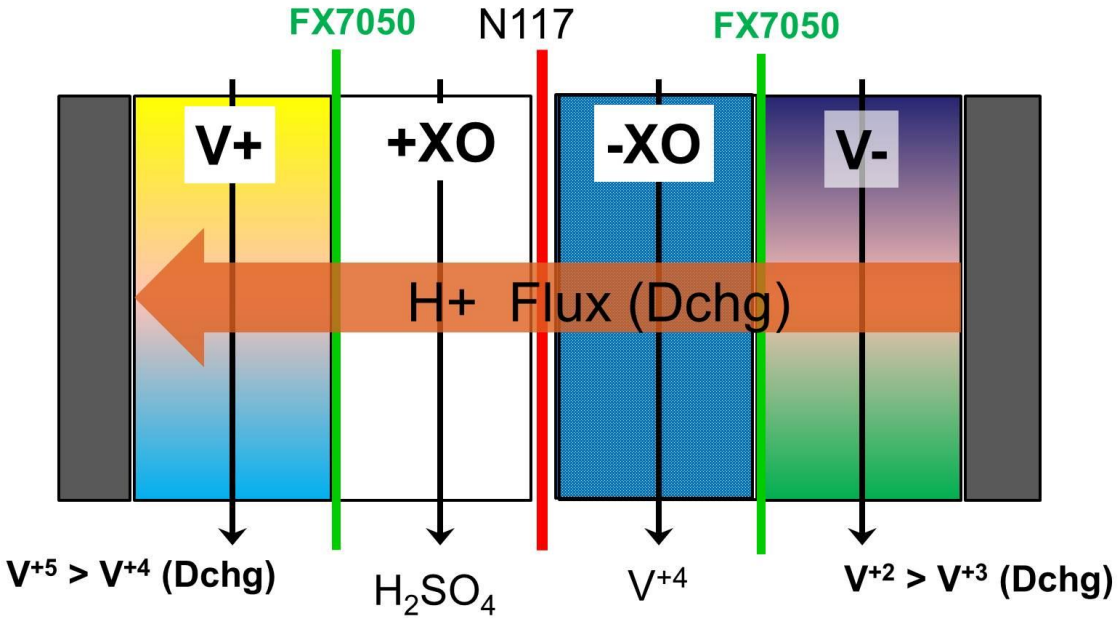

Figure 5.1 Experimental configuration for convective flow experiments.

This experimental configuration is similar to that described in section (4.3) of the previous chapter, in which cross-over between the two XO chambers of the cell was studied by flowing a solution of V^{+5} or V^{+4} on one side of the center N117 membrane and sulfuric acid on the other side. In those experiments the strength of the sulfuric acid solutions were adjusted so that the total sulfate concentrations on both sides of the center membrane matched. In the experiments described in this chapter, the concentration of the sulfuric acid in the –XO solution was reduced for some experimental runs to introduce an

osmotic pressure gradient across the center membrane and an accompanying bulk fluid flow. The +XO reservoir was filled with 25 mL of 5 M H_2SO_4 while the –XO reservoir was filled with 100 mL of a mixture of 0.5 M $VOSO_4$ (i.e. V^{+4}) with 4.5 M, 3.25 M, or 2 M sulfuric acid. In this way a sulfate concentration difference of zero, 1.25, or 2.5 M was imposed across the center N117 membrane. Fumatech FX-7050 membranes are used to separate the +XO and –XO chambers from the V+ and V- chambers of the cell. The FX-7050 membranes were found to have the lowest cross-over of the three membrane types tested, and the use of these membranes insures that the cross-over from the –XO chamber through the center N117 membrane is the dominant source of vanadium flowing into the +XO chamber of the cell.

Fluid volume increases of several mL were noted in the +XO reservoir when a 2.5 M difference in sulfate concentration existed across the membrane during the experiments. However, the reservoirs for the +XO and –XO pumping circuits were 25 mL graduated cylinders with a minimum graduation of 0.5 mL, so it was impossible to make accurate measurements of the volume changes. Table 5.1 lists the measured volume changes and calculated fluid flux rate for runs with a 2.5 M sulfate concentration difference. Smaller (< 0.5 mL) volume differences were noted when the sulfate difference was 1.25 M. The sulfate concentration difference was used as an independent variable instead of the fluid flux when analyzing the results from the experiment, with the implicit assumption that fluid flux is proportional to the sulfate concentration difference.

Figure 5.2 shows the measured effective mass transport coefficients for the experiment runs. The x-axis label lists the sulfate concentration difference and the current density for each run. The sulfate concentration had a large effect on the mass transfer coefficients, with m^* increased by more than a factor of three when a sulfate concentration difference of 2.5 M was present across the membrane.

Table 5.1 Fluid volume increases and water flux for runs with 2.5 M sulfate concentration difference.

Time	Current Density (mA/cm^2)	Delta Vol +XO fluid (ml)	Rate (ml/hr)	Flux Rate ($ml/hr\text{-}cm^2$)
9000	0	2.8	1.12	0.56
4600	0	1.6	1.25	0.63
4600	600	1	0.78	0.39
4400	600	1.2	0.98	0.49
4700	600	1.2	0.92	0.46
		Average	1.01	0.51
		StDev	0.18	0.09

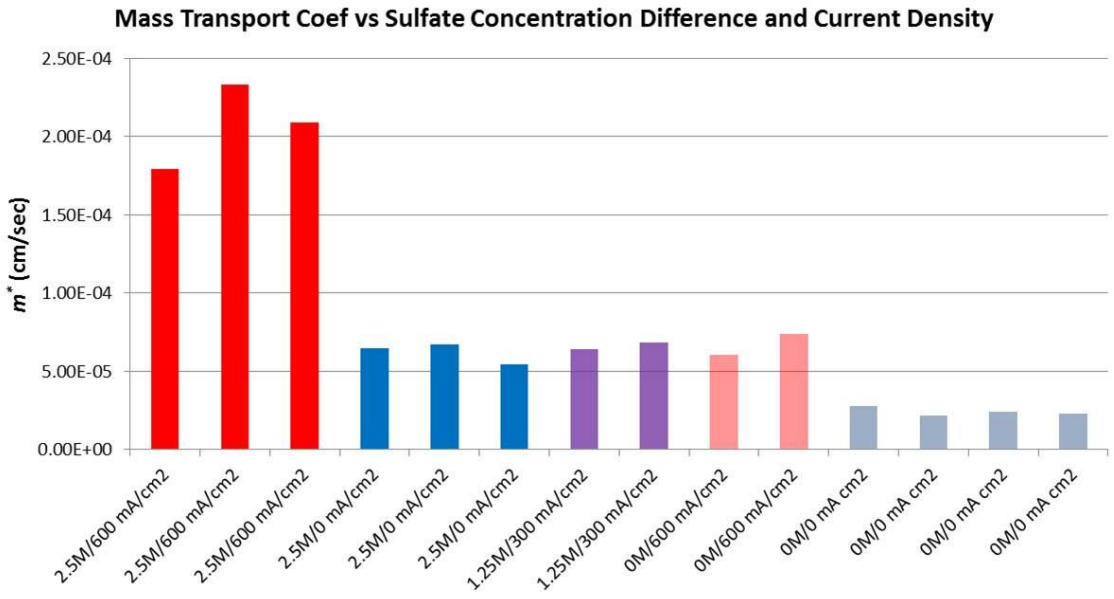

Figure 5.2 Calculated Mass Transport Coefficients for the variable sulfate experiments.

Data Analysis using a Full Factorial Model

The results were analyzed using a full factorial model of the form given by Equation (5.3) with linear variation in sulfate concentration difference ΔSO_4 and current density J_e and an interaction term proportional to $\Delta SO_4 * J_e$:

$$m^* = C_0 + C_J * J + C_{\Delta SO_4} * \Delta SO_4 + C_{J*\Delta SO_4} * \Delta SO_4 * J \tag{5.3}$$

The constant term C_0 and the coefficients C_J, C_{SO_4}, and C_{J*SO_4} are found using a least squares fitting algorithm. Table 5.2 lists the experimental run parameters, the measured mass transport coefficients, and the model coefficients and the full factorial model fits to the data. The average RMS error between the model and the measured m^* is approximately 13%. If the assumption is made that the convective flow velocity V is proportional to difference in sulfate concentration ΔSO_4 then a model for m^* which incorporates only the constant and linear terms in J and ΔSO_4 would be expected to provide an adequate representation of the experimental data. However, when a model of this form is fit to the data the error between the measured and model m^* is over three times larger than the error using the full factorial model results. Figure 5.3 shows the comparison between the measurements and the two different model fits.

The failure of the linear (i.e. J and ΔSO_4 terms only) model to fit the data does not mean that m^* does not vary linearly with J and V as predicted in Equation (5.2), it is just as likely that changing the difference in sulfate concentration difference has other effects than simply changing the fluid flux and the convective flow velocity V. Also, the implicit assumption in using an equation of the form of (5.1) is that dilute solution theory is valid for this application. The recent work by Michael [17] showed that a more appropriate method to treat the membrane is through the use of concentrated-solution theory and incorporating the mass transport equations for all of the species existing in the membrane ($H^+, SO_4^{-2}, HSO_4^{-1}, V^{+2}, V^{+3}, VO^{+2}, VO_2^+$). More detailed measurements of cross-over over a larger parameter space with more careful measurements of fluid fluxes is needed before conclusions can be made regarding the appropriateness of the dilute solution theory or a model based on concentrated-solution theory.

Table 5.2 Experimental Conditions and Results for variable sulfate experiments.

Sulfate	J (mA/cm^2)	Delta Sulfate (M)	Δ Sulfate x J	Mass Trans (cm/sec)	Model Fit (cm/sec)	Error
Low Sulfate	0	2.5	0	6.48E-05	5.86E-05	-9.5%
Low Sulfate	0	2.5	0	6.70E-05	5.86E-05	-12.5%
Low Sulfate	0	2.5	0	5.43E-05	5.86E-05	8.0%
Low Sulfate	600	2.5	1500	1.80E-04	2.04E-04	13.5%
Low Sulfate	600	2.5	1500	2.33E-04	2.04E-04	-12.6%
Low Sulfate	600	2.5	1500	2.09E-04	2.04E-04	-2.4%
Mid Sulfate	300	1.25	375	6.39E-05	8.66E-05	35.4%
Mid Sulfate	300	1.25	375	6.85E-05	8.66E-05	26.4%
Std Sulfate	0	0	0	2.79E-05	2.16E-05	-22.5%
Std Sulfate	0	0	0	2.18E-05	2.16E-05	-0.8%
Std Sulfate	0	0	0	2.42E-05	2.16E-05	-10.6%
Std Sulfate	0	0	0	2.28E-05	2.16E-05	-5.0%
Std Sulfate	600	0	0	6.05E-05	6.22E-05	2.8%
Std Sulfate	600	0	0	7.40E-05	6.22E-05	-16.0%

Constant C_0	J Term C_J	Sulfate Term C_{SO4}	Cross Term C_{J*SO4}
2.16E-05	6.76E-08	1.48E-05	6.98E-08

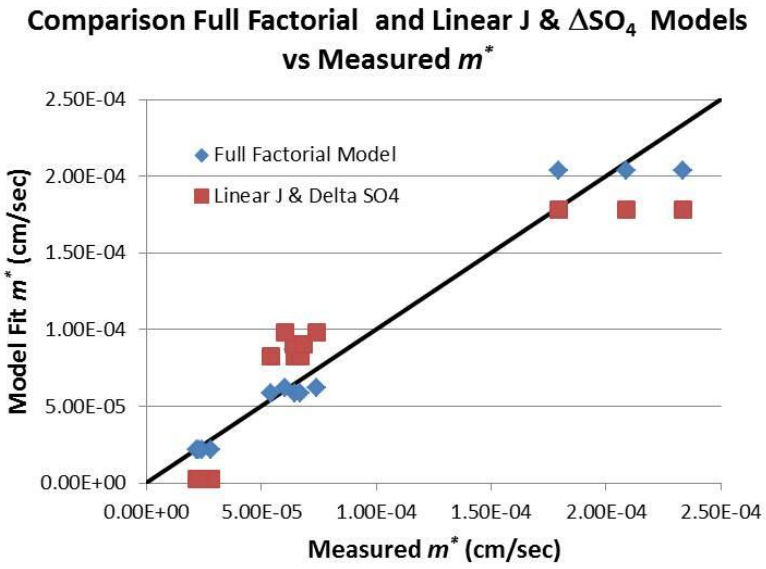

Figure 5.3 Comparison of Full Factorial and Linear Model fits to measured mass transport coefficient data.

5.3 COMPARISON OF VARIABLE SULFATE CONCENTRATION MODEL WITH RESULTS FROM CURRENT SCALING EXPERIMENTS

The results of the variable sulfate experiment reported in the previous section showed that mismatch in the sulfate concentration across the membrane can cause large effects on the cross-over rates of vanadium. A 2.5 M mismatch in the sulfate concentration caused an increase in the V^{+4} cross-over rate through Nafion N117 of over a factor of three at zero and 600 mA/cm^2 current density. The results of the variable sulfate experiment were fit to a full factorial model which can be used to predict the mass transport rate for V^{+4} through N117 as a function of current density and sulfate concentration difference across the membrane. The full factorial model is used to compare the V^{+4} mass transfer coefficients obtained with N212 membranes at low and high vanadium concentrations.

Figure 5.4 compares the measured V^{+4} m^* values for the different experiments described in the previous chapter against the experimental results from variable sulfate experiment at 600 mA/cm^2 and the predictions of the full factorial model with different sulfate concentrations. As noted earlier, the results for low (0.7 M) and high (1.5 M) concentration experiments with N212 membranes differed considerably. The discrepancy between the low and high concentration N212 data can explained using the results from the variable sulfate experiment if a 2.5 M sulfate concentration difference existed during the lower concentration experiments which added an additional source to the cross membrane transport. This amount of sulfate concentration mismatch is larger than the amount of error (~ 0.5 M) likely due to errors in solution preparation, so the reason for the discrepancy between the different experiments is still unknown.

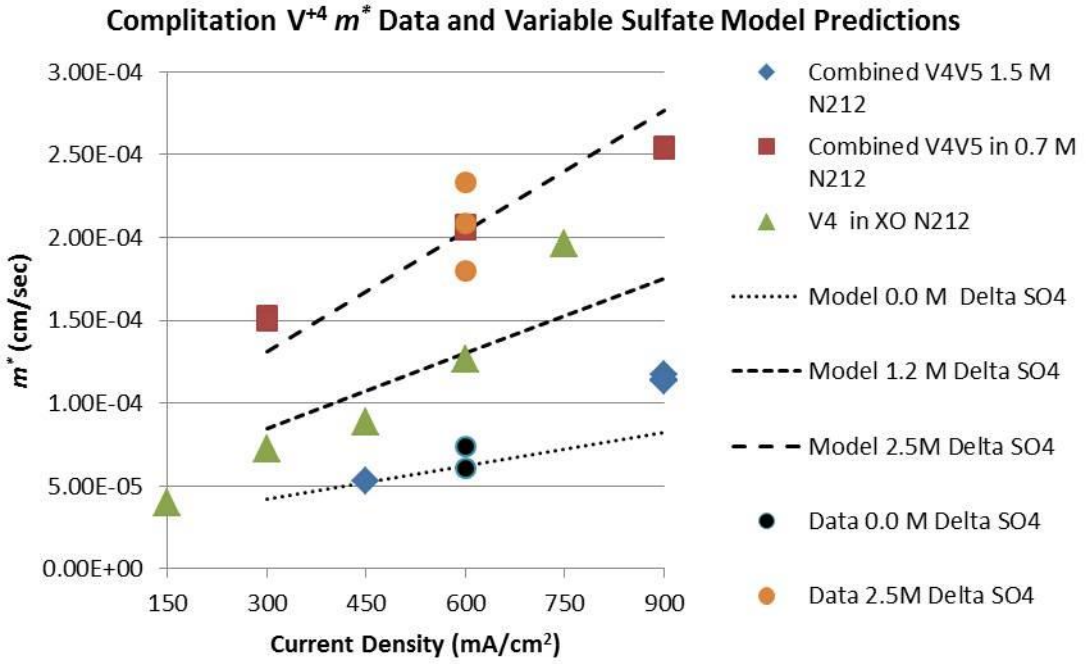

Figure 5.4 Comparison of V^{+4} m^* from different experiments (described in Chapter 4) with results from full factorial model of variable sulfate experiment.

5.4 CONCLUSIONS FOR CONVECTIVE FLOW EFFECTS ON CROSS-OVER

The effect of varying convective flow velocity as well as current density was tested in the experiment described in this chapter. The convective flow velocity was found to vary monotonically with the sulfate concentration difference across the ion exchange membrane. Cross-over rates at zero and 600 mA/cm^2 current density were observed to increase by more than a factor of three when a sulfate concentration difference of 2.5 M was imposed across a Nafion N117 membrane. A full factorial model with terms proportional to current density, sulfate concentration difference, and the product of the two was found to best describe the experimental results. The results show that convective flow effects have a large effect on the transport of vanadium through ion exchange membranes and needed to be taken into account when running cross-over experiments. However, the level of sulfate concentration mismatch needed to explain all of the variation in the mass transfer coefficients measured during the various experiments described in Chapter 4 of this thesis is larger than the likely variations that occurred during the experiments.

Chapter 6: Conclusions and Recommendations for Future Work

6.1 CONCLUSIONS

Spectroscopic measurement of Vanadium electrolyte mixtures

The characteristic colors of the aqueous solutions containing V^{+2}, V^{+3}, V^{+4} and V^{+5} had prompted many different groups to investigate the use of absorption spectroscopy to determine the composition and concentration of vanadium ion mixtures encountered in VRB work. However, problems with anomalous absorption which could not be reconciled with Beer's law had lead researchers to discount the usefulness of this method for determining the composition of mixtures of V^{+4} and V^{+5} ions. In this thesis, it was demonstrated that dilution of the solutions of vanadium ion mixtures was sufficient to allow the spectroscopic analysis of any mixture of vanadium ions, as long as the final concentration was less than 0.1 M. Methods to determine the composition and concentration of vanadium ion mixtures using absorption data at three different wavelengths were developed and applied in the analysis of the cross-over experiments reported in this thesis.

Triple Membrane Cell

The most important product from this work was the development of the Triple Membrane (or XO) cell for the study of electrolyte cross-over in a flow battery under realistic operating conditions. The XO cell is a standard porous electrode VRB with two additional chambers which connect the V+ and V- chambers of the cell. The additional chambers, called the positive and negative cross over, or +XO and –XO chambers for short, provide an ionic conduction path between the V+ and V- chambers of the VRB. The +XO and –XO chambers contain sulfuric acid solution which maintains ionic conduction across the cell as well as providing a medium for the collection and analysis

of electrolyte species which cross through the ion exchange membranes separating the XO chambers from the V+ and V- chambers.

Scaling of Cross-over with Current Density

The XO cell was successfully operated as a VRB and clearly demonstrated the powerful effect current density has on the transport of vanadium ions across an ion exchange membrane. The numerous experiments which were performed with the XO cell demonstrated that at current densities that have been achieved by leading edge research groups, the contribution of electric field effects to electrolyte cross-over often far exceeds that due to diffusion alone. At large positive current densities (up to 900 mA/cm^2) cross-over was increased by more than a factor of five (for N117) compared to the no current case. At large negative current densities (as small as -900 mA/cm^2) cross-over was suppressed by up to an order of magnitude compared to diffusion alone.

The current density scaling experiments were extended to include the comparison of three different ion exchange membranes: Nafion N212, N117, and Fumatech FX-7050. In head to head experiments, the Fumatech membrane was found to have up to a factor of three less cross-over at large positive current densities and an order of magnitude less cross-over at large negative current densities compared to either Nafion membrane. The difference between the two Nafion membranes was only apparent for current densities less than 450 mA/cm^2, at or above this level the cross-over of the thick (N117) and thin (N212) Nafion membranes were the same.

Prediction of Electrolyte imbalance

A simple model was developed which demonstrated how differences in cross-over rates between the V+ and V- sides of a VRB can lead to capacity loss due to the development of an electrolyte imbalance situation. Since the cross-over rates have great

sensitivity to the direction and magnitude of the current flow through the cell, any model which is used to predict capacity loss due to cross-over must incorporate the current density effects in addition to diffusion effects. The use of the XO cell to measure the net cross-over from V+ and V- chambers over multiple discharge and charge cycles was demonstrated in an experiment over two full discharge/charge cycles. Samples of the electrolyte from the +XO and –XO chambers of the XO cell were analyzed after each step of the experiment and the net cross-over rate was determined. The direct measurement of net cross-over by the XO cell over one or two cycles can allow the prediction of an electrolyte imbalance condition which would take many (20 to 50 cycles or more) to become apparent as a capacity loss in a conventional cell.

Demonstration of convective flow effects

The effect of osmotic pressure gradient driven convective flows on cross-over was studied in an experiment in which a deliberate mismatch in sulfate levels was used to modulate cross-over between the +XO and –XO chambers of the XO cell. Mismatches in sulfate level of 2.5 M were shown to lead to measureable fluid transfer (assumed to be water) during cross-over experiments. Cross-over rates with and without current density were affected by the osmotic pressure gradient caused by the sulfate concentration difference. The cross-over results were found to be best fit by a full factorial model which included linear terms in current density and sulfate concentration difference and a non-linear interaction term proportional to the product of the two. The interaction term is not predicted by dilute solution theory, but the strictly speaking the membrane-electrolyte system is best modeled with concentrated solution theory.

However, the differences in sulfate concentrations needed to explain the difference in cross-over rates with N212 membranes at low and high vanadium

concentration are larger than those that were likely to have occurred during electrolyte solution preparation. The results of the convective flow experiment do show the importance of careful preparation of the vanadium solutions and in the specification of the strength of the sulfuric acid solutions used to collect cross-over in the XO cell experiments. The results also demonstrated a method to isolate changes in transport due to convective flows from changes due to concentration gradients and electric field effects.

Oxidation of V^{+4} to V^{+5} during cross-over measurements

At moderately high current densities (> 300 mA/cm^2) the mass transport coefficient for V^{+5} increased rapidly with current density while that of V^{+4} showed signs of saturation. This effect was seen in current scaling experiments carried out with V^{+4} and V^{+5} at both high and low concentrations and with all three membranes tested. A mechanism was proposed in which leakage currents through the ion exchange membrane separating the +XO from the V+ chambers of the XO cell allowed oxidation of V^{+4} collected in the +XO chamber to converted to V^{+5}. A series of experiments were run in which solutions of either V^{+4} or V^{+5} were pumped through the +XO chamber, and cross-over to the –XO chamber was studied as a function of current density. This experimental configuration provided improved electrical isolation of the chamber of the cell which in which V^{+4} or V^{+5} is collected, and in this manner oxidation of V^{+4} was reduced. The large difference in the V^{+4} and V^{+5} mass transport coefficients at high current densities disappeared with the new experimental configuration, which suggests that un-intended oxidation of V^{+4} was present in the earlier experiments.

6.2 RECOMMENDATIONS FOR FUTURE WORK

Improvements in the VRB cell designs

All of the experimental VRB cells built for these experiments had problems with leaking electrolytes. Part of the problem was found to the porous nature of the graphite used to machine the current collectors of the VRB cells. Graphite was purchased from Glemco Inc, which supplies graphite for use in the semiconductor industry. Graphite parts used in semiconductor equipment are most often used in a vacuum environment, and graphite is not typically used in parts in which a vacuum seal to atmosphere is made. Consequently, the graphite parts used in the VRB cells which were wetted on one side and exposed to the atmosphere on the other side showed signs of liquid penetration. The other source of leakage was due to the design of the electrodes themselves. The sealing surface of the electrodes is approximately 4 mm wide and the electrodes were recessed into the PVC flange of the cell, making it difficult to verify the integrity of the electrode to flange seal. Simplification of the design to incorporate planar electrodes with simple flat gasket seals would eliminate the seal leakage problem. Elimination of leaking issues would allow the cells to be used over longer duration experiments and over multiple charge/discharge cycles, and for changes in electrolyte volume due to convective flow effects to be more easily detected.

Membrane selection within the XO cell

The membrane comparison studies revealed that the Fumatech FX-7050 membrane had very low cross-over rates, both in the forward and backward current flow directions, compared to the Nafion brand membranes. The Fumatech membrane is the best choice for the membrane to separate the +XO and –XO chambers of the XO cell when studying net cross-over between V+ and V- chambers, which is important for

predicting capacity loss due to electrolyte imbalance situtaions. The net cross-over experiment discussed in section 4.2 of this thesis used a Nafion N117 membrane to separate the +XO and the –XO chambers, and a measureable amount of vanadium was exchanged between those two regions of the cell. The bulk of the cross-over that contributed to the vanadium detected in the +XO and –XO electrolytes in those experiments was from the adjacent V+ and V- chambers. However, the small amount of vanadium exchanged between the XO chambers became more significant when the net cross over rate was calculated since the net cross over involves the difference between two comparably sized quantities (i.e. the V+ and V- cross-over rates).

Half Cell Mode Experiment Improvements

Many of the experiments were performed using the XO cell in the half cell mode, in which one side of the cell runs a redox reaction in the oxidation direction and the other side of the cell ran the same reaction in the opposite direction. Two separate reservoirs were used in the experiments, and the duration of the experiment was limited by the volume, concentration, and initial state of charge of the electrolytes stored in each reservoir. Recently, researchers at United Technologies have shown that by using a single electrolyte reservoir, a quasi-steady state half cell reaction can be maintained in a flow battery cell [19]. Both sides of the battery use the same flow circuit, with the electrolyte exiting one side of the cell immediately entering the other side of the cell. Reactants which are consumed in the first reaction are immediately restored during the second reaction. The use of the quasi-steady state half cell mode eliminates variations in the electrolyte composition during the experiments which are presently accounted for by averaging starting and ending compositions and assuming linear behavior during the

experiment. Also, experiments can be run indefinitely, which is useful when cross-over rates are very low.

Additional Experiments on Convective Flow Effects

The experiment described in Chapter 5 provides a method to produce convective flow effects through the variation in the sulfate concentration difference between the different electrolyte solutions. Electrolyte volume differences which can used to deduce convective flow velocity variations were observed and could be related to the sulfate concentration differences, but the type of electrolyte reservoir used in the experiments did not provide sufficient resolution for volume change measurements to be made accurately. Redesign of the electrolyte reservoirs to improve the ability to measure electrolyte volume differences is needed.

The results of the Chapter 5 experiment were best fit with an empirical model with linear terms in current density and sulfate concentration difference, and a nonlinear term proportional to the product of current density and sulfate difference. The original experiments only investigated five combinations of current density and sulfate concentration difference, more experiments to explore the two dimensional parameter space are needed to explore in greater detail the non-linear nature of the transport. Experiments with other species other than V^{+4} are also needed to obtain data important for understanding the importance of convective flow in cross-over for all of the species important for VRB's.

Experiments with Advanced VRB Cell Designs

The experiments described in this thesis were performed using a simple flow battery cell design utilizing carbon felt electrodes and capable of modest current densities (~ 250 mA/cm^2). Higher current densities for testing membrane cross-over were achieved

by the use of current defining apertures and by driving the cell with external power supplies (ie. potentiostats) during charging and discharge cycles with little regard to voltage or energy efficiency. The leading edge VRB cells optimized for peak power density are able to efficiently operate at current densities up to 1000 mA/cm^2 [10,20]. A logical extension of the work reported in this thesis is to modify a high performance VRB cell by adding the additional membranes and porous electrode chambers to directly measure cross-over. The additional membranes, porous electrodes, and electrolyte inlet and outlets that comprise the additional chambers of the XO cell can be fit within two 3 Mm thick Viton gaskets which can be sandwiched between the positive and negative half cells of current experimental VRB cells. In this way virtually any type of VRB cell can be made into an XO cell with dedicated chambers to collect cross-over from the positive and negative half cells.

Investigation of other Variables affecting Cross-over

The relatively large discrepancy (~ factor of 10) between the Nafion zero current diffusion coefficients reported in the literature and the results found in this work as well as the large variation seen in the literature demonstrates that all of the variables affecting cross-over through flow battery membranes are not known. One possible variable to explore in future work is the compression of the porous electrodes against the membranes. Various changes that were made to the graphite electrode gaskets in an attempt to control electrolyte leakage issues during this work caused variation in the degree of compression that the porous electrodes were subjected to. Also, many of the dialysis cell experiments reported in the literature were made with free standing membranes without any porous electrodes in contact with the membranes.

It is possible that the Nafion membranes that were used in the experiments described in this thesis were subjected to extreme conditions compared to the experiments described in the literature. Operation at extremely high current densities with large voltages and at nearly 100% SOC produces conditions which are known to damage graphite porous electrodes and current collectors. Wear patterns corresponding to the position of the 2 cm^2 Teflon aperture were observable in the graphite electrodes used in the XO cell experiments. Microscopic examination of the Nafion membranes which have been subjected to extreme conditions might reveal flaws which could lead to enhanced transport. The use of improved experimental techniques such as the quasi-steady state half cell mode and closer attention to osmotic pressure gradient effects would reduce other sources of variation and improve the chances of identifying other variables influencing electrolyte cross-over.

6.3 CLOSING REMARKS

The most important result of this thesis was not the actual experimental results, but the development of a method to directly measure electrolyte cross-over under realistic operating conditions using the triple membrane (XO) cell. The XO cell geometry, with the additional chambers between the half cells of a standard RFB, successfully demonstrated that cross-over from each side of the cell could be collected with minimal cross-talk between the two sides of the cell, and in the case of vanadium can easily be diagnosed with simple spectroscopic absorption measurements. The results of the experiments clearly showed the importance of current driven transport when considering cross-over of electrolytes in a VRB cell, and show how capacity loss can be predicted from the results of cross-over measurements over just a few charge/discharge cycles.

Appendix: Compilation of Experimental Run Data

CHAPTER 4 EXPERIMENTS

Table A1 Low Concentration (0.7 M) V^{+2}/V^{+3} and V^{+4}/V^{+5} N212 Cross-over Data (Figures 4.1, 4.2, 4.3, 4.4).

Date	Membrane	Species	Initial_C	Final_C	Dilution	Avg_Conc	XO_Conc	Time	Vol (CC)	J_Dens	Mass Trans	Diff_C	Exp_Type	Combined m
8/3/2012	N212	V5	0.004035	0.027261	10	0.1565	0.0047	7200	53	0	1.10E-04	5.51E-07	V4V5	9.51E-05
8/3/2012	N212	V4	0.035062	0.007561	10	0.2131	0.0049	7200	53	0	8.40E-05	4.20E-07	V4V5	
8/3/2012	N212	V5	0.026316	0.001157	10	0.1374	0.0040	7200	53	0	1.08E-04	5.38E-07	V4V5	9.19E-05
8/3/2012	N212	V4	0.009572	0.0377	10	0.2364	0.0053	7200	53	0	8.27E-05	4.14E-07	V4V5	
8/2/2012	N212	V5	0.004234	0.029676	10	0.1696	0.0077	7200	53	300	1.67E-04	8.36E-07	V4V5	1.53E-04
8/2/2012	N212	V4	0.034768	0.007705	10	0.2124	0.0082	7200	53	300	1.41E-04	7.07E-07	V4V5	
8/2/2012	N212	V5	0.027377	0.001992	10	0.1468	0.0040	7200	53	-300	1.01E-04	5.03E-07	V4V5	8.95E-05
8/2/2012	N212	V4	0.010074	0.037265	10	0.2367	0.0053	7200	53	-300	8.26E-05	4.13E-07	V4V5	
8/3/2012	N212	V5	0.027943	0.004049	10	0.1600	0.0033	7200	53	-300	7.50E-05	3.75E-07	V4V5	5.33E-05
8/3/2012	N212	V4	0.007327	0.035306	10	0.2132	0.0021	7200	53	-300	3.70E-05	1.85E-07	V4V5	
8/3/2012	N212	V5	0.002057	0.02891	10	0.1548	0.0076	7200	53	300	1.81E-04	9.07E-07	V4V5	1.50E-04
8/3/2012	N212	V4	0.037273	0.008238	10	0.2276	0.0079	7200	53	300	1.28E-04	6.40E-07	V4V5	
8/7/2012	N212	V5	0.003093	0.030102	10	0.1660	0.0104	3600	33	600	2.88E-04	1.44E-06	V4V5	2.07E-04
8/7/2012	N212	V4	0.035623	0.008329	10	0.2198	0.0070	3600	33	600	1.46E-04	7.32E-07	V4V5	
8/7/2012	N212	V5	0.028113	0.000107	10	0.1411	0.0008	3600	33	-600	2.70E-05	1.35E-07	V4V5	3.33E-05
8/7/2012	N212	V4	0.009474	0.038566	10	0.2402	0.0019	3600	33	-600	3.70E-05	1.85E-07	V4V5	
8/7/2012	N212	V5	0.030102	0.002754	10	0.1643	0.0014	3600	33	-600	3.91E-05	1.96E-07	V4V5	3.72E-05
8/7/2012	N212	V4	0.008329	0.036422	10	0.2238	0.0018	3600	33	-600	3.59E-05	1.79E-07	V4V5	
8/7/2012	N212	V5	0.000107	0.028634	10	0.1437	0.0108	3600	33	600	3.44E-04	1.72E-06	V4V5	2.04E-04
8/7/2012	N212	V4	0.038566	0.008029	10	0.2330	0.0060	3600	33	600	1.18E-04	5.91E-07	V4V5	
8/10/2012	N212	V5	0.032027	0.001775	10	0.1690	0.0007	3000	33	-900	2.14E-05	1.07E-07	V4V5	2.90E-05
8/10/2012	N212	V4	0.009973	0.041687	10	0.2583	0.0016	3000	33	-900	3.39E-05	1.69E-07	V4V5	
8/10/2012	N212	V5	0.003126	0.03248	10	0.1780	0.0138	3000	33	900	4.25E-04	2.12E-06	V4V5	2.55E-04
8/10/2012	N212	V4	0.040126	0.00831	10	0.2422	0.0057	3000	33	900	1.30E-04	6.52E-07	V4V5	
8/10/2012	N212	V5	0.001775	0.032214	10	0.1699	0.0139	3000	33	900	4.48E-04	2.24E-06	V4V5	2.53E-04
8/10/2012	N212	V4	0.041687	0.008975	10	0.2533	0.0056	3000	33	900	1.23E-04	6.13E-07	V4V5	
8/10/2012	N212	V5	0.03248	0.002632	10	0.1756	0.0006	3000	33	-900	2.02E-05	1.01E-07	V4V5	2.40E-05
8/10/2012	N212	V4	0.00831	0.040221	10	0.2427	0.0012	3000	33	-900	2.68E-05	1.34E-07	V4V5	
8/21/2012	N212	V5	0.034677	0.034677	10	0.3468	0.0047	3600	33	0	6.28E-05	3.14E-07	V2V3V4V5	6.34E-05
8/21/2012	N212	V4	0.01985	0.01985	10	0.1985	0.0028	3600	33	0	6.44E-05	3.22E-07	V2V3V4V5	
8/22/2012	N212	V5	0.035261	0.035261	10	0.3526	0.0042	3600	33	0	5.44E-05	2.72E-07	V2V3V4V5	5.78E-05
8/22/2012	N212	V4	0.020368	0.020368	10	0.2037	0.0028	3600	33	0	6.38E-05	3.19E-07	V2V3V4V5	
8/22/2012	N212	V3	0.013147	0.013147	10	0.1315	0.0017	3600	33	0	5.92E-05	2.96E-07	V2V3V4V5	7.68E-05
8/22/2012	N212	V2	0.034532	0.034532	10	0.3453	0.0063	3600	33	0	8.35E-05	4.18E-07	V2V3V4V5	
8/23/2012	N212	V5	0.038328	0.00672	10	0.2252	0.0005	6000	33	-600	6.41E-06	3.20E-08	V2V3V4V5	1.82E-05
8/23/2012	N212	V4	0.012891	0.047479	10	0.3019	0.0030	6000	33	-600	2.70E-05	1.35E-07	V2V3V4V5	
8/23/2012	N212	V3	0.006322	0.049324	10	0.2782	0.0213	6000	33	600	2.10E-04	1.05E-06	V2V3V4V5	1.74E-04
8/23/2012	N212	V2	0.036863	0	10	0.1843	0.0080	6000	33	600	1.20E-04	5.99E-07	V2V3V4V5	
8/23/2012	N212	V5	0.006834	0.032772	10	0.1980	0.0127	5031	33	600	2.11E-04	1.06E-06	V2V3V4V5	1.58E-04
8/23/2012	N212	V4	0.047472	0.017485	10	0.3248	0.0125	5031	33	600	1.26E-04	6.30E-07	V2V3V4V5	
8/23/2012	N212	V3	0.049324	0.008825	10	0.2907	0.0022	5031	33	-600	2.46E-05	1.23E-07	V2V3V4V5	
8/24/2012	N212	V5	0.033893	0.004484	10	0.1919	0.0008	10800	33	-300	6.20E-06	3.10E-08	V2V3V4V5	3.53E-05
8/24/2012	N212	V4	0.016739	0.048066	10	0.3240	0.0111	10800	33	-300	5.25E-05	2.63E-07	V2V3V4V5	
8/24/2012	N212	V3	0	0.042911	10	0.2146	0.0122	10800	33	300	8.68E-05	4.34E-07	V2V3V4V5	1.10E-04
8/24/2012	N212	V2	0.046886	0.006426	10	0.2666	0.0225	10800	33	300	1.29E-04	6.44E-07	V2V3V4V5	
8/24/2012	N212	V5	0.004484	0.033203	10	0.1884	0.0124	10800	33	300	1.01E-04	5.04E-07	V2V3V4V5	9.43E-05
8/24/2012	N212	V4	0.048066	0.015726	10	0.3190	0.0189	10800	33	300	9.05E-05	4.53E-07	V2V3V4V5	
8/24/2012	N212	V3	0.042911	0	10	0.2146	0.0064	10800	33	-300	4.55E-05	2.28E-07	V2V3V4V5	2.89E-05
8/24/2012	N212	V2	0.006426	0.044981	10	0.2570	0.0025	10800	33	-300	1.51E-05	7.53E-08	V2V3V4V5	
8/31/2012	N212	V3	0.03877	0.03877	10	0.3877	0.0126	7200	33	0	7.48E-05	3.74E-07	V3V2	9.33E-05
8/31/2012	N212	V2	0.036584	0.036584	10	0.3658	0.0180	7200	33	0	1.13E-04	5.64E-07	V3V2	
9/5/2012	N212	V3	0.004622	0.032967	10	0.1879	0.0128	7200	33	300	1.56E-04	7.82E-07	V3V2	1.55E-04
9/5/2012	N212	V2	0.028895	0.002224	10	0.1556	0.0105	7200	33	300	1.54E-04	7.71E-07	V3V2	
9/5/2012	N212	V3	0.033981	3.87E-05	10	0.1701	0.0026	7200	33	-300	3.48E-05	1.74E-07	V3V2	5.05E-05
9/5/2012	N212	V2	0	0.036584	10	0.1829	0.0052	7200	33	-300	6.51E-05	3.25E-07	V3V2	
9/6/2012	N212	V3	0.036069	0.003565	10	0.1982	0.0135	6800	33	300	1.65E-04	8.27E-07	V3V2	1.41E-04
9/6/2012	N212	V2	0	0.027786	10	0.1389	0.0061	6800	33	300	1.07E-04	5.33E-07	V3V2	
9/6/2012	N212	V3	0.004622	0.034462	10	0.1954	0.0032	6800	33	-300	4.02E-05	2.01E-07	V3V2	3.81E-05
9/6/2012	N212	V2	0.028895	0	10	0.1445	0.0021	6800	33	-300	3.53E-05	1.76E-07	V3V2	

Table A2 High Concentration (1.5 M) V^{+4}/V^{+5} with N212, N117, FX-7050 membranes (Figures 4.9. 4.10, 4.11, 4.12).

Date	Membran	Species	Initial_C	Final_C	Dilution	Avg_Conc	XO_Conc	Time	Vol (CC)	J_Dens	Mass Tran	Diff_C	Combined Mass
9/30/2013	7050	V5	0.000336	0.043796	20	0.441328	0.009005	7945	33	900	4.24E-05	2.12E-07	3.15E-05
9/30/2013	7050	V4	0.050311	0.003953	20	0.542637	0.005916	7945	33	900	2.26E-05	1.13E-07	
9/30/2013	7050	V5	0.041915	0	20	0.419146	0.000116	7945	33	-900	5.73E-07	2.86E-09	7.25E-07
9/30/2013	7050	V4	0.000104	0.047272	20	0.473753	0.000196	7945	33	-900	8.59E-07	4.3E-09	
9/30/2012	7050	V5	0	0.044309	20	0.443089	0.007593	12000	33	600	2.36E-05	1.18E-07	1.92E-05
9/30/2012	7050	V4	0.051247	0.003489	20	0.547362	0.00621	12000	33	600	1.56E-05	7.8E-08	
9/30/2012	7050	V5	0.044546	0	20	0.445463	0.000322	12000	33	-600	9.95E-07	4.98E-09	9.65E-07
9/30/2012	7050	V4	0.000372	0.046584	20	0.469562	0.00032	12000	33	-600	9.36E-07	4.68E-09	
9/29/2012	7050	V5	0.044546	0	20	0.445463	0.000322	12000	33	-600	9.95E-07	4.98E-09	9.65E-07
9/29/2012	7050	V4	0.000372	0.046584	20	0.469562	0.00032	12000	33	-600	9.36E-07	4.68E-09	
9/29/2012	7050	V5	0	0.044309	20	0.443089	0.007593	12000	33	600	2.36E-05	1.18E-07	1.92E-05
9/29/2012	7050	V4	0.051247	0.003489	20	0.547362	0.00621	12000	33	600	1.56E-05	7.8E-08	
9/28/2012	7050	V5	0.04276	0	20	0.427599	0.010843	7412	33	900	5.64E-05	2.82E-07	3.46E-05
9/28/2012	7050	V4	0.000636	0.046201	20	0.468367	0.003081	7412	33	900	1.46E-05	7.32E-08	
9/28/2012	7050	V5	0	0.044606	20	0.446055	0.005736	16105	33	450	1.32E-05	6.59E-08	1.21E-05
9/28/2012	7050	V4	0.047808	0.003673	20	0.514806	0.005572	16105	33	450	1.11E-05	5.54E-08	
9/27/2012	7050	V5	0.040318	0.040318	20	0.806353	0.001706	67380	33	0	5.18E-07	2.59E-09	5.33E-07
9/27/2012	7050	V4	0.051321	0.051321	20	1.026424	0.002281	67380	33	0	5.44E-07	2.72E-09	
9/22/2012	N117	V5	0.045405	0.045405	20	0.908094	0.045405	25440	33	0	3.24E-05	5.84E-07	1.84E-05
9/22/2012	N117	V4	0.056956	0.056956	20	1.139124	0.012663	25440	33	0	7.21E-06	1.3E-07	
9/23/2013	N117	V5	0.049716	0	20	0.497158	0.001448	18124.8	33	-450	2.65E-06	4.77E-08	3.14E-06
9/23/2013	N117	V4	0.001371	0.054253	20	0.556233	0.002188	18124.8	33	-450	3.58E-06	6.45E-08	
9/23/2013	N117	V5	0.000516	0.047664	20	0.481798	0.035427	18124.8	33	450	6.69E-05	1.2E-06	5.28E-05
9/23/2013	N117	V4	0.055473	0.002207	20	0.576809	0.025996	18124.8	33	450	4.1E-05	7.39E-07	
9/24/2012	N117	V5	0	0.049356	20	0.49356	0.035457	17655	33	450	6.71E-05	1.21E-06	5.72E-05
9/24/2012	N117	V4	0.047642	0.000896	20	0.485371	0.02447	17655	33	450	4.71E-05	8.48E-07	
9/24/2012	N117	V5	0.046676	0.000819	20	0.474953	0.001431	17655	33	-450	2.82E-06	5.07E-08	3.06E-06
9/24/2012	N117	V4	0.002368	0.058971	20	0.613392	0.002128	17655	33	-450	3.24E-06	5.83E-08	
9/24/2012	N117	V5	0.049498	0.000495	20	0.49993	0.001622	8507	33	-900	6.29E-06	1.13E-07	4.39E-06
9/24/2012	N117	V4	0.001049	0.057175	20	0.582243	0.000829	8507	33	-900	2.76E-06	4.97E-08	
9/24/2012	N117	V5	0.000947	0.051296	20	0.522428	0.043019	8507	33	900	0.00016	2.87E-06	1.06E-04
9/24/2012	N117	V4	0.059109	0.003504	20	0.626123	0.019511	8507	33	900	6.04E-05	1.09E-06	
9/25/2012	N117	V5	0.000621	0.043927	20	0.445483	0.041824	7998.8	33	900	0.000194	3.49E-06	1.27E-04
9/25/2012	N117	V4	0.046179	0.00241	20	0.485895	0.015365	7998.8	33	900	6.52E-05	1.17E-06	
9/25/2012	N117	V5	0.045691	0.00156	20	0.472506	0.001079	7998.8	33	-900	4.71E-06	8.48E-08	4.55E-06
9/25/2012	N117	V4	0.004605	0.051403	20	0.560086	0.0012	7998.8	33	-900	4.42E-06	7.96E-08	
9/19/2012	N212	V5	0.034342	0.034342	20	0.686845	0.026164	14220	33	0	4.42E-05	2.21E-07	3.77E-05
9/19/2012	N212	V4	0.010615	0.010615	20	0.212307	0.003047	14220	33	0	1.67E-05	8.33E-08	
9/19/2012	N212	V5	0.000935	0.035301	20	0.362363	0.021506	13501	33	450	7.25E-05	3.63E-07	5.32E-05
9/19/2012	N212	V4	0.054499	0.017827	20	0.723252	0.025727	13501	33	450	4.35E-05	2.17E-07	
9/19/2012	N212	V5	0.053329	0.018598	20	0.719269	0.004222	13501	33	-450	7.17E-06	3.59E-08	8.19E-06
9/19/2012	N212	V4	0.000311	0.038034	20	0.38345	0.003172	13501	33	-450	1.01E-05	5.05E-08	
9/20/2012	N212	V5	0.00088	0.045374	20	0.462541	0.046193	9000	33	900	0.000183	9.15E-07	1.17E-04
9/20/2012	N212	V4	0.05387	0.004502	20	0.583716	0.020757	9000	33	900	6.52E-05	3.26E-07	
9/20/2012	N212	V5	0.055481	0.003484	20	0.589655	0.00252	9000	33	-900	7.83E-06	3.92E-08	8.43E-06
9/20/2012	N212	V4	0.001693	0.053464	20	0.551566	0.002731	9000	33	-900	9.08E-06	4.54E-08	
9/20/2012	N212	V5	0.045374	0.002442	20	0.478164	0.00314	8584	33	-900	1.26E-05	6.31E-08	9.13E-06
9/20/2012	N212	V4	0.004502	0.052952	20	0.57454	0.001859	8584	33	-900	6.22E-06	3.11E-08	
9/20/2012	N212	V5	0.003484	0.057716	20	0.612005	0.05192	8584	33	900	0.000163	8.15E-07	1.13E-04
9/20/2012	N212	V4	0.053464	0.003122	20	0.565864	0.017327	8584	33	900	5.89E-05	2.94E-07	
9/21/2012	N212	V5	0.002489	0.045374	20	0.47863	0.046444	8481	33	900	0.000189	9.44E-07	1.14E-04
9/21/2012	N212	V4	0.057918	0.004502	20	0.6242	0.018145	8481	33	900	5.66E-05	2.83E-07	
9/21/2012	N212	V5	0.055238	0.003484	20	0.587221	0.002838	8481	33	-900	9.4E-06	4.7E-08	8.02E-06
9/21/2012	N212	V4	0.005737	0.053464	20	0.592008	0.002021	8481	33	-900	6.64E-06	3.32E-08	

Table A3 V^{+4}/V^{+5} Electrolyte in +XO (Figure 4.15).

Membrane	Species	Initial_C	Final_C	Dilution	Avg_Conc	Exp Type	XO_Conc	Time	Vol (CC)	J_Dens	Mass Tran	Diff_C
N117	V5	0.026856	0.026856	20	0.537121	V5 in XO	0.010812	9000	33	150	3.69E-05	6.64E-07
N117	V5	0.027068	0.027068	20	0.541351	V5 in XO	0.013101	9600	33	225	4.16E-05	7.49E-07
N117	V5	0.023563	0.023563	20	0.471269	V5 in XO	0.007809	9000	33	300	3.04E-05	5.47E-07
N117	V5	0.027291	0.027291	20	0.545826	V5 in XO	0.013264	6600	33	300	6.08E-05	1.09E-06
N117	V5	0.025	0.025	20	0.500009	V5 in XO	0.012225	6000	33	450	6.72E-05	1.21E-06
N117	V5	0.031979	0.031979	20	0.63958	V5 in XO	0.01755	5600	33	450	8.08E-05	1.46E-06
N117	V5	0.031163	0.031163	20	0.623266	V5 in XO	0.018544	5400	33	600	9.09E-05	1.64E-06
N117	V5	0.029119	0.029119	20	0.582377	V5 in XO	0.01632	4200	33	600	1.10E-04	1.98E-06
N117	V5	0.020408	0.020408	20	0.408167	V5 in XO	0.01707	3600	33	750	1.92E-04	3.45E-06
N117	V4	0.032119	0.032119	20	0.642379	V4 in XO	0.018648	12000	33	150	3.99E-05	7.18E-07
N117	V4	0.027872	0.027872	20	0.557448	V4 in XO	0.021891	9000	33	300	7.20E-05	1.30E-06
N117	V4	0.033393	0.033393	20	0.667858	V4 in XO	0.021507	6000	33	450	8.86E-05	1.59E-06
N117	V4	0.027214	0.027214	20	0.544275	V4 in XO	0.018066	4323.9	33	600	1.27E-04	2.28E-06
N117	V4	0.027321	0.027321	20	0.546422	V4 in XO	0.023348	3600	33	750	1.96E-04	3.53E-06
N117	V3	0.03762	0.03762	20	0.752399	V3 in XO	0.017721	7860	33	300	4.94E-05	8.90E-07
N117	V3	0.034965	0.034965	20	0.699295	V3 in XO	0.013122	4000	33	450	7.74E-05	1.39E-06
N117	V3	0.037196	0.037196	20	0.743924	V3 in XO	0.017016	3600	33	600	1.05E-04	1.89E-06
N117	V3	0.038369	0.038369	20	0.767387	V3 in XO	0.019779	3600	33	750	1.18E-04	2.13E-06

Table A4 Variable Sulfate (Figure 5.2).

Membrane	Species	Initial_C	Final_C	Dilution	Avg_Conc	Exp Type	XO_Conc	Time	Vol (CC)	J_Dens	Mass Trans	Diff_C	Comment
N117	V4	0.042708	0.042708	10	0.427085	V4 in XO	0.021807245	11040	33	0	7.63E-05	1.37E-06	Low Sulfate
N117	V4	0.05293	0.04836	10	0.506448	V4 in XO	0.02182425	9000	33	0	7.90E-05	1.42E-06	Low Sulfate
N117	V4	0.045671	0.052185	10	0.489277	V4 in XO	0.008723028	4600	33	0	6.39E-05	1.15E-06	low sulfate
N117	V4	0.048371	0.049871	10	0.491211	V4 in XO	0.02899157	4600	33	600	2.12E-04	3.81E-06	low sulfate
N117	V4	0.052366	0.053014	10	0.526901	V4 in XO	0.038649427	4400	33	600	2.75E-04	4.95E-06	low Sulfate
N117	V4	0.050939	0.050078	10	0.505085	V4 in XO	0.035410315	4700	33	600	2.46E-04	4.43E-06	low Sulfate
N117	V4	0.05027	0.052683	10	0.514767	V4 in XO	0.012695411	5400	33	300	7.54E-05	1.36E-06	Mid Sulfate
N117	V4	0.051977	0.049857	10	0.509169	V4 in XO	0.010591683	4252	33	300	8.07E-05	1.45E-06	Mid Sulfate
N117	V4	0.052444	0.049556	10	0.510001	V4 in XO	0.108071485	7500	33	0	4.66E-04	8.39E-06	No Sulfate
N117	V4	0.036968	0.036968	10	0.369684	V4 in XO	0.007962135	10800	33	0	3.29E-05	5.92E-07	Std Sulfate
N117	V4	0.04532	0.047178	10	0.462491	V4 in XO	0.006485902	9000	33	0	2.57E-05	4.63E-07	Std Sulfate
N117	V4	0.044539	0.046617	10	0.455781	V4 in XO	0.005673469	7200	33	0	2.85E-05	5.13E-07	Std Sulfate
N117	V4	0.046617	0.042811	10	0.447142	V4 in XO	0.005235782	7200	33	0	2.68E-05	4.83E-07	Std Sulfate
N117	V4	0.047854	0.05039	10	0.491218	V4 in XO	0.009673629	4560	33	600	7.13E-05	1.28E-06	Std Sulfate
N117	V4	0.049323	0.050268	10	0.497955	V4 in XO	0.013168604	5000	33	600	8.73E-05	1.57E-06	Std Sulfate

References

1. M. Rychcik and M. Skyllas-Kazacos, "Characteristics of a new all-vanadium redox flow battery", *J. Power Sources*, 22 (1988) 59-67.
2. K.W. Knehr, E. Kumbur," Open circuit voltage of vanadium redox flow batteries: Discrepancy between models and experiments", *Electrochemistry Communications*, 13 (2011) 342-345.
3. E. Kjeang, B. Proctorm A. Brolo, D. Harrington, N. Djilali, D. Sinton, "High performance microfluidic vanadium redox fuel cell*", Electrochimica Acta*, 52 (2007) 4942–4946.
4. A. Tang, J. Bao, M. Skylass-Kazacos, "Dynamic modeling of the effects of ion diffusion and side reactions on the capacity loss for vanadium redox flow battery", *J. Power Sources*, 196 (2011) 10737-10747.
5. K.W. Knehr, E. Agar, C. Dennison, A. Kalidindi, and E. Kumbar, "A Transient Vanadium Flow Battery Model Incorporating Vanadium Crossover and Water Transport through the Membrane", *J. Electrochem. Soc*., 159 (2012) A1446-A1459.
6. F. Grossmith, P. Llewellyn, A.G. Fane, M. Skyllas-Kazacos, "Evaluation of membranes for all-vanadium redox cell", *Proc. Electrochem. Soc. Symp*., Honolulu, October 1988, pp. 363-374.
7. E. Wiedemann, A. Heintz, R.N. Lichtenthaler, "Transport properties of vanadium ions in cation exchange membranes: Determination of diffusion coefficients using a dialysis cell", *J. Membrane Science* ,141 (1998) 215-221
8. C. Sun, J. Chen, H. Zhang, X. Han, Q. Luo, "Investigations on transfer of water and vanadium ions across Nafion membrane in an operating vanadium redox flow battery", *J. Power Sources*, 195 (2010) 890-897.
9. Q. Luo, L. Li, Z. Nie, W. Wang, X. Wei, B. Li, B. Chen, Z. Yang, "In-situ investigation of vanadium ion transport in redox flow battery", *J. Power Sources*, 218 (2012) 15-20.
10. Q. Liu, G. Grim, A. Papandrew, A. Turbin, T. Zawodzinski, M. Mench, "High Performance Vanadium Redox Flow Batteries with Optimized Electrode Configuration and Membrane Selection", *J. Electrochem. Soc.*, 159 (2012), A1246-A1252.
11. M. Skyllas-Kazacos, M. Kazacos, "State of charge monitoring methods for vanadium redox flow battery control", *J. Power Sources*, 2011, 196, 8822-8827.
12. Z. Tang, D. Aaron, A. Papandrew, T. Zawodzinski, "Monitoring the State of Charge of Operating Vanadium Redox Flow Batteries", *ECS Transactions*, 2012, 41 (23), 1-9.
13. P. Blanc, C. Madic, J. P. Launay, " Spectrophotometric identification of a mixed-vlaence cation-cation complex between aquadioxovanadium (V) and aquaovanadium (IV) ions in perchloric, sulfuric, and hydrochloric acid media", *Inorganic Chemistry*, 1982, 21, 2923-2928.

14. K. Okamoto, J. Woo-Sik, H. Tomiyasu, H. Fukutomi, "Vanadium-51 NMR line-broadening in the mixture of dioxovanadium(V) and oxovanadium(IV) ions in perchloric acid Solution", *Inorganica Chimica Acta*. 1988, 143, 217-221.
15. J. Newman, K. Thomas-Alyea, *Electrochemical Systems*, 3rd Edition (Hoboken NJ: Wiley, 2004).
16. K. Knehr, E. Agar, C. Dennison, A. Kalidindi, E. Kumbar, "A Transient Vanadium Flow Battery Model Incorporating Vanadium Crossover and Water Transport through the Membrane", *J. of the Electrochemical Soc*., 159 (2012) A1446-1459.
17. P.H. Michael, "*A Multicomponent Model for the Vanadium Redox Flow Battery*", Unpublished Masters Thesis, The University of Texas, Austin TX (2012).
18. R.M. Darling and M.L Perry, "*Pseudo-Steady-State Flow Battery Experiments*", paper #B6-0480 to be presented at the 223rd meeting of the Electrochemical Society. Toronto, Canada (2013).
19. M.L. Perry, R.M. Darling, R. Zaffou, "*High Power Density Flow Battery Cells*", paper #B6-0476 to be presented at the 223rd meeting of the Electrochemical Society. Toronto, Canada (2013).
20. W.B. Stine and M. Geyer, *"Power from the Sun"*, published online http://www.powerfromthesun.net/book.html, (2001).